UNIVERSIDADE DE SÃO PAULO

CENTRO DE ENERGIA NUCLEAR NA AGRICULTURA

LUIZA SANTOS REIS

Pleistocene and Interdisciplinary Reconstitution of Lacustrine Deposits in the Serra Sul de Carajás, southeastern Amazonia

Piracicaba

2020

LUIZA SANTOS REIS

Pleistocene and Interdisciplinary Reconstitution of lacustrine deposits in the Serra Sul de Carajás, southeastern Amazonia

Thesis presented to Center for Nuclear Energy in Agriculture, University of São Paulo as a requisite to the Doctoral Degree in Sciences

Concentration Area: Nuclear Energy in Agriculture and Environment

Supervisor: Prof. Dr. Luiz Carlos Ruiz Pessenda

Co-supervisor: Dr. José Tasso Felix Guimarães

Piracicaba

2020

AUTORIZO A DIVULGAÇÃO TOTAL OU PARCIAL DESTE TRABALHO, POR QUALQUER MEIO CONVENCIONAL OU ELETRÔNICO, PARA FINS DE ESTUDO E PESQUISA, DESDE QUE CITADA A FONTE

Dados Internacionais de Catalogação na Publicação (CIP)

Seção Técnica de Biblioteca - CENA/USP

Reis, L. S.

Reconstituição Pleistocênica e interdisciplinar de depósitos lacustres da Serra Sul de Carajás, sudeste da Amazônia / Pleistocene and Interdisciplinary Reconstitution of lacustrine deposits in the Serra Sul de Carajás, southeastern Amazonia / Luiza Santos Reis; orientador Luiz Carlos Ruiz Pessenda; coorientador José Tasso Felix Guimarães. - - Piracicaba, 2020.

133 p. : il.

Tese (Doutorado – Programa de Pós-Graduação em Ciências. Área de Concentração: Energia Nuclear na Agricultura e no Ambiente) – Centro de Energia Nuclear na Agricultura da Universidade de São Paulo, Piracicaba.

1. Ácidos graxos 2. Compostos orgânicos 3. Datação ^{14}C 4. Geoquímica 5. Isótopos estáveis 6. Lipídeos 7. Mudança climática 8. Paleoambiente 9. Paleoclima – Amazônia 10. Palinologia 11. Quaternário 12. Sedimentologia lacustre I. Título

CDU 551.583.7 : 902.67 (811.3)

Elaborada por:
Marilia Ribeiro Garcia Henyei
CRB-8/3631
Resolução CFB Nº 184 de 29 de setembro de 2017

I dedicate this thesis to my parents, José and Helena
and my sister, Lorena.

I also devote my thesis to all those people who dedicate their lives to Science.

ACKNOWLEDGMENTS

First of all, I thank God for this achievement and for all the blessings I have obtained, including four years of doctorate full of learning and valuable experiences shared with wonderful people.

Secondly, I thank my family which is my strength and my greatest support. Thanks to my parents' teachings and dialogues, along with the model of honesty, kindness and moral values they showed me, I have become the person I am today and I got here. Love you all!

Furthermore, I thank the University of São Paulo, the Vale Institute of Technology, and the Center of Nuclear Energy in Agriculture, including the Laboratory of Stable Isotopes (Prof. Dr. Albertino Bendassolli) and Laboratory of Nutrients Cycling (Prof. Dr. Marisa Piccolo) for all the supports which provided the development and completion of this research project. Additionally, I thank for the high standard education, scientific and pedagogical basis that contributed to my personal and professional growth.

Thanks to the São Paulo Research Foundation (FAPESP) for granting the scholarship (grant - 2015/25744-8).

I am also very grateful to Prof. Dr. Luiz Carlos Ruiz Pessenda for opening the lab doors and guided me into this adventure, at times very arduous but with excellent rewards.

Special thanks also to Dr. Tasso Guimarães for believing in my potential and for all conversations and advice, always on time.

I thank Dr. Prafulla Sahoo for valuable discussions regarding geochemical data.

Thanks to Ioanna Bouloubassi and Mercedes Mendez-Millan from Laboratoire d'Océanographie et du Climat: Expérimentations et Approches Numériques and Institut de Recherche pour le Développement (UMR LOCEAN-IPSL-SU-CNRS-IRD-MNHN), who supervised me during my internship at the Sorbonne Universités, France. Thanks to all the team which provided all technical and intellectual support, and access to instrumental platforms that allowed me to be trained in the field of molecular and isotopic organic geochemistry.

Thanks to all my great colleagues from Laboratory C-14 – Flávio, Beatriz, Elton, Thiago, Evandro, Álvaro - and those who shared special moments with me during my doctorate – Ana, Cleverson, Rodolfo, Débora, Rodrigo(s), Bárbara, Wanderlei, Plácido, Leonardo, Adriana, Cindy, Letícia, Lucas, Marlon, Joana, Alice. Thanks for the companionship and for making my days more pleasant and joyful.

Finally, my personal thanks to Amine for bringing lightness to my journey. And yet, for being so present in my life even with an entire ocean between us.

“Todas as batidas de um coração humano abrem um universo de possibilidades.” –
Trecho do livro *Shantaram*

ABSTRACT

REIS, L. S. **Pleistocene and interdisciplinary reconstitution of lacustrine deposits in the Serra Sul de Carajás, southeastern Amazonia.** 2020. 133 p. Tese (Doutorado em Ciências) – Centro de Energia Nuclear na Agricultura, Universidade de São Paulo, Piracicaba, 2020.

Several studies have been performed within the Amazon basin in order to better understand the effects of Northern Hemisphere climatic events over the rainfall regime and vegetation dynamic. However, there is no broad consensus, since most studies is based only on pollen data. Due to the limitations of this technique, a multiproxy approach is essential to obtain a better interpretation of climatic variations. In this way, molecular and isotopic analyses of plant waxes ($\delta^{13}C$ and δD) and bulk organic matter ($\delta^{13}C$ and $\delta^{15}N$) together with sedimentary facies, palynological, multi-elemental geochemistry, micro- and macro-charcoal fragments analyses were performed on sedimentary cores from Lake Amendoim and revealed important environmental changes over the last ~22 ka. Low sedimentation rate and siderite precipitation episodes during the Last Glacial Maximum (LGM) and Late Glacial, besides mixed C_3/C_4 plant communities and enriched plant wax δD, evidence less humid conditions at Carajás. The occurrence of cool-adapted taxa such as *Podocarpus*, *Alnus*, and *Hedyosmum* also reveals cooler conditions during this interval, attesting the key role of changes in temperature over vegetation composition and distribution inside the Amazon basin. During LGM, colder sea surface temperature (SST) probably caused a decrease in the Atlantic Ocean moisture supply to northern South America which led to reduced precipitation amount. The Pleistocene-Holocene transition and the beginning of the Early Holocene are characterized by the large occurrence of fire events and precipitation of siderite nodules, besides reduced detrital input into the lake basin. On the other way, the data also show a higher concentration of pollen grains from forest formation and palms as well as depleted plant wax δD and $\delta^{13}C$ values, indicating the onset of seasonal features. A well-marked episode of intense precipitation between 11-10 ka shows a high correspondence with the Heinrich Stadial 0 and the Holocene Thermal Maximum, evidencing their influences over the rainfall regime within Amazonia. From Early to Late Holocene, a pronounced increase in C_3-dominated community together with a steady decrease in plant wax δD and $\delta^{13}C$ values points to an expansion of ombrophylous forest over the plateau slopes in Serra Sul de Carajás and a change to predominantly wet climatic conditions similar to the current one from the last 5 ka.

Keywords: Late Quaternary. Paleoclimate. Paleovegetation. Stable isotopes. Plant waxes.

RESUMO

REIS, L. S. **Reconstituição Pleistocênica e interdisciplinar de depósitos lacustres da Serra Sul de Carajás, sudeste da Amazônia**. 2020. 133 p. Tese (Doutorado) – Centro de Energia Nuclear na Agricultura, Universidade de São Paulo, Piracicaba, 2020.

Diversos estudos foram realizados na bacia amazônica com o intuito de compreender os efeitos dos eventos climáticos ocorridos no Hemisfério Norte sobre o regime de chuvas e na dinâmica da vegetação. No entanto, não há um amplo consenso, uma vez que a maioria dos estudos se baseia apenas em dados palinológicos. E devido às limitações desta técnica, uma abordagem "*multi-proxy*" é essencial para obter uma melhor interpretação das variações climáticas. Dessa forma, análises moleculares e isotópicas de ceras vegetais ($\delta^{13}C$ e δD) e de matéria orgânica sedimentar ($\delta^{13}C$ e $\delta^{15}N$), juntamente com fácies sedimentares, análises palinológicas, geoquímica multi-elementar, micro e macro-fragmentos de carvão foram realizadas em testemunhos sedimentares proveninetes do Lago Amendoim que revelram importantes mudanças ambientais ao longo dos últimos ~ 22 mil anos. As baixas taxas de sedimentação e episódios de precipitação de siderita durante o Último Glacial Máximo (UMG) e Glacial Tardio, além da comunidade mista de plantas C_3/C_4 e valores enriquecidos de δD, evidenciam condições menos úmidas em Carajás. A ocorrência de táxons adaptados ao frio, como *Podocarpus*, *Alnus* e *Hedyosmum*, revela condições mais frias durante esse intervalo, atestando o importante papel das mudanças na temperatura sobre a composição e distribuição da vegetação na bacia amazônica. Durante o UMG, baixas temperaturas da superfície do mar (TSM) provavelmente causaram uma diminuição no aporte de umidade do Oceano Atlântico para o norte da América do Sul, o que levou a uma redução na precipitação. A transição Pleistoceno-Holoceno e o início do Holoceno Inferior são caracterizados pela grande ocorrência de eventos de incêndio e precipitação de nódulos de siderita, além de menor aporte de detritos para o interior da bacia lacustre. Por outro lado, os dados também mostram uma maior concentração de grãos de pólen de formação florestal e palmeiras, bem como valores empobrecidos de δD e $\delta^{13}C$ de cera vegetal, indicando o início de condições sazonais. Um episódio de intensa precipitação entre 11 e 10 mil anos mostra uma alta correspondência com os eventos Heinrich Stadial 0 e o Holoceno Thermal Maximum, evidenciando suas influências sobre o regime de chuvas na Amazônia. A partir do Holoceno Inferior até o Holoceno Tardio, ocorre um aumento pronunciado na comunidade de plantas C_3, e o empobrecimento contínuo dos valores de δD e $\delta^{13}C$ de cera vegetal. Isto indica uma expansão da floresta ombrófila nas encostas do planalto na Serra Sul de Carajás e uma mudança para condições climáticas predominantemente úmidas semelhantes às atuais a partir dos últimos 5 mil anos.

Palavras-Chave: Quaternário Tardio. Paleoclima. Paleovegetação. Isótopos estáveis. Ceras foliares.

CONTENTS

1. INTRODUCTION

The Amazonia has been by far one of the most studied biomes in the context of environmental and vegetation dynamics due to its huge terrestrial biodiversity and importance in carbon sequestration and storage, playing a crucial role in the maintenance of the global climate system (FEARNSIDE, 2008; GRACE et al., 1995). It also provides a massive amount of heat and moisture to the atmosphere in the tropics, contributing 25-50% to the precipitation within the Amazon basin (ELTAHIR; BRAS, 1994; VAN DER ENT et al., 2010), and around 20% to the precipitation over La Plata Basin (MARTINEZ; DOMINGUEZ, 2014).

The evolutionary history and spatial patterns of Amazon biodiversity have already been well established (HOORN et al., 2010), however, the long-term climate variability and its potential influence on the biodiversity still remain poorly understood. Earlier palynological and paleobotany records from the Amazon basin indicate that the greatest diversity existed during the Miocene when environmental conditions – i.e. low seasonality, high rainfall, and heterogeneous soil substrates – were highly favorable for forest maintenance (JARAMILLO et al., 2010). However, with Andean tectonism throughout the Neogene (around 20 million years ago), important geomorphological displacement occurred and led to changes in the drainage system as well as in the climate setting over the Amazon basin (VAN DER HAMMEN; HOOGHIEMSTRA, 2000). These processes probably caused considerable stress on the plant community and may have led to extinction species less adapted to environmental disturbances. On the other hand, these environmental and climate perturbations may have induced intense speciation and evolution which resulted in the high biodiversity of the neotropical flora (HOORN; WESSELINGH, 2010).

Recently, it was proposed that greater biodiversity is maintained by relatively stable climate (HÄGGI et al., 2017), while climate perturbances may lead to loss in biodiversity and/or an increase in extinction rates (CHENG et al., 2013), which can explain the west-east diversity gradient that has been reported for some groups of Amazon organisms, such as trees and mammals (HOORN et al., 2010). Nevertheless, accurate characterization of hydroclimate variability in Amazonia on a wide range of timescales is still of great importance to understanding the possible link between climate change and biodiversity, and an indispensable step towards an assessment of the spatial-temporal patterns of tropical forest response to potential future climate change in South America (CHENG et al., 2013).

Despite a broad set of paleoclimate data from the Amazon basin, including lowland (COHEN et al., 2014; GUIMARÃES et al., 2013; LIMA et al., 2018; MAYLE; BURBRIDGE; KILLEEN, 2000; PESSENDA et al., 2009; SMITH et al., 2012; and references therein), and highland regions (BUSH et al., 2004; D'APOLITO; ABSY; LATRUBESSE, 2013; HOOGHIEMSTRA; VAN DER HAMMEN, 2004; PADUANO et al., 2003; URREGO et al., 2016; and references therein), climatic conditions in western and eastern Amazonia during Northern Hemisphere cold events – specifically the Last Glacial Maximum (LGM) – remain controversial.

Paleoclimatic studies based on pollen record have reported a cooling of 4-5°C in western Amazonia (BUSH; PHILANDER, 1999; BUSH et al., 2004; COLINVAUX et al., 1996; COLINVAUX; OLIVEIRA, 2000; VAN DER HAMMEN; HOOGHIEMSTRA, 2000), besides a decrease of 3°C in eastern Amazonia (REIS et al., 2017b), and around 5-8°C in high Andean and Altiplano (BAKER; FRITZ; BAKER, 2015; FORNACE et al., 2016; FRITZ et al., 2007; PADUANO et al., 2003) during the LGM. This caused changes in total rainfall amount, besides shifts in plant community distribution such as the incursion of cool-adapted species from Andean region into Amazonian lowland (COHEN et al., 2014; LIMA et al., 2018; REIS et al., 2017b), and maybe the expansion of savanna (C_4 plants) due to its higher water use efficiency and adaptation to drier conditions compared to C_3 plants (LARA; ANDREO, 2011).

Nevertheless, the extent of the dry episodes throughout the LGM and its impact on plant community composition and distribution (e.g. rainforest vs. savanna) over Amazon basin is largely debated and controversial (BUSH et al., 2004; COLINVAUX; OLIVEIRA, 2000; D'APOLITO; ABSY; LATRUBESSE, 2013). Pollen records from Lake Pata have shown that the rainforest persisted over the last 50,000 years under relatively stable climate in western Amazonia (COLINVAUX et al., 1996). Moreover, paleoecology records from Maicuru Plateau, in northern Amazonia, indicated the presence of forest throughout the LGM (COLINVAUX et al., 2001), similarly to the pollen data recorded at Lakes Dragão, Verde and Pata (BUSH et al., 2002; 2004). Although, new data from Lake Pata in the Hill of Six Lakes (D'APOLITO; ABSY; LATRUBESSE, 2013) revealed drier conditions during the LGM with a decrease of annual rainfall, raising new questions concerning past climate features for this region.

Considering the eastern Amazonia, several studies based on pollen data, geochemistry, and sedimentary records have suggested drier climate conditions in Carajás during the last glacial period (GUIMARÃES et al., 2016; HERMANOWSKI et al., 2012; SIFEDDINE et al., 2001) as evidenced by a hiatus in sedimentation and lower lake level (ABSY et al., 1991; SIFEDDINE et al., 1994). Cooler conditions in turn induced the formation of no-modern-analog communities composed of cool-adapted taxa and lowland species (REIS et al., 2017). On the other hand, some inconsistencies are observed in Holocene records for the eastern Amazonia. For instance, speleothem record from Paraíso cave revealed greater precipitation (142%) relative to current levels during the mid-Holocene epoch (about 6,000 years ago) (WANG et al., 2017), while pollen data have reported the occurrence of a dry episode evidenced by a decrease in forest abundance, high charcoal accumulation rates, and lower detrital input into the lacustrine deposits (CORDEIRO et al., 2008; HERMANOWSKI et al., 2012; REIS et al., 2017; SIFEDDINE et al., 2001).

Thus, in order to elucidate the questions mentioned above, we present a multi-proxy approach and the first hydrogen and carbon isotope records of plant waxes from southeastern Amazonia (Lake Amendoim), which brings new insights into paleoenvironmental and vegetation dynamics over the last ~22 ka. Combined with existing records, we also highlight the main forcing and climate control factors and address questions regarding major hydroclimate changes at the study site during relevant climate events in the Northern Hemisphere.

1.1. INTRODUÇÃO

A Amazônia tem sido de longe um dos biomas mais estudados no contexto da dinâmica ambiental e da vegetação, devido à sua enorme biodiversidade terrestre e importância no seqüestro e armazenamento de carbono, desempenhando um papel crucial na manutenção do sistema climático global (FEARNSIDE, 2008; GRACE et al., 1995). Além disso, fornece uma quantidade maciça de calor e umidade para a atmosfera nos trópicos, contribuindo com 25-50% para a precipitação na bacia amazônica (ELTAHIR; BRAS, 1994; VAN DER ENT et al., 2010) e com cerca de 20% para precipitação sobre a Bacia do Prata (MARTINEZ; DOMINGUEZ, 2014).

A história evolutiva e os padrões espaciais da biodiversidade da Amazônia já estão bem estabelecidos (HOORN et al., 2010), no entanto, a variabilidade climática a longo prazo e sua potencial influência na biodiversidade ainda permanecem pouco compreendidas. Registros palinológicos e paleobotânicos anteriores da bacia amazônica indicam que a maior diversidade existiu durante o Mioceno, quando as condições ambientais - ou seja, baixa sazonalidade, alta pluviosidade e substratos heterogêneos do solo - eram altamente favoráveis à manutenção da floresta (JARAMILLO et al., 2010). No entanto, com o tectonismo andino ao longo do Neogeno (em torno de 20 milhões atrás), ocorreram importantes deslocamentos geomorfológicos que levaram às mudanças no sistema de drenagem e no cenário climático da bacia amazônica (VAN DER HAMMEN; HOOGHIEMSTRA, 2000). Esses processos provavelmente causaram considerável estresse na comunidade vegetal e podem ter levado à extinção de espécies menos adaptadas à distúrbios ambientais. Por outro lado, tais perturbações ambientais e climáticas podem ter induzido intensa especiação e evolução, o que resultou na alta biodiversidade da flora neotropical (HOORN; WESSELINGH, 2010).

Recentemente, foi proposto que uma maior biodiversidade é mantida por um clima relativamente estável (HÄGGI et al., 2017), enquanto as perturbações climáticas podem levar à perda de biodiversidade e/ou a um aumento nas taxas de extinção (CHENG et al., 2013), o que pode explicar o gradiente de diversidade oeste-leste relatado para alguns grupos de organismos amazônicos, como árvores e mamíferos (HOORN et al., 2010). No entanto, a caracterização precisa da variabilidade do hidroclima na Amazônia em uma ampla escala de tempo ainda é de grande importância para a compreensão do possível vínculo entre mudança climática e biodiversidade, e um passo indispensável para uma avaliação dos padrões

espaço-temporais da resposta das florestas tropicais à potenciais mudanças climáticas futuras na América do Sul (CHENG et al., 2013).

Apesar de um amplo conjunto de dados paleoclimáticos da bacia amazônica, incluindo terras baixas (COHEN et al., 2014; GUIMARÃES et al., 2013; LIMA et al., 2018; MAYLE; BURBRIDGE; KILLEEN, 2000; PESSENDA et al., 2009; SMITH et al., 2012; e referências nela) e regiões montanhosas (BUSH et al., 2004; D'APOLITO; ABSY; LATRUBESSE, 2013; HOOGHIEMSTRA; VAN DER HAMMEN, 2004; PADUANO et al., 2003; URREGO et al., 2016; e referências nelas), as condições climáticas na Amazônia ocidental e oriental durante os eventos frios do Hemisfério Norte - especificamente o Último Máximo Glacial (UMG) - permanecem controversas.

Estudos paleoclimáticos baseados em registros polínicos relataram um resfriamento de 4-5°C no oeste da Amazônia (BUSH; PHILANDER, 1999; BUSH et al., 2004; COLINVAUX et al., 1996; COLINVAUX; OLIVEIRA, 2000; VAN DER HAMMEN; HOOGHIEMSTRA, 2000), além de uma diminuição de ~3°C no leste da Amazônia (REIS et al., 2017), e de cerca de 5-8°C nas regiões Andinas e Altiplano (BAKER; FRITZ; BAKER, 2015; FORNACE et al., 2016; FRITZ et al., 2007; PADUANO et al., 2003) durante o UMG. Isto causou mudanças na quantidade total de chuvas, além de mudanças na distribuição da comunidade de plantas, como a incursão de espécies adaptadas a frio da região andina na planície amazônica (COHEN et al., 2014; LIMA et al., 2018; REIS et al., 2017) e talvez a expansão da savana (plantas C_4) devido à sua maior eficiência no uso da água e adaptação às condições mais secas em comparação às plantas C3 (LARA; ANDREO, 2011).

No entanto, a extensão dos episódios secos em todo o UMG e seu impacto na composição e distribuição da vegetação (por exemplo, floresta tropical vs. savana) sobre a bacia amazônica é amplamente debatida e controversa (BUSH et al., 2004; COLINVAUX; OLIVEIRA, 2000; D'APOLITO; ABSY; LATRUBESSE, 2013). Registros palinológicos da Lagoa da Pata mostraram que a floresta tropical persistiu nos últimos 50,000 anos sob clima relativamente estável no oeste da Amazônia (COLINVAUX et al., 1996). Além disso, os registros paleoecológicos do planalto de Maicuru, no norte da Amazônia, indicaram a presença de florestas ao longo de todo período glacial (COLINVAUX et al., 2001), semelhante aos dados de pólen registrados nos Lagos Dragão, Verde e Pata (BUSH et al., 2002; 2004). Contudo, novos dados da Lagoa da Pata no Morro dos Seis Lagos (D'APOLITO; ABSY; LATRUBESSE, 2013) revelaram condições mais secas durante o

UMG, que resultou na diminuição da precipitação anual, levantando novas questões a respeito das características climáticas passadas desta região.

Considerando o leste da Amazônia, diversos estudos baseados em dados polínicos, de geoquímica e sedimentares sugeriram condições climáticas mais secas em Carajás durante o último período glacial (GUIMARÃES et al., 2016; HERMANOWSKI et al., 2012; SIFEDDINE et al., 2001), evidenciado por um hiato na sedimentação e diminuição do nível d'água dos lagos (ABSY et al., 1991; SIFEDDINE et al., 1994). As condições mais frias, por sua vez, induziram a formação de comunidades não-análogas às modernas compostas por taxa adaptados ao frio e espécies de planícies (REIS et al., 2017). Por outro lado, algumas inconsistências são observadas nos registros holocênicos para o leste da Amazônia. Por exemplo, o registro de espeleotemas da caverna Paraíso revelou maior precipitação (142%) em relação aos níveis atuais durante o Holoceno Médio (cerca de 6,000 anos atrás) (WANG et al., 2017), enquanto registros polínicos relataram a ocorrência de um episódio seco evidenciado por diminuição na abundância florestal, altas taxas de acúmulo de carvão e diminuição no aporte detrítico para as bacias lacustres (CORDEIRO et al., 2008; HERMANOWSKI et al., 2012; REIS et al., 2017; SIFEDDINE et al., 2001).

Assim, para elucidar as questões mencionadas acima, apresentamos uma abordagem multi-proxy e o primeiro registro isotópico de hidrogênio e carbono de ácidos graxos provenientes do Lago do Amendoim, que traz novos abordagens sobre a dinâmica paleoambiental e da vegetação ao longo dos últimos ~ 22,000 anos, no sudeste da Amazônia. Juntamente com os registros existentes, destacamos também as principais forçantes e fatores controladores da configuração climática e abordamos questões relacionadas às principais mudanças hidroclimáticas na área do estudo durante eventos climáticos relevantes no Hemisfério Norte.

References

ABSY, M. L. et al. Mise en évidence de quatre phases d'ouverture de la forêt dense dans le Sud-Est de l'Amazonie au cours des 60 000 dernières années : Première comparaison avec d'autres régions tropicales. **Comptes Rendus de l'Académie des Sciences**, v. 312, n. 6, p. 673–678, 1991.

BAKER, P. A.; FRITZ, S. C.; BAKER, P. A. Nature and causes of Quaternary climate variation of tropical South America. **Quaternary Science Reviews**, v. 124, p. 31–47, 2015.

BUSH, A. B. G.; PHILANDER, G. S. H. The climate of the Last Glacial Maximum: Results from a coupled atmosphere-ocean general circulation model. **Journal of Geophysical Research**, v. 104, n. D20, p. 24509–24525, 1999.

BUSH, M. B. et al. Orbital forcing signal in sediments of two Amazonian lakes. **Journal of Paleolimnology**, v. 2, p. 341–352, 2002.

BUSH, M. B. et al. Amazonian paleoecological histories: one hill, three watersheds. **Palaeogeography, Palaeoclimatology, Palaeoecology**, v. 214, n. 4, p. 359–393, 2004.

CHENG, H. et al. Climate change patterns in Amazonia and biodiversity. **Nature Communications**, v. 4, p. 1–6, 2013.

COHEN, M. C. L. et al. Late Pleistocene glacial forest of Humaitá-Western Amazonia. **Palaeogeography, Palaeoclimatology, Palaeoecology**, v. 415, p. 37–47, 2014.

COLINVAUX, P. A. et al. A long pollen record from Lowland Amazonia: Forest and Cooling in Glacial Times. **Science**, v. 274, n. 5284, p. 85–88, 1996.

COLINVAUX, P. A. et al. A paradigm to be discarded: Geological and paleoecological data falsify the HAFFER & PRANCE refuge hypothesis of Amazonian speciation. **Amazoniana**, v. 16, p. 609–646, 2001.

COLINVAUX, P. A.; OLIVEIRA, P. E. DE. Palaeoecology and climate of the Amazon basin during the last glacial cycle. **Journal of Quaternary Science**, v. 15, n. 4, p. 347–356, 2000.

CORDEIRO, R. C. et al. Holocene fires in East Amazonia (Carajás), new evidences, chronology and relation with paleoclimate. **Global and Planetary Change**, v. 61, n. 1–2, p. 49–62, 2008.

D'APOLITO, C.; ABSY, M. L.; LATRUBESSE, E. M. The Hill of Six Lakes revisited: New data and re-evaluation of a key Pleistocene Amazon site. **Quaternary Science Reviews**, v. 76, p. 140–155, 2013.

ELTAHIR, E. A. B.; BRAS, R. L. Precipitation recycling in the Amazon basin. **Quarterly Journal of the Royal Meteorological Society**, v. 120, n. 518, p. 861–880, 1994.

FEARNSIDE, P. M. Amazon Forest Maintenance as a Source of Environmental Services. **Anais da Academia Brasileira de Ciências**, v. 80, n. 1, p. 101–114, 2008.

FORNACE, K. L. et al. Late Quaternary environmental change in the interior South American tropics: New insight from leaf wax stable isotopes. **Earth and Planetary Science Letters**, v. 438, p. 75–85, 2016.

FRITZ, S. C. et al. Quaternary glaciation and hydrologic variation in the South American tropics as reconstructed from the Lake Titicaca drilling project. **Quaternary Research**, v. 68, n. 3, p. 410–420, 2007.

GRACE, J. et al. Carbon Dioxide Uptake by an Undisturbed Tropical Rain Forest in Southwest Amazonia, 1992 to 1993. **Science**, v. 270, p. 778–780, 1995.

GUIMARÃES, J. T. F. et al. An integrated approach to relate Holocene climatic, hydrological, morphological and vegetation changes in the southeastern Amazon region. **Vegetation History and Archaeobotany**, v. 22, n. 3, p. 185–198, 2013.

GUIMARÃES, J. T. F. et al. Late Quaternary environmental and climate changes registered in lacustrine sediments of the Serra Sul de Carajás, south-east Amazonia. **Journal of Quaternary Science**, v. 31, n. 2, p. 61–74, 2016.

HÄGGI, C. et al. Response of the Amazon rainforest to late Pleistocene climate variability. **Earth and Planetary Science Letters**, v. 479, p. 50-59, 2017.

HERMANOWSKI, B. et al. Palaeoenvironmental dynamics and underlying climatic changes in southeast Amazonia (Serra Sul dos Carajás, Brazil) during the late Pleistocene and Holocene. **Palaeogeography, Palaeoclimatology, Palaeoecology**, v. 365–366, p. 227–246, 2012.

HOOGHIEMSTRA, H.; VAN DER HAMMEN, T. Quaternary Ice-Age dynamics in the Colombian Andes: developing an understanding of our legacy. **Philosophical Transactions of the Royal Society B**, v. 359, p. 173–181, 2004.

HOORN, C. et al. Amazonia through time: Andean uplift, climate change, landscape evolution, and biodiversity. **Science**, v. 330, n. 6006, p. 927–931, 2010.

HOORN, C.; WESSELINGH, F. P. **Amazonia, landscape and species evolution**: A look into the past. 1. ed. Malaysia: Wiley-Blackwell, 2010.

JARAMILLO, C. et al. The Origin of the Modern Amazon Rainforest: Implications of the Palynological and Palaeobotanical Record. In: HOORN, C.; WESSELINGH, F. P. (Ed.). **Amazonia, landscape and species evolution**: A look into the past. 1. ed. Malaysia: Wiley-Blackwell, 2010. p. 317–334.

LARA, M. V.; ANDREO, C. S. C4 Plants Adaptation to High Levels of CO2 and to Drought Environments. In: SHANKER, A. (Ed.). **Abiotic stress in plants -** mechanisms and adaptations. 1. ed. New York: Intech, 2011. p. 415–428.

LIMA, W. J. S. et al. Late Pleistocene glacial forest elements of Brazilian Amazonia. **Palaeogeography, Palaeoclimatology, Palaeoecology**, v. 490, p. 617–628, 2018.

MARTINEZ, A. J.; DOMINGUEZ, F. Sources of atmospheric moisture for the La Plata River Basin. **Journal of Climate**, v. 27, n. 17, p. 6737–6753, 2014.

MAYLE, F. E.; BURBRIDGE, R.; KILLEEN, T. J. Millennial-scale dynamics of southern Amazonian rain forests. **Science**, v. 290, n. 5500, p. 2291–2294, 2000.

PADUANO, G. M. et al. A Vegetation and Fire History of Lake Titicaca since the Last Glacial Maximum. **Palaeogeography, Palaeoclimatology, Palaeoecology**, v. 194, p. 259–279, 2003.

PESSENDA, L. C. R. et al. The evolution of a tropical rainforest/grassland mosaic in southeastern Brazil since 28,000 14C yr BP based on carbon isotopes and pollen records. **Quaternary Research**, v. 71, n. 3, p. 437–452, 2009.

REIS, L. S. et al. Environmental and vegetation changes in southeastern Amazonia during the late Pleistocene and Holocene. **Quaternary International**, v. 449, p. 83–105, 2017a.

REIS, L. S. et al. Environmental and vegetation changes in southeastern Amazonia during the late Pleistocene and Holocene. **Quaternary International**, v. 449, p. 83–105, 25 ago. 2017b.

SIFEDDINE, A. et al. La sédimentation lacustre indicateur de changements des paléoenvironnements au cours des 30 O00 dernières années (Caraias, Amazonie, Brésil). **Académie des Sciences de Paris**, v. 318, p. 1645–1652, 1994.

SIFEDDINE, A. et al. Variations of the Amazonian rainforest environment: A sedimentological record covering 30,000 years. **Palaeogeography, Palaeoclimatology, Palaeoecology**, v. 168, n. 3–4, p. 221–235, 2001.

SMITH, C. B. et al. Holocenic proxies of sedimentary organic matter and the evolution of Lake Arari-Amazon Region. **Catena**, v. 90, p. 26–38, 2012.

URREGO, D. H. et al. Millennial-scale vegetation changes in the tropical Andes using ecological grouping and ordination methods. **Climate of the Past**, v. 12, p. 697–711, 2016.

VAN DER ENT, R. J. et al. Origin and fate of atmospheric moisture over continents. **Water Resources Research**, v. 46, n. 9, p. 1–12, 2010.

VAN DER HAMMEN, T.; HOOGHIEMSTRA, H. Neogene and Quaternary history of vegetation, climate, and plant diversity in Amazonia. **Quaternary Science Reviews**, v. 19, n. 27, p. 725–742, 2000.

WANG, X. et al. Hydroclimate changes across the Amazon lowlands over the past 45,000 years. **Nature**, v. 541, n. 7636, p. 204–207, 2017.

2. MULTI-PROXY EVIDENCE OF PALAEOENVIRONMENTAL AND PALAEOVEGETATION CHANGES IN THE SOUTHEASTERN AMAZONIA

Abstract

The west-eastern Amazonia dipole pattern has been strongly debated in the scientific community, and no such broad consensus on drier climate conditions in eastern Amazonia has been reached so far. We performed a multi-proxy approach on a sediment core from Lake Amendoim which covers the last ~25 ka. During the Last Glacial Maximum (LGM), very low sedimentation rate, siderite precipitation, and formation of no-modern-analog communities indicated less humid and cooler conditions. Lower global temperatures as well as colder Atlantic Sea Surface Temperature (SST) probably caused a decrease in ocean moisture supply to northern South America and led to lower rainfall amount. The Pleistocene-Holocene transition and Early Holocene were characterized by the large occurrence of fire events and siderite precipitation, besides the decrease in detrital input to the lake basin. On the other hand, the presence of forest formation and palms, as well as depleted $\delta^{13}C$ values, suggest seasonal (warmer) conditions in the study site. Higher northern summer insolation probably induced the northward Intertropical Convergence Zone (ITCZ) displacement, leading to periods with reduced precipitation amount over southeastern Amazonia from Early to Middle Holocene. An expansion of ombrophylous forest over the plateau slopes in the Serra Sul de Carajás and a change to predominantly wet climatic conditions was observed from the last 5 ka until the present. Therefore, cool climate events in the northern hemisphere and summer insolation played a key role in climate conditions, which led to relevant environmental and vegetation changes in the southeastern Amazonia.

Keywords: Late Quaternary, Paleoclimatology, Eastern Amazonia, Palynology, Fire events, Lake sediments.

2.1. Introduction

The Amazon basin covers nearly 7,179,100 km^2, including the Amazon River and its tributaries (HUBBELL et al., 2008), and represents around 40% of the world's remaining tropical forest, which is renowned for the exceptional diversity of species that comprises 14,003 plant species, of which 6,727 are trees (CARDOSO et al., 2017). The moisture provided via tree evapotranspiration is essential for the regional water cycle, as the flow of water vapor maintains convection in the Amazon region and increases rainfall events (FISCH; MARENGO; NOBRE, 1998). Those convective activities, in turn, are crucial mechanisms for heating the tropical atmosphere, in terms of intensity and position (ADAMS; PEREIRA DE SOUZA; COSTA, 2009), and therefore, they play a fundamental role in regulating and sustaining the water budget, the valuable biodiversity as well as its ecosystem services and the climate in a local to global scale.

Although the forest acts permanently in climate regulation, several changes in vegetation cover and climatic conditions unrolled in response to millennial to orbital-scales events mainly associated with the Northern Hemisphere cooling (CLARK et al., 2009; VON DEIMLING et al., 2006). Previous studies reported a decrease in temperature between 4.5 to 5°C (COLINVAUX et al., 1996; STUTE et al., 1995; VAN DER HAMMEN; HOOGHIEMSTRA, 2000) in Amazon basin and between 5 and 9°C in the Andes (BUSH et al., 2004; PADUANO et al., 2003) during the Last Glacial Maximum (LGM, 26-19 ka; CLARK et al., 2009), due to increased ice-sheet cover (CLARK; MIX; BARD, 2006), low atmospheric CO_2 levels (PETIT et al., 1999), and decreased Atlantic and Pacific SSTs (LEA; PAK; SPERO, 2000; MOSBLECH et al., 2012).

Lower temperature in tropics, specifically in Amazonia, led to dynamical circulation change associated with reduced convective mass flux (GASTMANS et al., 2017; WANG et al., 2017), the incursion of cool-adapted taxa from high altitudes (*Podocarpus*, *Weinmannia*, *Alnus* and *Hedyosmum*) into Amazonian lowlands (BUSH et al., 2002; 2004; BUSH; SILMAN; URREGO, 2004; COHEN et al., 2014; COLINVAUX et al., 1996; COLINVAUX; DE OLIVEIRA, 2000; REIS et al., 2017) and savanna expansion in the eastern Amazonia (ABSY et al., 1991; HERMANOWSKI et al., 2012), due to cool and dry climate conditions during the LGM. Meanwhile, relatively humid conditions prevailed in the Andes and western and southwestern Amazonia (BAKER et al., 2001; BUSH et al., 2004; COHEN et al., 2014; COLINVAUX et al., 1996; COLINVAUX; DE OLIVEIRA, 2000; FREITAS et al., 2002).

The occurrence of a western and eastern Amazonia dipole pattern has been strongly debated due to significant uncertainties about climate conditions in eastern Amazonia since previous studies were mostly based on pollen data (ABSY et al., 1991; BUSH et al., 2004; COLINVAUX et al., 1996; COLINVAUX; OLIVEIRA, 2000; HERMANOWSKI et al., 2012; SIFEDDINE et al., 1994). Thus, a multi-proxy approach was applied in order to obtain a broader interpretation of the environmental changes and vegetation cover dynamics over the past ~25 ka in the Serra Sul de Carajás, southeastern Amazonia. Moreover, we attempt to answer the following questions: (A) what were the main effects of the climate changes on the sedimentary dynamics of Lake Amendoim? (B) What were the main environmental changes? (C) how did the vegetation respond to the climate changes? (D) what were the key climatic factors or events responsible for those changes?

2.2. Study area

Lake Amendoim is located in Serra Sul de Carajás (Figure 1; 6°25’0” S – 6°20’0” S and 50°25’0” W - 50°17’30” W), southeastern Amazonia. It lies within the Carajás National Forest – a Sustainable Use Reserve with an area of 3,927 km^2 – west of the National Park of Ferruginous Fields in the Pará state. The plateau is around 730 m above mean sea level (a.m.s.l.) and lies within the domain of the ombrophylous forest phytophysiognomies subdivided into dense (montane, submontane) and open (submontane) ombrophylous forest. On a smaller scale, "*Campos rupestres*" (SILVA, 1991) occurs with a predominance of herbaceous-shrub species over ferruginous crust at the top of the plateau (NUNES et al., 2015; SKIRYCZ et al., 2014).

Geology

In the regional context, crystalline complexes composed of high-grade Granite-gneiss rocks and Greenstone belts of Archean ages, besides volcanic-sedimentary supra crust sequences, as well as granites (Archaean to Paleoproterozoic) and mafic-ultramafic (basic-ultrabasic) compose the Mineral Province of Carajás (MACAMBIRA; LAFON, 1995; NOGUEIRA; TRUCKENBROD; PINHEIRO, 1995; RÄMÖ et al., 2002). The Banded-Iron Formations (BIF’s) from Carajás Formation are included in the Grão-Pará Group and represented in the Serra dos Carajás as belonging to the Itacaiúnas Supergroup (OLSZEWSKI et al., 1989). Associated with the BIF’s are the lateritic crusts or “*cangas*” which are the product of the rock alteration and responsible for the formation and perpetuation of lakes in the central depressions of the plateaus.

Figure 1 - (a) Map of South American continent with the mean January (2017) precipitation (mm/day).and major atmospheric systems; (b) Aerial view of the Serra Sul de Carajás; (c) illustrative scheme of catchment basins in the Lake Amendoim (left). (Adapted from Sahoo et al., 2016)

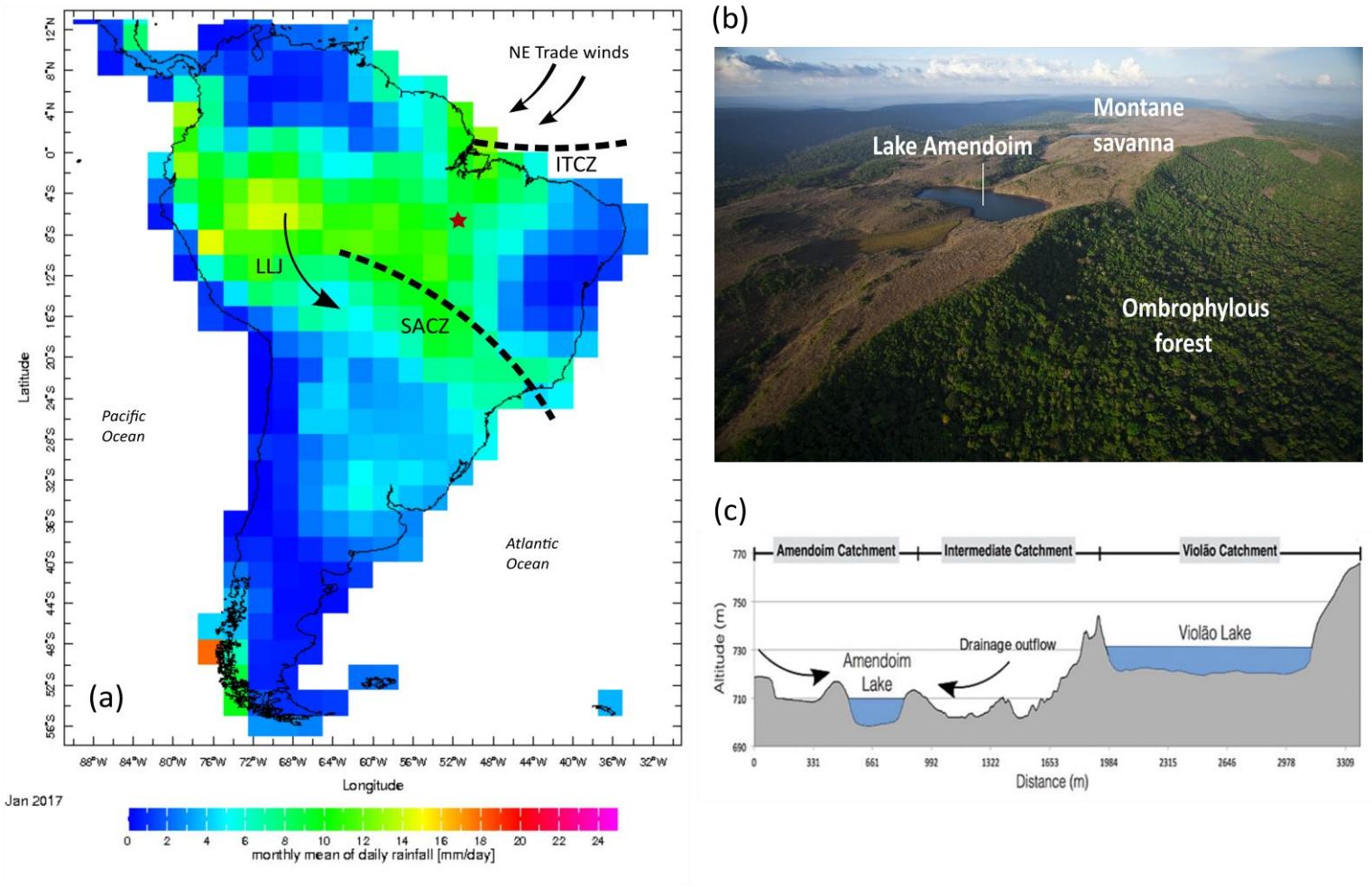

Those lakes constitute depositional environments with variable accommodation space for sediment deposition, being classified as active and inactive lake systems (REIS et al., 2017; SAHOO et al., 2017). The Lake Amendoim is an active lake formed by structural processes and degradation of the lateritic profile (MAURITY; KOTSCHOUBEY, 1995). It has an elongated rectangular shape with orientation in the N-S direction and a surface area of 1.23 km^2, and an altitude around 730 m a.m.s.l. A steep morphology composed of lateritic rocks characterizes the surroundings of the lake, except for the drainage areas (south- and northwest edges) where the borders are smoother. The lake's bottom, in turn, is irregular and muddy (DA SILVA et al., 2018; GUIMARÃES et al., 2017a).

Vegetation

The catchment basin of the lake is predominantly composed of montane savanna, forest patches ("Capão Florestal") and ombrophylous forest (Figure 1). The montane savanna is mainly represented by *Vellozia glauca* Pohl, *Bauhinia pulchella* Benth., *Callisthene microphylla* Warm., *Perama carajensis* J.H. Kirkbr., *Sobralia liliastrum* Salzm. ex Lindl., *Tibouchina edmundoi* Brade, *Ipomoea marabensis* D.F. Austin & Secco and *Norantea guianensis* Aubl., associated with ferruginous crust; forest patches are mainly composed by *Licania* Aubl., *Aparisthmium cordatum* (A. Juss.) Baill., *Myrcia multiflora* (Lam.) DC., *Miconia cuspidata* Naudin, *Matayba guianensis* Aubl., *Anadenanthera peregrina* (L.) Speg., and *Aspidosperma multiflorum* A. DC. and developed over Cambisols on degraded crust (ABSY et al., 2014; NUNES et al., 2015). Forest formations, in turn, are situated on the slopes of the plateau. The dense ombrophylous forests are mainly represented by Fabaceae, Moraceae and Sapotaceae and occur on deeper soils and softer reliefs. On the other hand, the open ombrophylous forests occupy steep slopes, with a predominance of lianas and/or palms. Seasonal deciduous forests occur in the middle of the ombrophylous forest, integrating and merging into different communities. Among the dominating species are *Myracrodruon urundeuva* Allemão, *Maclura tinctoria* (L.) D. Don ex Steud., and *Aspidosperma parvifolium*. Finally, the lake bottom is largely colonized by macrophytes, including *Isoetes cangae* J.B.S. Pereira, Salino & Stützel (GUIMARÃES et al., 2017a; NUNES et al., 2018; PEREIRA et al., 2016).

Climate

The regional climate is tropical monsoon (ALVARES et al., 2013) with two well-defined seasons (LOPES; DE SOUZA; FERREIRA, 2013). The total annual rainfall varies from 1,545 to 1,863 mm during the rainy season (November to May) and from 159 to 321 mm during the dry season (June to October) (SILVA JÚNIOR et al., 2017). The mean temperature is around 27.2° C, with minimum (January) and maximum (September) annual temperatures of 26.6° C and 28.1° C, respectively (TAVARES et al., 2018).

Seasonal and annual rainfall variability within Amazon basin is mainly associated with the South American Summer Monsoon (SASM) (LIEBMANN; MECHOSO, 2011), which is strongly influenced by two important meteorological systems, such as the South Atlantic Convergence Zone (SACZ) and the Intertropical Convergence Zone (ITCZ) (SCHNEIDER; BISCHOFF; HAUG, 2014). The migration of the ITCZ occurs seasonally over South America and the tropical Atlantic in response to changes in summer insolation and the southern SST gradient, reaching maximum latitude to the north (10° N) in August and the maximum latitude south of the equator (2° S) in March (NOBRE et al., 2012; NOBRE; SHUKLA, 1996). The SACZ, in turn, intensifies between November and February by the Low-Level Jets (LLJ) (MARENGO et al., 2004), which transports moisture from the tropical Atlantic Ocean to the western Amazon and the adjacent Andes, flowing along the eastern flank of the Andes. Humidity crosses the Bolivian Amazon and later, reaches the southeast of Brazil, where the SACZ begins to form. Thus, the southward migration of the ITCZ and the intensification of the SACZ contribute to the strengthening of SAMS and for enhanced precipitation in the Amazon basin.

2.3. Materials and Methods

One sedimentary core was sampled from Amendoim Lake in the Serra Sul de Carajás in July 2016, using a Livingstone sampler (LIVINGSTONE, 1955). The geographical position of the core (AM2: 6°23'57.61" S, 50°22'20.03" W; Figure 1) was determined by GPS. The description of sedimentary facies followed the Walker and James (1992) proposal, which includes color, lithology, texture and sedimentary structures descriptions. The sediment classification scheme of the Global Lake Drilling Program was also employed to describe the core (SCHNURRENBERGER; RUSSELL; KELTS, 2003).

Radiocarbon dating and age-depth model

At the base and top of each sedimentary facies, 11 samples of ~2 g each were submitted to radiocarbon dating at the Beta Analytic facilities (Miami, FL, USA). Radiocarbon ages are expressed as ^{14}C year B.P. normalized to a $\delta^{13}C$ of -25‰ VPDB (STUIVER; POLACH, 1977). The age-depth model was developed on Bacon (BLAAUW; CHRISTEN, 2011) using an R software package (R DEVELOPMENT CORE TEAM, 2013) as an interface and using the Intcal13.14c calibration dataset (REIMER et al., 2013), hereafter expressed in ka.

Palynological analysis

One cm^3 of sediment was collected at intervals of 2 cm for pollen and spores grain analysis. Prior to the pollen extractions, a tablet of exotic spores *Lycopodium clavatum* (STOCKMARR, 1971) containing ~20,848 grains/tablet was added to each sample for further calculation of the pollen and spore's concentration (grains/cm^3). All samples were prepared by Paleoflora Ltda (Colombia). At the counting stage, all pollen grains and spores found on the slides were counted due to the low concentration. For the identification of pollen and spores specialized books and manuals were consulted (CARREIRA; BARTH, 2003; COLINVAUX; OLIVEIRA; PATIÑO, 1999; ROUBIK; MORENO, 1991), in addition to the reference collections of the ICB/MPEG, ITV/GABA*N*-VALE, and C-14 Laboratory/CENA. Tilia and Tilia Graph software were used to plot pollen diagrams, as percentages of total pollen and spores counted, and pollen and spore concentration per cm^3 of sediment. The ecological groups were divided into montane savanna, forest formation (including forest patches and ombrophylous forest), cool-adapted taxa, palms, macrophytes, pteridophytes and algae (ABSY et al., 2014; GUIMARÃES et al., 2014; 2017a; NUNES et al., 2015). The pollen diagrams were statistically subdivided into zones of pollen assemblages (pollen zones) based on square-root transformations of the percentage data and stratigraphically constrained cluster analysis by the method of the total sum of squares using CONISS (GRIMM, 1987).

Charcoal fragments analysis

For macro-charcoal analysis, a total of 60 subsamples (1 cm^3) were collected at intervals of 2 cm. Samples were processed following the sieving method (STEVENSON; HABERLE, 2005). Each sub-sample was submerged in deflocculant (5% solution of Sodium Pyrophosphate) for 24 h and then carefully washed through sieves with a fraction of 250 μm, for the removal of finer organic and inorganic materials. The counts of the fragments

retained in the sieves were made using a binocular microscope (magnification x10-15). The resulting dataset was converted to charcoal concentration (number of charcoal particles cm^{-3}). For micro-charcoal analysis, only black, opaque and angular fragments (10-100 μm) were counted on the same pollen slides (SADORI; GIARDINI, 2007).

Isotopic and elemental analyses of C and N

Carbon ($\delta^{13}C$) and Nitrogen ($\delta^{15}N$) isotopes, besides C/N ratio, were analyzed in subsamples of sediments extracted at intervals of 4 cm along with the sedimentary facies. The sediment samples were analyzed at the Stable Isotope Laboratory of CENA/USP, in which total organic carbon (TOC), total nitrogen (TN) and carbon and nitrogen isotopes were analyzed by ANCA SL 2020 mass spectrometer. TOC and TN values were expressed as percent dry weight and used to calculate the C/N ratio (weight/weight). The $\delta^{13}C$ and $\delta^{15}N$ values were calculated in relation to international standards VPDB (Vienna Pee Dee Belemnite) and atmospheric N_2, respectively, with 0.2‰ of precision and expressed in per mil (‰). For the interpretations regarding sources of organic matter, previous works were used (CORDEIRO et al., 2008; 2011; GUIMARÃES et al., 2017a; MARTINELLI et al., 1994, 2009; MEYERS, 1994; 1997; MOREIRA et al., 2013; SAHOO et al., 2016).

Multi-element geochemistry analysis

For geochemical analysis about 15-20 g of samples were collected every 5 cm. Subsequently, samples were dried (50°C), disaggregated and then analyzed by inductively coupled plasma optical emission spectrometry (ICP-OES, for major and minor elements) and by inductively coupled plasma mass spectrometry (ICP-MS, for trace elements including rare earth elements) in the Acme Laboratory Analytical (Vancouver, Canada) after tetraborate fusion followed by dilute nitric acid digestion (GRIEPINK; TOLG, 1989; VAN LOON et al., 1989). The precision and accuracy were verified through parallel analyzes of reference standards. The analytical error for the major and minor elements is approximately ± 2%, whereas for the trace elements is around ± 10%. Biogenic Si (BSi) was determined by subtracting biogenic Si from total Si, where BSi = SiO2 - 2.8 × Al_2O_3 according to Robinson (1994). The weathering effect was calculated using the chemical index of alteration (CIA = [Al_2O_3 / (Al_2O_3 + CaO* + Na_2O + K_2O) × 100). CIA values below 60 represent low weathering, between 60 and 80 moderate weathering and higher than 85 extreme chemical weathering (NESBITT et al., 1996).

S*tatistical analysis*

Elemental associations (major, minor and REEs) in lake sediments were determined using Spearman correlation. Principal component analysis (PCA) was used to determine relationships among variables and to simplify the data interpretation based on major controlling factors. This was performed on the open-source software Past (HAMMER et al., 2001). All variables (major and trace elements concentration) were normalized and standardized prior to PCA analysis in order to eliminate the influence of different measurement units and minimize the variances. A detailed description of the standardization method is found in Sahoo et al. (2015).

2.4. Results and Discussions

2.4.1. Sedimentary facies and age-depth model

The AM2 core (150 cm) covers the last ~25 ka based on age-depth modeling using ^{14}C ages. The radiocarbon dates and the sedimentary facies descriptions are shown in Tables 1-2 and Figure 2, respectively. An age inversion is observed between ~25 and 21,5 ka (140-150 cm), probably caused by the diagenetic formation of siderite or iron carbonate ($FeCO_3$) (GUIMARÃES et al., 2016). Thus, the last ^{14}C dating was not considered in the age model.

Based on the age model, the sedimentation rates range from 0.02 to 0.16 mm year^{-1}. During the LGM, the sedimentation rates vary between 0.03 and 0.10, with maximum values from ~25 to 24,8 ka (0.08-0.1 mm year^{-1}), and minimum values between 24,8 and 19,4 ka (0.03-0.09 mm year^{-1}). This period is followed by an increase in sedimentation rates (0.09-0.12 mm year^{-1}), extending from LGM to Late Glacial (19,4-16,5 ka). Between 16,5 and 12,9 ka, sedimentation rates reach values of 0.02-0.03 mm year^{-1} and subsequently increase to 0.05-0.16 mm year^{-1} between 12,9 and 10,2 ka. From 10,2 ka, there is a gradual decrease in sedimentation rates with minimum values (<0.03 mm year^{-1}) during the Middle to Late Holocene.

Considering the lithology and sedimentary facies, during the LGM, between ~25 and 24,5 ka, the core AM2 is composed of laminated mud (Ml) deposited gradually by suspension (GUIMARÃES et al., 2016). From LGM to Late Glacial (24,5 to 17,4 ka), the layer is composed by siderite mud (Ms). During diagenetic processes of siderite formation, Fe is rearranged within siliciclastic horizons, which causes the formation of small nodules (individual or agglomerates) of $FeCO_3$ and changes the primary characteristics of the

sedimentary deposit (BAILEY et al., 1994). From Pleistocene-Holocene transition to the Early Holocene (17,4 to 10.9 ka), the deposit is composed of laminated mud interbedded with peat (M/P), indicating alternate between autochthonous and allochthonous organic matter input. This deposit is overlaid by herbaceous peat, and points to less contribution of allochthonous material to the lake basin and to a predominance of autochthonous organic matter throughout the Early Holocene (~10,9 to 8.5 ka). From Mid- to Late Holocene (last 8.5 ka), the layer consists of laminated mud (39-22 cm; 8.5-4.5 ka) superimposed by mud intercalated with herbaceous peat (21-0 cm: last 4.5 ka).

Table 1 - ^{14}C dating (AMS) and calibrated ages of the sediment samples from core AM2, collected in Lake Amendoim, Serra Sul de Carajás

Code	Sample ID	Pre-treatment material	$^{13}C/^{12}C$ (‰)	^{14}C age (yr AP)	Cal. age, 2σ range (cal yr AP)
BETA445926	AM2 -10-11	(organic sediment): acid washes	-26.9	940 +/- 30	924-792
BETA443169	AM2 -20-21	(organic sediment): acid washes	-26.4	3780 +/- 30	4244-4082
BETA445927	AM2 -39-40	(organic sediment): acid washes	-27.1	7660 +/- 30	8522-8400
BETA443173	AM2 -50-51	(organic sediment): acid washes	-26.5	8880 +/- 40	10179-9886
BETA445928	AM2 -60-61	(organic sediment): acid washes	-25.1	9540 +/- 30	11076-10943
BETA443172	AM2 -70-71	(organic sediment): acid washes	-24.2	10050 +/- 40	11765-11386
BETA445929	AM2 -85-86	(organic sediment): acid washes	-20.4	13560 +/- 40	16538-16163
BETA445930	AM2 -111-112	(organic sediment): acid washes	-18.8	15480 +/- 40	18847-18621
BETA443170	AM2 -120-121	(organic sediment): acid washes	-19.4	16820 +/- 60	20494-20075
BETA445931	AM2 -139-140	(organic sediment): acid washes	-20.8	20220 +/- 60	24498-24073
BETA443171	AM2 -147-148	(organic sediment): acid washes	-20.3	17580 +/- 60	21491-20994

2.4.2. Macro-charcoal fragments analysis

The charcoal concentration (Figure 4) varies from 0 to 330 particles/cm^3. During the LGM (~25-19 ka), rare charcoal fragments (0-1 particle/cm^3) were found. A slight increase (45 particles/cm^3) is observed at the Late Glacial period between 17,8 and 16,7 ka. The highest charcoal concentrations occur during the Early Holocene from 10,9 to 8 ka (62-330 particles/cm^3), which suggests the high occurrence of fire events. From 8.3 ka, the charcoal concentration considerably decreases and over the past 6 ka, it ranges from 0 to 27 particles/cm^3.

2.4.3. Isotopic analysis ($\delta^{15}N$ e $\delta^{13}C$) and C/N ratio

The $\delta^{15}N$ and $\delta^{13}C$ values (Table 3; Figures 3, 4b) range from 0.33‰ to 6.62‰ and from -27.14‰ to -14.53‰, respectively. The C/N ratio varies between 11 and 43, which indicates terrestrial C_3 plants (MARTINELLI et al., 1994, $\delta^{13}C$ from -21‰ to 32‰, C/N ratio >12, DEINES, 1980; 1998; MEYERS, 1994; MEYERS; EADIE, 1993; PESSENDA et al., 1998a) and/or a mixture with macrophytes, e.g. *Isoëtes sp.* ($\delta^{13}C$ and $\delta^{15}N$ values of -25‰ and 4.7‰, respectively; SAHOO et al., 2016) and freshwater algae ($\delta^{13}C$ values between -25‰ and -30‰, C/N ratio from 4 to 10; MEYERS, 1994) as predominant sources of sedimentary organic matter.

Figure 2 - Lithological profile of the core AM2 with the age model as a function of the depth calculated from the ^{14}C dating in R program

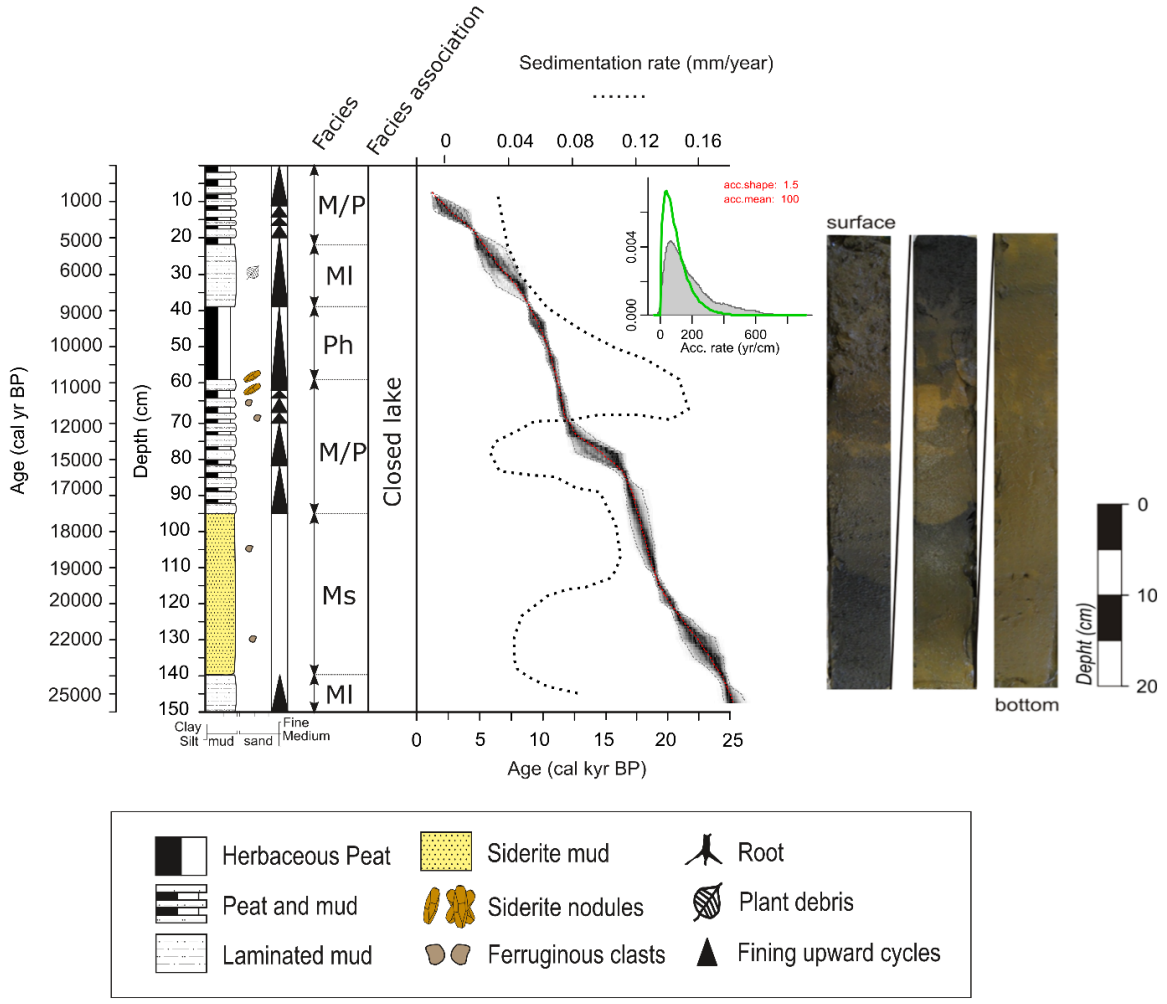

Table 2 - Summary of facies descriptions and sedimentary processes in the core AM2

Facies	Description	Formation/Process	Sedimentation rate (mm yr^{-1})
Herbaceous peat (Ph)	Olive gray (5Y 4/2) peat, massive, with herbaceous roots fragments in growth position from Isoëtes.	Low dendritic input. Stagnant and reduced water conditions with an herbaceous plant as the main source of the deposit.	0.05-0.1
Mud and peat (M/P)	Dark grayish brown (2.5Y 4/1) to black (5Y 2.5/1) mud. Some Yellow (5Y 7/8) to olive-yellow (5Y 6/8) spots are also present, besides clasts.	Equal periods of mud inflow from suspension and input of autochthonous organic matter under reduced conditions, which favored a higher degree of organic matter preservation.	0.02-0.1
Laminated mud (Ml)	Dark gray (5Y 4/1) to olive-gray (5R 5/2) mud.	Low energy flows with mud input from suspension into the lake basin and high preservation of organic matter.	0.03-0.4
Siderite mud (Ms)	Olive yellow (5Y 6/6) to Olive (5Y 5/4) mud, massive, oxidized, with yellow (5Y 7/8) to olive-yellow (5Y 6/8) spots. Besides, nodules of siderite and clasts are present. Mud is also a present forming incipient matrix.	Siderite is an early diagenetic mineral, forming in pore waters close to the sediment-water boundary layer. Siderite precipitation usually occurs under reducing conditions in slightly to strongly reducing methanogenic zones because of low sulfate and high organic carbon content (LEMOS et al., 2013).	0.04-0.2

Enriched $\delta^{13}C$ values recorded between ~25 and 16,5 ka (150-86 cm, Figure 4) are mainly associated with siderite mud facies. Siderite precipitation is strongly related to methanogenesis occurrence which causes the formation of ^{13}C-enriched bicarbonates, leading to heavier $\delta^{13}C$ values (BERNER, 1980; LENG et al., 2013; LIM et al., 2004; TAKIGIKU et al., 1991). In addition, diagenetic processes may also cause an increase in the C/N ratio as a result of the progressive degradation of OM, which selectively destroys the nitrogen compounds (LENG et al., 2006). Higher C/N values (up to 43) are observed from 21,5 to 17,7 ka (140-98 cm), and corresponds to the siderite layer.

Regarding $\delta^{15}N$ values, processes such as denitrification and volatilization of ammonia also occur under anoxic and alkaline conditions (similar conditions to siderite formation), respectively, which favor the reaction of ^{14}N molecules and lead to an increase in ^{15}N molecules (LENG et al., 2006). Thus, the highest $\delta^{15}N$ values (> 6) recorded in the siderite layer during the LGM (140-98 cm) points to significant fractionation effects caused by changes in redox conditions. The decrease in C/N values (<15) from Mid- to Late Holocene (last 7.6 ka; 34-2 cm) suggests lower input of terrestrial plants OM and higher contribution of organic matter from algae and/or aquatic plants to the sedimentary deposit.

Table 3 - Isotopic ($\delta^{13}C$ e $\delta^{15}N$, per mil ‰) and elemental (TOC, TN, %) composition and C/N ratio from core AM2

Depth (cm)	$\delta^{13}C$ (‰)	$\delta^{15}N$ (‰)	TOC (%)	TN (%)	C/N
2 - 4	-27.11	1.93	12.22	0.9	13.58
8-10	-26.80	2.71	10.17	0.71	14.32
14-16	-26.63	2.98	9.18	0.5	18.36
20-22	-26.54	3.88	8.02	0.7	11.46
26-28	-26.61	3.37	9.65	0.52	18.56
32-34	-26.98	1.18	11.65	0.93	12.53
38-40	-27.13	0.76	21.71	1.03	21.08
40-42	-27.14	1.15	20.74	1.01	20.53
44-46	-26.36	0.33	21.71	1.13	19.21
50-52	-26.18	1.26	17.86	0.93	19.20
56-58	-25.81	2.15	12.56	0.59	21.29
62-64	-25.05	3.71	7.09	0.37	19.16
68-70	-23.60	5.39	2.67	0.16	16.69
74-76	-24.25	5.36	3.58	0.2	17.90
80-82	-24.13	4.91	6.25	0.31	20.16
86-88	-20.52	4.39	5.27	0.27	19.52
92-94	-19.36	4.49	4.7	0.23	20.43
98-100	-15.80	6.10	3.56	0.11	32.36
104-106	-15.33	6.22	3.38	0.1	33.80
110-115	-14.96	6.32	3.88	0.09	43.11
124-126	-16.74	6.62	2.73	0.08	34.13
130-132	-15.77	6.36	2.96	0.09	32.89
136-138	-17.19	6.51	2.09	0.09	23.22
142-144	-19.75	6.10	1.41	0.08	17.63
148-150	-22.47	4.07	4.64	0.24	19.33

Figure 3 - Binary plot of (a) $\delta^{13}C$ (‰) vs. $\delta^{15}N$ (‰) of the sedimentary organic matter from core AM2; (b) C/N ratio vs. $\delta^{13}C$ (‰) (Fields based on DEINES, 1980; HAMILTON; LEWIS, 1992; THORNTON; MCMANUS, 1994; MEYERS, 1997; TROXLER; RICHARDS, 2000); Sedimentary facies: Mud and peat – M/P, Laminated mud – Ml, Herbaceous peat – Ph, Siderite mud – Ms)

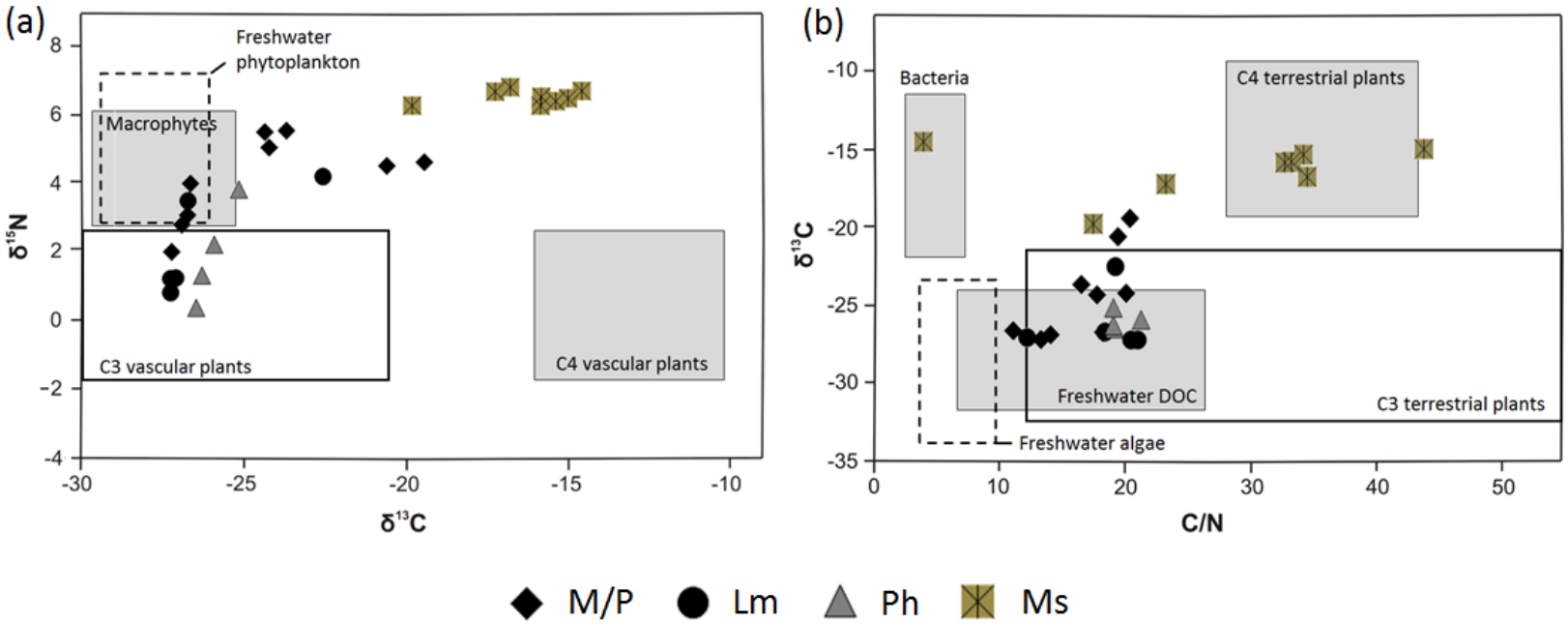

2.4.4. Pollen and micro-charcoal fragments analysis

Six pollen zones were statically recognized according to the identification of 68 morphotypes (Figure 4).

Zone AM2-1 (~25-21 ka; facies Ml-Ms)

During this period the highest amounts of charcoal (~3,500-1,000,000 particles cm^{-3}) are recorded, suggesting the high occurrence of fire events. The pollen diagram is characterized by high abundance of montane savanna (max. 100%, 1,630,000 grains cm^{-3} and 9 spp) and macrophytes (max. 89%, ~1,700,000 grains/spores cm^{-3} and 3 spp) followed by forest formation (max. 14%, 31,272 grains cm^{-3} and 6 spp). Montane savanna is mainly represented by Poaceae (46-56%), *Borreria* (10-29%) followed by Asteraceae (6-16%), *Serjania*, *Amaranthus*, *Vernonia*, *Hyptis*, *Byrsonima* and Fabaceae (<7%). Macrophytes are composed of *Isoëtes* (90-99%), Cyperaceae (0-7%) and *Phyllanthus* (<2%). Anacardiaceae (0-7%), *Alchornea*, *Moraceae*, *Pouteria*, Melastomataceae and Burseraceae (<4%) represent forest formation. Cool-adapted taxa (max. 2%, 20,848 grains cm^{-3} and 1 spp) and palms (max. 1%, 718 grains cm^{-3} and 1 spp) are also present, however in low concentration as well as pteridophytes (max. 8%, ~146,000 spores cm^{-3} and 3 spp) and algae (max. 1%, ~21,000 colonies cm^{-3} and 1 spp).

Zone AM2-2 (21-18 ka; facies Ms)

This zone presents lower charcoal concentration (3,000-19,000 particles cm^{-3}) compared to the previous period. The pollen diagram is characterized by high abundance of montane savanna (max. 89%, 11,245 grains cm^{-3} and 13 spp) and macrophytes (max. 93%, ~98,560 grains/spores cm^{-3} and 2 spp). Taxa from forest formation (max. 10%, ~1,130 grains cm^{-3} and 13 spp) are represented by *Alchornea*, Moraceae, Anacardiaceae, *Zanthoxylum*, *Pouteria*, *Schefflera*, *Paullinia*, *Sapium*, *Dioclea*, *Acalypha*, Melastomataceae, Myrtaceae and Rutaceae (<5%); cool-adapted taxa (max. 3%, ~327 grains cm^{-3} and 4 spp) are represented by *Alnus*, *Hedyosmum* and *Podocarpus* (<3%); and palms (max. 1%, 69 grains cm^{-3} and 1 spp) are also present, but in low concentrations. Pteridophytes (max. 5%, ~700 spores cm^{-3} and 1 spp.), algae (max. 5%, ~700 colonies cm^{-3} and 1 spp) occur with low frequencies. This zone presents a greater number of species within ecological groups but in considerably lower concentrations compared to the previous zone.

Figure 4 - Pollen diagram. (a) Percentage (%) of pollen and spore grains (b) Percentage of most abundant ecological groups together with elemental and isotopic data, and charcoal concentration from core AM2.

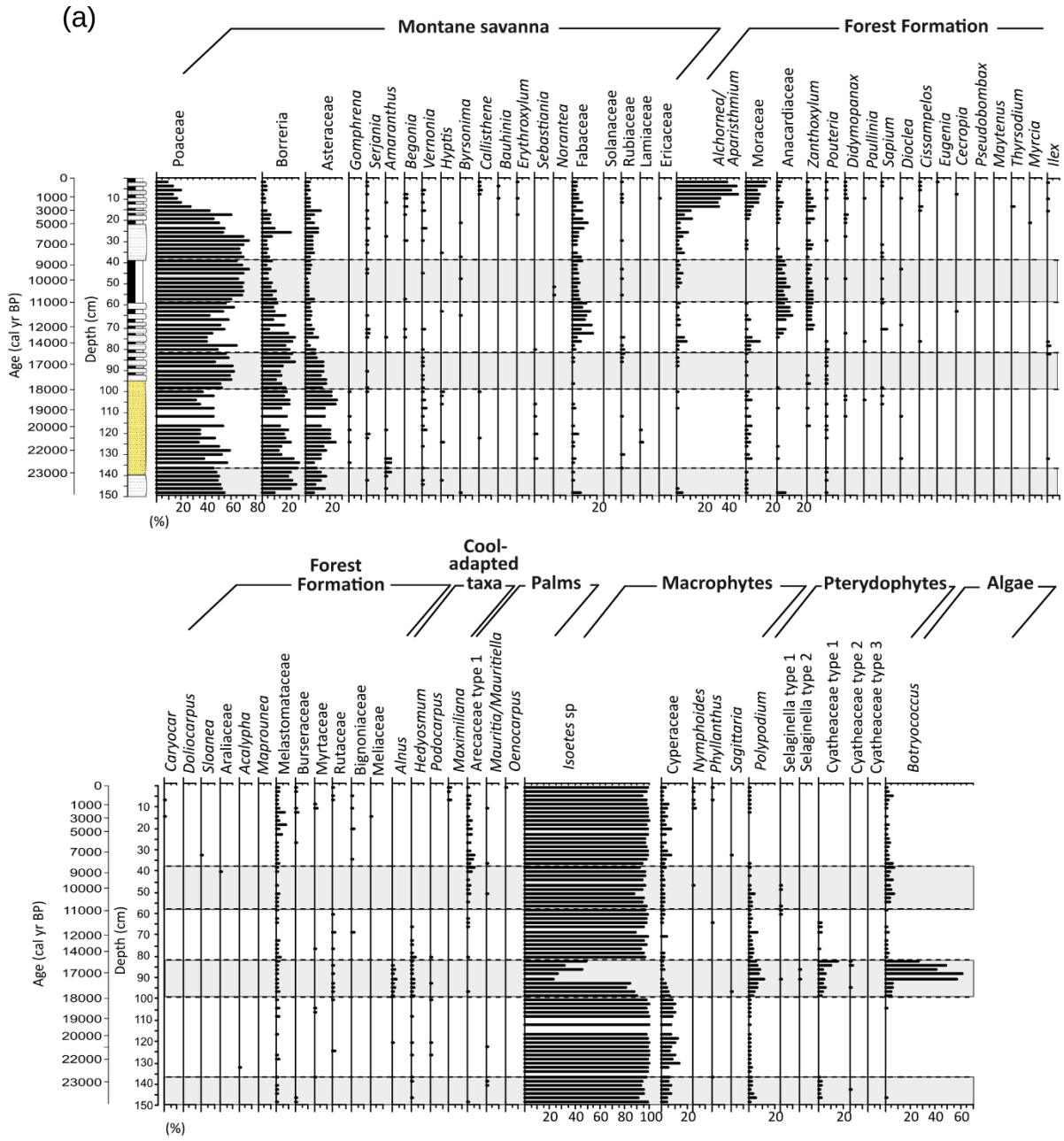

(b)

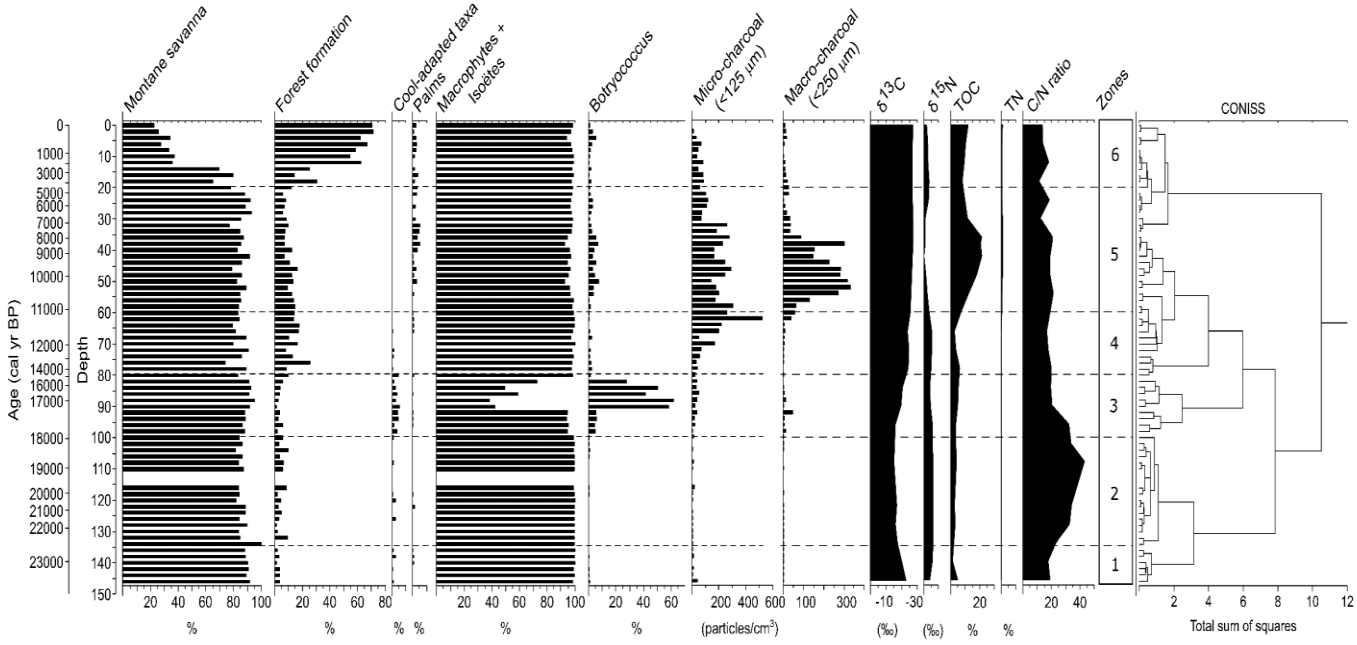

Zone AM2-4 (15-11 ka; facies M/P)

Higher amounts of charcoal (22,000-523,000 particles cm^{-3}) are recorded between ~11,2 and 11 ka. The montane savanna (max. 90%, ~215,000 grains cm^{-3} and 12 spp) is mainly composed by Poaceae (40-64%), *Borreria* (5-27%), Fabaceae (0-15%), Asteraceae (2-10%), *Serjania*, *Amaranthus*, *Begonia*, *Vernonia*, *Hyptis*, *Byrsonima* and *Sebastiania* (<2%), while macrophytes (max. 82%, ~817,500 grains/spores cm^{-3} and 3 spp) are represented by *Isoëtes* (88-98%), Cyperaceae (0-3%) and *Phyllanthus* (<1%). This zone is characterized by the increase in percentage values and richness of forest formation group (max. 24%, ~35,440 grains cm^{-3} and 15 spp), composed by Anacardiaceae (0-12%), Moraceae (0-11%), *Alchornea* (0-7%), *Zanthoxylum* (0-4%), *Sapium* (0-3%), *Pouteria*, *Schefflera*, *Paullinia*, *Dioclea*, *Cissampelos*, *Cecropia*, Melastomataceae, Myrtaceae, Rutaceae and Bignoniaceae (<2%). However, there is a decrease in the occurrence of cool-adapted taxa (max. 5%, 5,380 grains cm^{-3} and 2 spp), palms (max. <1%, ~2,084 grains cm^{-3} and 1 spp), pterydophytes (max. 7%, ~14,600 spores cm^{-3} and 3 spp) and algae (max. 3%, ~7,445 colonies cm^{-3} and 2 spp) compared to the previous zone.

Zone AM2-5 (11-8 ka; facies Ph)

Large amounts of charcoal (144,600-291,000 particles cm^{-3}) are also found in this layer. The pollen diagram presents characteristics similar to others zone in which montane savanna (max. 91%, ~76,000 grains cm^{-3} and 10 spp) and macrophytes (max. 73%, ~185,700 grains/spores cm^{-3} and 3 spp) are the dominant groups. This layer is highlighted by the decrease in the percentage of forest formation group (max. 16%, ~15,830 grains cm^{-3} and 9 spp.) composed by Anacardiaceae (3-10%), *Zanthoxylum* (0-4%), *Alchornea* (0-4%), *Pouteria*, *Schefflera*, *Sapium*, *Dioclea*, Araliaceae and Melastomataceae (<2%); and absence of cool-adapted taxa. Palms (max. 5%, 2,207 grains cm^{-3} and 2 spp) and algae (max. 7%, 7,848 colonies cm^{-3} and 1 spp) presented a small increase in concentration and percentage values in relation to the previous layer. Pteridophytes (max. 4%, ~2,919 spores cm^{-3} and 2 spp), on the other hand, occurred with low frequency.

Zone AM2-6 (<8 ka; facies M/P)

During this period a decrease in charcoal concentration (2,500-280,000 particles cm^{-3}) in comparison to the previous layer is observed. The uppermost pollen zone presents high frequencies of the main studied ecological groups. The spore concentration is higher than the previous zones. Thus, Poaceae (8-74%), *Borreria* (2-23%), Asteraceae (0-23%) and Fabaceae (0-5%) are the main taxa of montane savanna (max. 92%, ~93,800 grains cm^{-3} and 15 spp.). As in other zones, macrophytes (max. 97%, ~4,000,000 grains/spores cm^{-3} and 5 spp) remained dominant. Palms (max. 5%, ~5,200 grains cm^{-3} and 4 spp.) and forest formation show the highest values of percentage and species richness (max.71%, 47,950 grains cm^{-3} and 22 spp.) during this period. Among the main forest taxa are *Alchornea* (0-48%), Moraceae (0-17%), *Zanthoxylum* (0-6%) and Anacardiaceae (0-4%). Algae (max. 5%, 59,565 colonies cm^{-3} and 1 spp.) were also observed, while ferns (max. <1%, ~3,680 spores cm^{-3} and 1 spp.) occur in low frequency in this zone.

2.4.5. Multi-element geochemical data

The concentrations of major, minor and rare earth elements (Table 4) were evaluated using principal components analysis (Figure 5). Ratios between elements are also presented as indicators of paleoproductivity, authigenic precipitation, and detrital input to the lake, intensity of chemical weathering, surface runoff and changes in the redox condition and lake water level (Table 5). Two principal components (PC) with eigenvalues >1 were extracted

from core AM2, which explained 74.9% of the total variance. Six geochemical zones were defined in accordance with the pollen zones described above.

Group 1 (145-130 cm) presents high positive loading on PC1 and low loading on PC2 and shows a strong relationship with major (Al_2O_3, SiO_2, TiO_2, K_2O, and MgO) and trace elements (V, Ga, Hf, Zr, and Th), indicating the terrigenous source. Major and trace elements are main terrestrial components – abundant in the Earth's crust – used as provenance indicator since their amount in lakes and pelagic environments are mainly controlled by parent soils or rocks composition as well as by the intensity of weathering/erosion on catchment basin (CHEN et al., 2013). The Al_2O_3/TiO_2 ratio ranged from 10.3 to 13.3 wt% and suggests that mafic and felsic rocks are important detrital sources (SAHOO et al., 2015). Higher Al, Ti, Hf, Zr, and REEs contents are observed in zone AM2-1 (Figure 6), similar distribution pattern and moderate to strong positive correlations between these elements (r = > 0.64) reinforce their detrital and terrigenous origin, mainly associated with Al-enriched lateritic crusts, including basalts and soils (SAHOO et al., 2019).

The SiO_2 content varied between 9.7 wt% (AM2-6) and 20.8 wt% (AM2-1). The temporal distribution of Si shows a marked enrichment during periods with high detrital input into the lake basin and a similar distribution pattern of major and trace elements (Figure A.1). The strong positive correlation between SiO_2 and Al_2O_3 (r = 0.71) and a weak correlation between Si/Al and calculated biogenic Si, indicate that Si is mainly derived from detrital silicate minerals, and to a lesser extent from organic compounds such as siliceous algae.

Table 4 - Summary of the concentration of the inorganic component (major, trace, REEs) in sediments of core AM2, from Lake Amendoim

	Rare earth elements				**Major and minor oxides**		
	Concentration (mg/Kg)				Concentration (%)		
	Min[1]	Max[2]	Avg[3]		Min	Max	Avg
La	20.90	37.30	29.49	**Al_2O_3**	6.95	12.57	9.90
Ce	41.90	77.00	60.63	**Fe_2O_3**	42.26	56.63	52.21
Pr	4.21	7.42	5.80	**K_2O**	0.03	0.14	0.10
Nd	14.50	26.00	19.92	**MgO**	0.02	0.09	0.06
Sm	2.51	4.45	3.68	**MnO**	<0.01	0.02	<0.01
Eu	0.58	1.00	0.77	**CaO**	<0.01	0.02	0.02
Gd	1.89	3.60	3.01	**Na_2O**	<0.01	0.02	<0.01
Dy	1.86	3.82	2.86	**P_2O_5**	0.50	0.83	0.65
Tb	0.34	0.63	0.49	**SiO_2**	9.75	20.08	16.70
Er	1.02	2.31	1.73	**TiO_2**	0.52	1.20	0.89
Ho	0.37	0.80	0.58				
Tm	0.16	0.36	0.25				
Yb	1.03	2.28	1.74				
Lu	0.17	0.37	0.26				

	Trace elements						
	Concentration (mg/Kg)						
	Min	Max	Avg		Min	Max	Avg
Ba	10.00	50.00	24.12	**Cu**	19.90	51.90	26.76
Sr	1.00	2.60	1.87	**Zn**	26.00	78.00	47.71
Rb	0.70	5.20	3.25	**As**	2.00	4.10	2.66
Pb	14.00	21.40	16.71	**Se**	2.30	7.90	3.89
Th	5.90	12.10	9.28	**Mo**	2.03	4.77	2.84
U	0.92	1.49	1.18	**Hg**	0.03	0.29	0.09
Zr	5.40	30.60	23.33	**V**	58.00	98.00	76.47
Hf	0.15	0.74	0.55	**Cr**	35.00	53.00	44.12
Nb	0.76	2.33	1.45	**Ga**	12.70	20.80	16.46
Sn	1.50	2.40	1.95	**Co**	0.70	3.00	1.98
Y	5.10	8.32	6.83	**Ni**	5.40	14.20	7.77

[1] Min: minimum; [2] Max: maximum; [3] Avg: average

Figure 5 - Principal Component Analysis of geochemical components (major and trace elements) of the core AM2

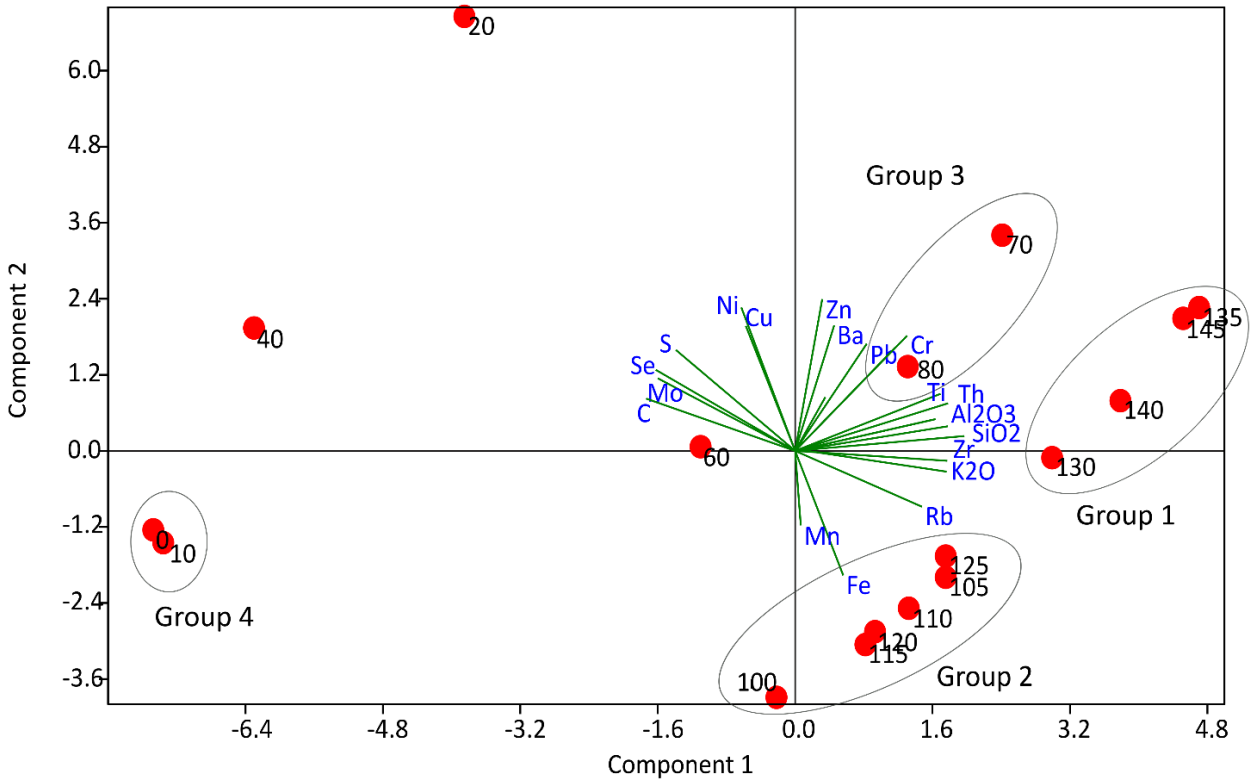

Group 2 (125-100 cm) is most related to Fe, Fe_2O_3 and Mn with weak loading on PC1 and high negative loading on PC2. The concentration of Fe ranges from 26.4 wt% (AM2-6) to 35.8 wt% (AM2-4) and shows a distinct distribution compared to detrital fraction elements; additionally, its association with siderite mud facies reinforces the occurrence of diagenetic processes in this interval. Positive values of Ce anomaly along the entire profile indicate oxidant conditions in sediments. Therefore, these values are probably reflecting the redox conditions prior to the diagenetic processes which usually occur in a depleted-oxygen environment (GUIMARÃES et al., 2016). The high association of Group 3 (70-80 cm) with trace elements (Zn, Ba, Pb, Y, Cr, and U) observed in the zone AM2-4 (Laminated mud facies) indicate that they are mainly linked to the detrital phase since they are commonly found in the earth's crust, specifically igneous and metamorphic rocks. High Zn concentration (53-58 ppm) may also indicate erosion of catchment laterites since most of it is distributed as a minor constituent of Fe-enriched rocks (ADRIANO, 1986). Low Al_2O_3/Fe_2O_3 ratios (< 0.2)

and lower Al_2O_3 content (6.9 – 12.5 wt%) compared to Fe_2O_3 content (42.2 – 56.6 wt%) in sediments confirm the contribution of Fe-enriched lateritic crust and hence an important source of sediments for lake basin.

Trace elements such as Se, Hg, Mo are clustered with C (Total Carbon) in the zone AM2-5 (60-40 cm), while Nb, As, Cu and Ni, are related to S in the zone AM2-6 (40-20 cm). Since As and Mo are redox-sensitive elements and some trace elements (Cu, Ni) have high affinities for organic matter (ADRIANO, 1986), therefore their association with C and S suggests that these elements are mainly controlled by organic matter content and by the redox environment conditions (GUIMARÃES et al., 2016; SAHOO et al., 2019). An increase in Mo/Al and Fe/Al ratios between 70 and 40 cm indicate a change in the redox condition of the lake and support the precipitation of siderite nodules between 70 and 60 cm, respectively. Group 4 in turn composed by the upper part of the core (20-0 cm) presents high and weak negative loading on PC1 and PC2, respectively. The opposite distribution of these samples compared to major and trace elements pattern indicates that this layer is not associated with terrigenous components but rather with the organic fraction (Herbaceous peat). High Mo/Al ratios indicate slightly reducing conditions – which favors the preservation of organic matter – and low Hf, Zr and REEs among other elements from detrital fraction support this statement. The CIA index ranges from 98 to 99 which is similar to catchment laterites and soils, indicates a high degree of chemical weathering in the lake catchment basin (SAHOO et al., 2019).

Thus, the geochemical data shows that lake sediments in Serra Sul de Carajás are associated with parent rocks and local geology surrounding the catchment basin of the lake (GUIMARÃES et al., 2016; SAHOO et al., 2015; 2016a), however, they are mainly derived from weathered crust, including Fe-enriched laterites and adjacent soils (SAHOO et al., 2019).

Table 5 - Geochemical proxies, elemental ratios, and concentration along with the profile of core AM2, from Lake Amendoim

		Paleoproductivity proxy	**Indicator of biogenic silica**	**Indicators of detrital input to the lake**			**Provenance**	**Indicators of chemical weathering**		
Depth (cm)	Zones	Ba/Al	Si/Ti	Al (%)	Ti (%)	Ca/Ti	Al_2O_3/TiO_2	CIA[1]	Ti/K	Th/U
0-10	AM2-6	3.23	120.37	3.10	0.08	0.12	12.44	99.30	8.10	5.73
10-20		3.36	151.08	2.98	0.07	0.14	13.37	99.29	7.40	5.48
20-40		13.59	208.94	3.68	0.09	0.11	12.24	98.83	4.70	5.22
40-60	AM2-5	6.37	133.79	3.14	0.09	0.11	11.13	98.83	4.35	5.36
60-70	AM2-4	4.96	125.94	4.03	0.10	0.10	11.85	98.94	3.37	5.56
70-80		11.52	150.75	4.34	0.11	0.09	12.45	98.84	3.53	5.41
80-100	AM2-3	10.39	196.77	3.85	0.09	0.11	11.46	98.50	2.33	5.49
100-105	AM2-2	5.87	196.51	3.41	0.09	0.12	11.00	98.49	2.87	5.61
105-110		5.25	193.87	3.81	0.09	0.11	10.88	98.53	2.33	5.41
110-115		5.46	195.71	3.66	0.09	0.11	10.98	98.45	2.28	5.64
115-120		5.62	197.19	3.56	0.09	0.11	10.93	98.45	2.97	5.70
120-125		5.88	195.38	3.40	0.09	0.11	10.84	98.52	3.03	4.80
125-130		5.83	191.75	3.43	0.10	0.10	10.53	98.52	3.23	5.19
130-135		5.68	192.35	3.52	0.10	0.10	10.38	98.55	5.10	5.02
135-140	AM2-1	4.95	182.55	4.04	0.11	0.09	10.36	98.62	3.67	4.98
140-145		5.26	168.93	3.80	0.11	0.09	10.33	98.69	5.60	5.14
145-150		7.39	160.17	4.06	0.12	0.08	10.48	98.67	6.05	5.23

		Paleoredox proxies		Indicator for authigenic precipitation			Terrestrial runoff proxies			Proxy for lake level change	
Depth (cm)	Zones	Mo/Al	Ce anomaly[2]	U/Th	V/Cr	Fe/Al	ΣREE[3]	Hf (ppm)	Zr (ppm)	P (ppm)	Fe (%)
0-10	AM2-6	1.32	3.34	0.18	1.20	10.55	101.85	0.15	5.40	2760	32.70
10-20		1.60	3.29	0.15	1.28	11.74	111.91	0.26	11.90	2600	35.00
20-40		1.11	3.24	0.14	1.19	7.17	141.10	0.56	19.30	2090	26.40
40-60	AM2-5	1.28	3.36	0.13	1.50	9.33	118.74	0.41	15.70	2730	29.30
60-70	AM2-4	0.77	3.47	0.12	1.43	8.88	139.54	0.58	24.40	3260	35.80
70-80		0.65	3.56	0.13	1.31	7.79	167.64	0.74	30.60	2970	33.80
80-100	AM2-3	0.68	3.53	0.12	1.37	8.18	168.21	0.56	24.60	2240	31.50
100-105	AM2-2	0.60	3.69	0.12	0.25	10.06	130.38	0.54	23.20	2170	34.30
105-110		0.61	3.68	0.12	1.30	9.11	135.87	0.72	29.00	2030	34.70
110-115		0.60	3.65	0.12	1.53	9.32	144.02	0.68	27.10	1950	34.10
115-120		0.57	3.59	0.12	1.48	9.63	150.09	0.58	24.00	2080	34.30
120-125		0.63	3.42	0.12	1.60	10.09	182.44	0.52	23.50	2440	34.30
125-130		0.63	3.63	0.12	1.41	9.77	151.22	0.56	24.40	2550	33.50
130-135		0.63	3.62	0.12	1.39	9.26	169.31	0.60	25.30	2690	32.60
135-140	AM2-1	0.69	3.75	0.12	1.54	8.12	172.37	0.69	30.60	2920	32.80
140-145		0.66	3.80	0.13	1.41	8.84	156.82	0.63	28.10	3140	33.60
145-150		0.61	3.65	0.13	1.48	8.20	168.77	0.63	29.50	3100	33.30

[1]CIA = [Al2O3/ (Al2O3 + CaO + Na2O + K2O) *100]
[2]Ce anomaly = 2*Ce/(La+Pr)
[3]ΣREE = [Y+La+Ce+Pr+Nd+Sm+Eu+Gd+Dy+Tb+Er+Ho+Tm+Yb+Lu

2.4.6. Depositional processes according to lake filling

Isolated lakes distributed along the Serra Sul de Carajás such as Lago do Amendoim have closed or restricted basins, i.e., they respond directly to variations in the precipitation-evaporation balance, which, in turn, affects the intensity of weathering and erosion processes, surface runoff and transport of detrital material to the lacustrine sedimentation basins (SAHOO et al., 2016b; 2019). Thus, the geochemical signature and associated indicators can be interpreted in terms of paleohydrological and paleoenvironmental changes.

A trend of decreasing concentration of REEs, Hf, and Zr observed from 25 to 20 ka, as well as decreasing of Al and Ti contents and Ca/Ti ratio suggests a progressive decrease in surface runoff and detrital input into the lake, respectively. Additionally, increased Fe/Al ratio and Fe concentration indicate precipitation of siderite under lower lake level in response to less humid climatic conditions between 21 and 20 ka in the Serra Sul de Carajás. Low Ti/K and Th/U ratios which are indicators of chemical weathering also support this statement. Subsequently, an increase in detrital fraction (terrigenous elements) indicates a rise and fluctuation of water level. This is followed by low amounts of Al and Ti around 18 ka which suggests reduced detrital input due to less erosive rainfall events and/or high catchment stability (GUIMARÃES et al., 2016), probably caused by drier conditions compared to the present. This can be also supported by the occurrence of siderite mud and high Fe/Al ratio during this period. From 18 to 15 ka, a slight decrease in CIA index, plus reduced detrital input (Al, Ti and Ti/K, among other trace elements) and surface runoff (Hf, Zr and REEs) indicate the maintenance of less humid conditions until ~17 ka. High levels of Fe associated with the siderite mud layer indicate authigenic precipitation of siderite under the suboxic condition at the sediment-water interface (WAGNER et al., 2013). The interval between 17 and 15 ka is characterized by a change to oxidizing conditions, inhibiting the formation of siderite. Higher Ba/Al and Si/Ti ratios and slightly depleted $\delta^{15}N$ suggest a period of high productivity under relatively low lake levels (SAHOO et al., 2019). P and Fe content may also be a paleoproductivity proxies, since a combination of increased Fe and P concentration stimulate biomass increasing, leading to greater phytoplankton communities (NORTH et al., 2007). Thus, fluctuation in the Fe and P content from 22 to 15 ka can be due to the variation in biomass growth as well as in lake level, since both are strongly related. In modern conditions, this feature increases the contribution of autochthonous organic matter, such as siliceous sponge spicules, algae and aquatic vegetation due to the greater availability of solar radiation (SAHOO et al., 2017; TOLU et al., 2017). In addition, the increase in the detrital fraction (Ti/Al, Ti, Al, Zr, Hf and REEs) associated with the organic mud layer suggests an

increase in rainfall and runoff events leading to the transport of terrigenous material to the lake basin and a rising trend in lake level in response to the onset of warm conditions.

From 15 to 11 ka, the period which corresponds to the Pleistocene-Holocene transition is characterized by a trend of increasing Mo/Al and decreasing Ce anomaly indicating a possible change to the depleted-oxygen environment. Higher Ba/Al ratio and P and Fe content suggest increasing biomass growth from algae, probably associated with decreased lake level evidenced by depleted $\delta^{15}N$. On the other hand, lower Ca/Ti ratio and slightly higher CIA index, REEs, Ti/K, Hf, Zr, Al and Ti values than in the previous period indicate a discrete increase in surface runoff as well as in weathering, transport and detrital input to the lake at the same period. These divergent trends are probably associated with seasonal changes and warmer climatic conditions, which led to the erosion of the catchment basin and transport of terrigenous material to the lake basin during the rainy season; and reduced surface flow and detrital input, lower lake level and predominant deposition of autochthonous material during dry seasons (GUIMARÃES et al., 2016).

The following interval from 11 to 8 ka is distinguished by the significant reduction of detrital input and predominant deposition of organic material in the lake basin, possibly associated with the higher frequency of dry events or prolonged dry seasons, which led to low-energy transport and high accumulation of autochthonous material. Higher Mo/Al ratio and decreased Al, Ti, Ti/K, REEs, Hf and Zr values related to the herbaceous peat layer support this statement. Additionally, those dry events probably caused a decrease in the lake level and a small change in its redox condition around 11 ka, which favored the formation of siderite nodules under relatively reducing conditions at the water-sediment interface, as indicated by higher Mo/Al, Fe/Al, Fe, and P content and corroborated by facies description.

Subsequently, variations in REEs, Hf, Zr, Al and Ti/K values indicate the occurrence of alternate rainy and dry events. Dry episodes from ~ 6 ka marked by high productivity, changes in water level and fluctuations in the detrital input into the lake basin evidence the establishment of well-defined seasons in the Serra Sul de Carajás under predominantly humid climatic conditions similar to the present.

2.4.7. Vegetation dynamics, fire-history, and climate inferences

~25-21 ka (LGM-I)

The pollen diagram indicates a broad distribution of montane savanna and ombrophylous forest over the plateau and its slopes. Palms and ferns (*Polypodium* and Cyatheaceae) may support the presence of forest formation due to the strong association

currently existing in the study site (GUIMARÃES et al., 2017a). The cool-adapted taxa recorded are entirely represented by *Hedyosmum*, which is normally associated with open areas and gallery forests (FLORA DO BRASIL, 2020). *Hedyosmum* pollen grains (including *Alnus* and *Podocarpus*) are commonly dispersed by wind (ZANIOLO, 2002), thus long-distance transport of those pollen grains i.e. by wind from remote areas (e.g. Andes and/or Brazilian central plateau), where such species are currently distributed was considered. Moreover, considering that the majority of the pollen grains dispersed by the wind is not carried out more than 0.5 km beyond the source (BRADLEY, 1999), we assume that the presence of pollen grains from *Hedyosmum*, *Alnus* and *Podocarpus* evidence the expansion of those species in plateaus near southeastern Pará, i.e. in the central-western and southeastern Brazil due to cooler temperatures, which can be also a evidence of ancient connection between Amazonia and Atlantic forest (BOUIMETARHAN et al., 2018; CHENG et al., 2013; WANG et al., 2004).

Fire events in regional scale recorded by high micro-charcoal concentration (<100 µm) around 21.7 ka suggests a gradual shift to less humid conditions. These conditions coupled with high biomass availability as shown by the pollen data probably favored an increase in the frequency or intensity of fire events. Besides regional fires (within 20-100 km around a site), micro-charcoal fragments may also reflect the occurrence of local low-intensity fires probably associated with a high frequency of thunderstorms and lightning in the plateau at the end of dry seasons (REIS et al., 2017). Thus, with the onset of the rainy season, the charcoal fragments formed were gradually transported and deposited into the lake basin.

Previous studies performed on Serra Sul de Carajás have reported less humid climatic conditions for the LGM based on rare occurrence of forest taxa and low lake level (HERMANOWSKI et al., 2012), as well as decrease in pollen and spores richness and predominance of autochthonous SOM, which suggest periods with reduced terrigenous detrital input into the lake basin due to low surface runoff as a consequence of relatively dry conditions (REIS et al., 2017).

On Noel Kempff Mercado National Park (NKMNP), southwestern Amazonia Basin, pollen and charcoal records revealed expansion of dry forests and savanna due to longer dry season associated with drier conditions during the last glacial period (BURBRIDGE; MAYLE; KILLEEN, 2004). The occurrence of a sedimentary hiatus and absence of pollen grains during the LGM recorded on old fluvial terraces of Madeira River (COHEN et al., 2014), southern Amazonia, support the climatic conditions proposed previously.

On Hill of Six Lakes, northwestern Amazonia, lower lake level and reduced lacustrine productivity also evidenced the occurrence of drier conditions (CORDEIRO et al., 2011) compared to the present. On the other hand, pollen data previously obtained in the same site revealed the continuous presence of rainforest and high occurrence of cool-adapted taxa suggesting humid and cooler conditions (BUSH et al., 2004; COLINVAUX et al., 1996). The occurrence of cool-adapted taxa (*Alnus*, *Hedyosmum*, *Weinmannia*, *Podocarpus*) within Amazonian lowlands during the LGM and Late Glacial have been extensively reported in different regions of the Amazonia (BUSH et al., 2004; COHEN et al., 2014; COLINVAUX et al., 1996; COLINVAUX; DE OLIVEIRA, 2000; FONTES et al., 2017; HABERLE; MASLIN, 1999; MAYLE; BURBRIDGE; KILLEEN, 2000; REIS et al., 2017) and Andes (BUSH; SILMAN; URREGO, 2004; PADUANO et al., 2003).

Thus, cooler climatic conditions (approximately 5°C below the present) (BURBRIDGE; MAYLE; KILLEEN, 2004; BUSH; GEORGE; PHILANDER, 1999; STUTE et al., 1995) associated with the LGM was a relevant factor on migration of cool-adapted taxa to lower altitudes, leading to the formation of no-modern-analog communities along the Amazonian lowlands (HOOGHIEMSTRA; VAN DER HAMMEN, 2004; RACZKA; BUSH; DE OLIVEIRA, 2018).

21-18 ka (LGM-II)

This period was mainly characterized by the siderite formation as a result of changes in redox conditions, i.e. from oxidizing to anoxic conditions, at the sediment-water interface due to a decrease in the lake water level around 20 ka caused by relatively dry climatic conditions (GUIMARÃES et al., 2016; HERMANOWSKI et al., 2012; REIS et al., 2017). Under anoxic conditions the microorganisms can use Fe^{3+} as electron acceptors, causing organic matter oxidation and furthermore the energy gain for maintenance and growth. Thus, microbiological activity modulates diagenetic processes and methanogenesis, in which the organic matter is degraded, generating CO_2. Under these conditions, Fe (III) is reduced to Fe (II), subsequently reacts with the available carbonate, and causes the massive siderite precipitation (LEMOS et al., 2007; WAGNER et al., 2013).

The pollen diagram showed the lowest concentration for all ecological groups during this period. Forest formation and cool-adapted taxa were observed even in low percentages (<10%), indicating the presence of these phytophysiognomies on slopes of the plateau or associate with forest patches (“*Capões florestais”*). The maintenance of these forest formations including cold-adapted taxa, even under less wet conditions, is probably associated

with colder temperatures which favored the reduction of photorespiration and evapotranspiration (CORDEIRO et al., 2011; COWLING; MASLIN; SYKES, 2001). On the other hand, a high percentage of montane savanna (Poaceae, *Borreria* and Asteraceae) and macrophytes (*Isoëtes*) was observed, suggesting selective preservation. Pollen grains from anemophilous plant (wind pollination) as *Borreria* and Asteraceae are more resistant to degradation process, while pollen grains of Poaceae are produced in much larger quantities compared to entomophilous species (insect pollination), which explains its abundance relative to the others. The high occurrence of *Isoëtes* is probably associated with the high production of microspores/megaspores since this submerged macrophyte are broadly found on lake bottom (~6 m depth; GUIMARÃES et al., 2017a; PEREIRA et al., 2016).

Enriched $\delta^{15}N$ values (> 6‰) observed during this period may be related to the aquatic plants' contribution to SOM or to volatilization of ammonia and denitrification processes (LENG et al., 2006). An increase in C/N ratio was recorded, however, no significant change was observed in the TOC (%) and TN (%) values. Thus, the isotopic and elemental values recorded on this interval are strongly associated with the diagenetic processes instead of organic matter sources.

Low LGM fire occurrence in Carajás inferred from charcoal records is in agreement with the records obtained in several regions of both hemispheres. Globally, 66% of charcoal records showed less-than-present fire events, including low latitudes in South America (POWER et al., 2008). Among the main factors that govern regional climate changes since the LGM are seasonal and latitudinal distribution of insolation (BUSH et al., 2002; CRUZ et al., 2009), expansion/contraction of Northern Hemisphere ice-sheets (CLARK et al., 2009), changes in Southern Hemisphere ice caps (JOUZEL et al., 2007), in sea surface temperature patterns and changes in atmospheric CO_2 levels (BARNOLA et al., 1987; EGGLESTON et al., 2016). All these factors directly or indirectly influence regional-scale atmospheric circulation patterns, leading to changes in precipitation amount, season length, vegetation distribution and fire events.

Within biomes or on a local scale, fire frequency and the amount of biomass burned mainly vary with changing climate, fuel (type, amount and arrangement) and ignition (anthropogenic or lightning) (POWER et al., 2008; PYNE; ANDREWS; LAVEN, 1996). Considerable changes on vegetation types and distribution within Amazonian region (GUIMARÃES et al., 2011; PESSENDA et al., 2009) indicate that the fire regime also results from variations in the plant community and fuels conditions (MARLON; BARTLEIN; WHITLOCK, 2006; MILLSPAUGH; WHITLOCK; BARTLEIN, 2000).

Therefore, a coherent pattern of low fire occurrence during the LGM is consistent with a cooler global climate than the present (STUTE et al., 1995). At a regional to local scale, pollen, geochemistry and lake level data from Amazon basin reinforced the temperature decrease around 4.5 to 5°C compared to the present, and the migration of montane forest species (*Alnus*, *Podocarpus*, *Hedyosmum*) to Amazonian lowlands in response to the colder conditions in the Northern Hemisphere (CLARK et al., 2009), lowered sea levels, cooler sea-surface temperatures, and decreased atmospheric carbon dioxide (EGGLESTON et al., 2016). Thus, these factors led to an overall reduction of terrestrial biomass (FRANÇOIS et al., 1999; FRIEDLINGSTEIN et al., 1995) and consequently, a decrease in fuel availability (MARLON; BARTLEIN; WHITLOCK, 2006).

18-15 ka (Late Glacial)

Diagenetic formation of siderite under anoxic conditions at the interface water-sediment of the lake associated with reduced water level is observed around 17 ka which suggests the permanence of cooler and less humid climatic conditions compared to the present. From 17 ka, a considerable change in the redox conditions or pH at the sediment-water interface is evidenced by the absence of siderite formation probably associated with a shift to less anoxic conditions and/or more acid waters. Mud and peat deposits are indicators of seasonal conditions marked by allochthonous and autochthonous SOM input during the wet and dry seasons, respectively. The occurrence of ombrophylous forest taxa (*Alchornea*, *Moraceae,* Anacardiaceae, *Zanthoxylum, Pouteria*, *Sapium*, Melastomataceae, and Rutaceae) and higher percentage and richness of cool-adapted taxa (*Alnus*, *Hedyosmum* and *Podocarpus*), besides pteridophytes and palms, indicate the continuous presence of forest formation on the plateau slopes and probably over degraded crust as patches forests under cool and relatively humid climatic conditions.

An abrupt decrease in the macrophytes concentration, mainly composed by *Isoëtes,* followed by the algae bloom (*Botryococcus braunii*) suggests a considerable change in the trophic state of the lake between ~17 and 15 ka. The variability of the lake's trophic state is mainly associated with regional and local weather changes, rainfall, catchment basin characteristics and lake level which, in turn, control the water quality, nutrients levels as well as phytoplankton biomass (SAHOO et al., 2017). Changes in the Amendoim Lake's trophic state – for example, from oligotrophic to eutrophic – marked by algae bloom strongly suggest lower lake level during the Late Glacial.

High primary productivity in the water column of tropical lakes usually occurs in transitional periods (GARCIA FERESIN et al., 2010). In Lake Amendoim, a limnological study showed that the phytoplankton biomass is strongly dependent on seasonal dynamics of the nutrients profile, catchment characteristics of the basin, rainfall regime and its variability (SAHOO et al., 2016b). In addition, morphological feature such as shallow depth is also a potential factor for high eutrophic conditions (DA SILVA et al., 2018; SAHOO et al., 2017). As algae bloom can block out the sunlight for other organisms, limiting photosynthesis and decreasing oxygen levels in the water (SHARMA et al., 2010), it is very likely that the decrease in lake level during dry seasons was the key factor which favored the increase in primary productivity and consequently the decrease of macrophytes, particularly *Isoëtes*, situated at the lake bottom. Alternate deposits of mud and peat, more depleted values of $\delta^{13}C$, plus a noticeable increase in TN and in the Ba/Al ratio support this statement.

Therefore, changes in floristic composition with cool-adapted taxa expansion (*Alnus*, *Hedyosmum*, *Podocarpus*) due to low temperatures led to the permanence of no-modern-analog communities in the Amazon basin (BUSH; SILMAN; URREGO, 2004; COHEN et al., 2014; COLINVAUX et al., 1996; HABERLE; MASLIN, 1999, and references therein), including Carajás (HERMANOWSKI et al., 2012; REIS et al., 2017), while seasonal variations in the precipitation amount caused lower lake levels (BUSH et al., 2004; HERMANOWSKI et al., 2012; HERMANOWSKI; DA COSTA; BEHLING, 2015) and / or even the absence of sedimentation (FONTES et al., 2017; SIFEDDINE et al., 2001) in different sites. Thus, those evidence reinforce the occurrence of cool and seasonal conditions (prolonged dry seasons) during the late glacial period.

15-11 ka (Pleistocene-Holocene transition)

The mud and peat facies, as well as the isotopic ($\delta^{13}C$, $\delta^{15}N$) and elemental (TN) values, indicate revealed the alternate of autochthonous (macrophytes and/or algae) and allochthonous (terrestrial C_3 plants) material during this interval. The formation of siderite nodules between 12 and 11 ka and low sedimentation rate (0.02 mm yr^{-1}) are also evidence of change in redox conditions at the water-sediment interface due to lower lake levels during prolonged dry seasons. High frequency and richness of ombrophylous forest taxa besides palms (represented by *Mauritia*/*Mauritiella* and Arecaceae) and pteridophytes occurrence indicate the presence of forest formations and swampy environments on the Serra Sul, respectively, likely maintained by the humidity provided during the rainy season. On the other hand, decreased cool-adapted taxa concentration indicates a gradual disappearance of those

taxa from Serra Sul due to an increase in global temperature, particularly in the Southern Hemisphere (JOUZEL et al., 2007).

A rapid change to warmer climatic conditions occurs between 14 and 13 ka, probably associated with increasing atmospheric CO_2 concentrations (BARNOLA et al., 1987; POWER et al., 2008). The last occurrence of *Podocarpus* and *Hedyosmum* between 12 and 11 ka, similar to previous studies (ABSY et al., 1991; HERMANOWSKI et al., 2012; HERMANOWSKI; DA COSTA; BEHLING, 2015; REIS et al., 2017) reinforces the deglacial warming trend from 14 ka. In addition, the absence of *Alnus* (disappearance between 16 and 15 ka) during this interval reveals lower tolerance of this species to higher temperatures and increased water stress compared to the *Podocarpus* and *Hedyosmum*. And therefore, its current distribution is restricted to areas of high altitudes such as the Andean region (GBIF.ORG, 2019).

The higher concentration of charcoal particles, in turn, revealed an increase in fire events at local (>250 μm) and regional (<100 μm) scales. This is consistent with previous charcoal records that reported an increase in global temperature and considerable changes in vegetation at a global scale between the Late Glacial and Early Holocene interval (MARLON; BARTLEIN; WHITLOCK, 2006; POWER et al., 2008). In the Southern Hemisphere, remarkable changes in South American Summer Monsoon (SASM) intensity (CRUZ et al., 2005) associated with decreased summer insolation led to weakened SASM and lower continental convection and caused reduced precipitation in the Amazon basin (CHENG et al., 2013; CRUZ et al., 2005; WANG et al., 2006). Therefore, such conditions combined with higher atmospheric CO_2 concentrations, increased temperature, and biomass/fuel availability were probably the main factors responsible for enhanced biomass burning and vegetation cover changes during the Pleistocene-Holocene transition and Early Holocene as well (MARLON; BARTLEIN; WHITLOCK, 2006; POWER et al., 2008).

11-8 ka (Early Holocene)

In South America, particularly in the Amazon basin, dramatic changes in the regional precipitation pattern occurred during the Early Holocene leading to warmer and drier conditions relative to modern levels (FREITAS et al., 2001; PESSENDA et al., 1998a, b). In Carajás, such conditions led to lower lake levels and reduced *Isoëtes* population on the lake bottom. The predominance of autochthonous organic matter and low detrital input showed by decreased sedimentation rate as well as low CIA, Zr, Hf and Al values also suggest reduced surface runoff and catchment erosion due to reduced precipitation amount. The non-formation

of siderite nodules is probably due to the prevalence of peat rather than detrital material to which this mineral is associated.

High incidence of fire during the Early Holocene possibly affected the vegetation cover, causing its reduction over Serra Sul as indicated by the large decrease in the concentration of phytophysiognomies composed by woody plants as forest formations, including forest patches, and montane savanna. The presence of palms and macrophytes associated with swamps suggests seasonal conditions and therefore moisture availability could have occurred during the rainy season, which allowed the maintenance of those environments in the study site (HERMANOWSKI et al., 2012).

Variability in the tropical hydrological cycle has been proved to be primarily driven by summer solar radiation, which is controlled by the Earth's precessional cycle (CRUZ et al., 2005). Thus, decreased summer insolation led to reduced continental convection activity and upward motion causing the weakening of the SASM (WANG et al., 2006). This system coupled with a northward shift in the mean position of the ITCZ probably provided low rainfall amount over eastern Amazonia between 11 and 8 ka. Moreover, in Tropical South America, El-Niño Southern Oscillation (ENSO) may have also affected the precipitation over Amazonia (GRIMM; BARROS; DOYLE, 2000; PHILANDER, 1983). El-Niño (La Niña) episodes are commonly associated with below (above) average precipitation in western-eastern Amazonia (CHENG et al., 2013; KANE, 2006; LI et al., 2011), since the east-west Walker circulation and the local meridional divergent circulation are important constituents in seasonal climatology, as well as interannual variability (MARENGO; HASTENRATH, 1993; YOON; ZENG, 2010). In addition, warm and dry weather caused by the El Niño event coupled with biomass availability is the ideal conditions for the increase of fires events in the Amazon basin.

Changes in climatic conditions during Early to Middle Holocene were also observed in previous studies from Serra Norte (CORDEIRO et al., 2008; TURCQ et al., 1998) and Serra Sul de Carajás (HERMANOWSKI et al., 2012; HERMANOWSKI; DA COSTA; BEHLING, 2015; REIS et al., 2017; SIFEDDINE et al., 2001). Drier conditions have been also recorded in Southern Rondônia and Amazonas (Humaitá region) States, Southern Amazonia (FREITAS et al., 2001; PESSENDA et al., 1998a, b), NKNP (BURBRIDGE; MAYLE; KILLEEN, 2004; MAYLE; BURBRIDGE; KILLEEN, 2000), Hill of the Six Lakes (BUSH et al., 2004) and Bolivian Altiplano (BAKER et al., 2001). In general, our record strongly suggests less humid conditions in Carajás.

<8 ka (Middle to Late Holocene)

Deposition of autochthonous and allochthonous material over the last 8 ka supports the occurrence of well-defined seasons in Serra Sul de Carajás. An increase in $\delta^{15}N$ values and high concentration of algae between 6 and 4 ka suggests a shift in trophic state of the lake and in its water level since the bloom algae are highly associated with less humid conditions and low lake level. Low forest formation and pteridophytes concentration support this statement and indicate a phase with reduced precipitation amount or occurrence of prolonged dry seasons possibly due to the intensified ENSO episodes (BARR et al., 2019; LABEYRIE et al., 2003) over Amazon basin.

The occurrence of a warm-dry interval in the Mid-Holocene was also recorded in Carajás and along the Amazon Basin and it is associated with: (1) low sedimentation rates (GUIMARÃES et al., 2016), a drop in lake level (CORDEIRO et al., 2008a; HERMANOWSKI et al., 2012; REIS et al., 2017) and reduced tropical forest taxa (HERMANOWSKI; DA COSTA; BEHLING, 2015; SIFEDDINE et al., 2001) in Carajás; (2) expansion of open savanna and seasonal forest elements in Lago do Saci, southern Amazonia, between 7.5 and 5 ka (FONTES et al., 2017); in NKMNP between 6 and 3 ka (BURBRIDGE; MAYLE; KILLEEN, 2004) and in Rondônia/Amazonas border from 9 to 3 ka (FREITAS et al., 2001; PESSENDA et al., 1998a; b); (3) high frequency of fire events in Rondônia between 7 and 6 ka (PESSENDA et al., 1998a); (4) a gap in sedimentation due to a complete dryness of the Comprido Lake between 7.8 and 3 ka (MOREIRA et al., 2013); and (5) a prolonged low lake level in Lake Titicaca between 8.5 and 3.5 ka (BAKER et al., 2001), with a peak between 6 and 4 ka marked by a change in the composition of aquatic community (PADUANO et al., 2003).

Lower charcoal concentrations correspond to a progressive increase in the summer insolation at the Southern Hemisphere over the last 5 ka. This possibly led to the strengthening of the SASM (WANG et al., 2006) and consequently reduced fire events. These factors combined with increased atmospheric CO_2 levels probably favored the establishment of the tropical rainforest under similar present-day climatic conditions. Previous studies also indicated the expansion of ombrophylous forest under warm and wet climatic conditions in the Serra Sul de Carajás between 5 and 3 ka (ABSY et al., 1991; CORDEIRO et al., 2008; GUIMARÃES et al., 2016; 2017b; HERMANOWSKI et al., 2012; HERMANOWSKI; DA COSTA; BEHLING, 2015; REIS et al., 2017; SIFEDDINE et al., 2001) and throughout Amazonia basin (BAKER et al., 2001; BURBRIDGE; MAYLE; KILLEEN, 2004; BUSH et al., 2004; COHEN et al., 2014; FREITAS et al., 2001; FONTES et al., 2017; GUIMARÃES

et al., 2011; MAYLE; BURBRIDGE; KILLEEN, 2000; PADUANO et al., 2003; PESSENDA et al., 1998a; b).

2.4.8. Western and Eastern Amazonia dipole

Considering climatic features during LGM, humid climatic conditions in the eastern Andes and western Amazonia have been strongly reported from previous records obtained in Lake Titicaca (BAKER et al., 2001), Lake Consuelo (BUSH; SILMAN; URREGO, 2004) and Hill of Six Lakes (BUSH et al., 2004), which showed the continuous presence of vegetation over the last 50 ka. On the other hand, drier climatic conditions than the current one prevailed in the southern (BURBRIDGE; MAYLE; KILLEEN, 2004) and eastern Amazonia (ABSY et al., 1991; FONTES et al., 2017; HERMANOWSKI et al., 2012; HERMANOWSKI; DA COSTA; BEHLING, 2015; REIS et al., 2017; SIFEDDINE et al., 1994; 2001) and northeastern (NE) Brazil (CRUZ et al., 2009; WANG et al., 2004). Divergent climatic conditions between western and eastern Amazonia show a dipole pattern (CHENG et al., 2013) and they are strongly associated with abrupt changes in atmospheric and oceanic circulation dynamics induced by North Atlantic climatic events occurred in centennial to millennial-scales (MOSBLECH et al., 2012).

During the glacial period, cooler North Atlantic SST, led to the AMOC weakening and a southward displacement of the ITCZ (ARBUSZEWSKI et al., 2013; CHIANG et al., 2003; DUBOIS et al., 2014). Thus, we propose reduced moisture incursion into northern South American via northeasterly trade winds, however, limited to the western Amazon basin, which favored atmospheric water vapor export to the eastern side of the Andes (physical barrier) and central-west, south-east and southern Brazil through low-level jets, increasing precipitation in those areas (CRUZ et al., 2009; WANG et al., 2006; 2007). Moreover, low moisture transport from Atlantic Ocean to South American continent may have weakened the SASM (MOSBLECH et al., 2012), leading to a reduced intensity and coverage area, and consequently lower precipitation amount in eastern Amazonia (WANG et al., 2017). Meanwhile, the western Amazon remained humid.

Regarding the Pacific Ocean effects on Amazon rainfall pattern during the LGM, it has been reported a decrease in the Tropical Pacific SST around 2.8 ± 0.7°C (LEA; PAK; SPERO, 2000), and dominance of La Niña-like conditions during glacial terminations (PENA et al., 2008). La Niña (El Niño) episodes are generally associated with higher (lower) precipitation amount in the entire Amazonia basin and NE Brazil (BRUM et al., 2018; CHENG et al., 2013; KANE, 2006; LI et al., 2011). However, the decreased moisture transport and convection activity induced by low evaporation due to lower Pacific SST coupled with a change in the mean position of the Hadley atmospheric cell (CRUZ et al., 2005; MOSBLECH et al., 2012; WANG et al., 2006) may have contributed to the reduction of precipitation in eastern Amazonia and played a fundamental role in the west-eastern Amazonia dipole pattern.

Finally, the formation of no-modern analogs communities at Amazonian lowlands due to the occurrence of cold-adapted taxa (*Alnus*, *Hedyosmum* and *Podocarpus*) near Serra Sul de Carajás attests cooler temperatures in the tropical regions during the LGM, and evidence a strong connection between Amazonia and Northern Hemisphere climate events. Although cooler climatic conditions have been recorded throughout the Amazon basin and the Andes, our records show that the establishment of west-eastern Amazonia dipole pattern is associated with precipitation amount variability linked to shifts in ITCZ and SACZ position, intensity and extent over the Amazon basin.

2.5. Conclusions

A multi-proxy approach applied on a sediment core (AM2) from Lake Amendoim revealed remarkable climate changes during the Late Pleistocene and Holocene which led to considerable environmental and vegetation cover changes in the Serra Sul de Carajás, southeastern Amazonia.

During the LGM and Late Glacial, relatively dry climatic conditions caused considerable fluctuations in the lake level and detrital input. Additionally, cooler conditions favored the establishment of cool-adapted taxa, i.e. *Alnus*, *Podocarpus*, and *Hedyosmum* in the Amazonian lowlands, respectively, and led to the formation of no-modern-analogs communities in southeastern Amazonia.

In Serra dos Carajás, variation in surface runoff and detrital input, besides a small increase in the occurrence of fire events, are linked to changes in the global climatic configuration (e.g. decrease in ice-sheet cover, rising sea level and increasing Atlantic and Pacific SST and atmospheric CO_2 levels), which possibly led to shifts in local rainfall patterns, evidencing a strong connection between Amazonia and Northern Hemisphere climate events.

From the Pleistocene-Holocene transition, increase in fire events and the decline of cool-adapted species point to warmer conditions as the main factor responsible for changes in vegetation composition and distribution in southeastern Amazonia during this period. From Early to Mid-Holocene, lower lake level and greater-than-present fire events suggest less humid conditions and correspond to low summer insolation in the southern hemisphere and consequently weakened SASM. Finally, from Middle to Late Holocene, a strong influence of ENSO episodes and a progressive increase in summer insolation in the Southern Hemisphere, and consequently, strengthened SASM, probably led to the establishment of well-defined seasons under predominantly humid conditions in the Serra Sul de Carajás.

References

ABSY, M. L. et al. Mise en évidence de quatre phases d'ouverture de la forêt dense dans le Sud-Est de l'Amazonie au cours des 60 000 dernières années : Première comparaison avec d'autres régions tropicales. **Comptes Rendus de l'Académie des Sciences**, v. 312, n. 6, p. 673–678, 1991.

ABSY, M. L. et al. Palynological differentiation of savanna types in Carajás, Brazil (southeastern Amazonia). **Palynology**, v. 38, n. 1, p. 78–89, 2014.

ADAMS, D. K.; PEREIRA DE SOUZA, E.; COSTA, A. A. Convecção úmida na Amazônia: implicações para modelagem númerica. **Revista Brasileira de Meteorologia**, v. 24, n. 2, p. 168–178, 2009.

ADRIANO, D. C. **Trace element in the terrestrial environment**. Heidelberg: Springer, 1986.

ALVARES, C. A. et al. Köppen's climate classification map for Brazil. **Meteorologische Zeitschrift**, v. 22, n. 6, p. 711–728, 2013.

ARBUSZEWSKI, J. A. et al. Meridional shifts of the Atlantic intertropical convergence zone since the Last Glacial Maximum. **Nature Geoscience**, v. 6, p. 959–962, 2013.

BAILEY, A. M.; ROBERTS, H. H.; BLACKSON, J. H. Diagenetic mineral formation in sediments of the Mississippi River delta plain. **Mineralogical Magazine**, v. 58, p. 38–39, 1994.

BAKER, P. A. et al. The History of South American Tropical Precipitation for the Past 25 , 000 Years. **Science**, v. 291, p. 640–643, 2001.

BARNOLA, J.-M. et al. Vostok ice core provides 160,000-years record of atmospheric CO2. **Nature**, v. 329, p. 408–414, 1987.

BARR, C. et al. Holocene el Niño-southern Oscillation variability reflected in subtropical Australian precipitation. **Scientific Reports**, v. 9, p. 1–9, 2019.

BERNER, R. A. **Early diagenesis** : a theoretical approach. Princeton: Princeton University Press, 1980.

BLAAUW, M.; CHRISTEN, J. A. Flexible paleoclimate age-depth models using an autoregressive gamma process. **Bayesian Analysis**, v. 6, n. 3, p. 457–474, set. 2011.

BOUIMETARHAN, I. et al. Intermittent development of forest corridors in northeastern Brazil during the last deglaciation: Climatic and ecologic evidence. **Quaternary Science Reviews**, v. 192, p. 86–96, 2018.

BRADLEY, R. S. **Paleoclimatology**: reconstructing climates of the Quaternary. 2. ed. New York: Academic Press, 1999.

BRUM, M. et al. ENSO effects on the transpiration of eastern Amazon trees. **Philosophical Transactions B**, v. 373, p. 1–12, 2018.

BURBRIDGE, R. E.; MAYLE, F. E.; KILLEEN, T. J. Fifty-thousand-year vegetation and climate history of Noel Kempff Mercado National Park, Bolivian Amazon. **Quaternary Research**, v. 61, n. 2, p. 215–230, 2004.

BUSH, A. B. G.; GEORGE, S.; PHILANDER, H. The climate of the Last Glacial Maximum: Results from a coupled atmosphere-ocean general circulation model. **Journal of Geophysical Research**, v. 104, p. 509–525, 1999.

BUSH, M. B. et al. Orbital forcing signal in sediments of two Amazonian lakes. **Journal of Paleolimnology**, v. 2, p. 341–352, 2002. BUSH, M. B. et al. Amazonian paleoecological histories: one hill, three watersheds. **Palaeogeography, Palaeoclimatology, Palaeoecology**, v. 214, n. 4, p. 359–393, 2004.

BUSH, M. B.; SILMAN, M. R.; URREGO, D. H. 48,000 Years of climate and forest change in a biodiversity hot spot. **Science**, v. 303, n. 5659, p. 827–829, 2004.

CARDOSO, D. et al. Amazon plant diversity revealed by a taxonomically verified species list. **Proceedings of the National Academy of Sciences of the USA**, v. 114, p. 10695–10700, 2017.

CARREIRA, L. M. M.; BARTH, O. M. **Atlas de pólen da vegetação de Canga da Serra de Carajás**. 1. ed. Belém: Museu Paraense Emílio Goeldi, 2003.

CHEN, H.-F. et al. The Ti/Al molar ratio as a new proxy for tracing sediment transportation processes and its application in aeolian events and sea level change in East Asia. **Journal of Asian Earth Sciences**, v. 73, p. 31–38, 2013.

CHENG, H. et al. ARTICLE Climate change patterns in Amazonia and biodiversity. **Nature Communications**, v. 4, p. 1–6, 2013.

CHIANG, J. C. H. et al. Sensitivity of the Atlantic ITCZ to Last Glacial Maximum boundary conditions. **Paleoceanography**, v. 18, n. 4, p. 1094, 2003. doi:10.1029/2003PA000916.

CHIANG, J. C. H.; KUSHNIR, Y.; GIANNINI, A. Deconstructing Atlantic Intertropical Convergence Zone variability: Influence of the local cross-equatorial sea surface temperature gradient and remote forcing from the eastern equatorial Pacific. **Journal of Geophysical Research**, v. 107, n. D1, p. 4004, 2002.

CLARK, P. U. et al. The Last Glacial Maximum. **Science**, v. 325, p. 710–714, 2009.

CLARK, P. U.; MIX, A. C.; BARD, E. Ice sheets and sea level of the Last Glacial Maximum. **Eos, Transactions American Geophysical Union**, v. 82, n. 22, p. 241–241, 2006.

COHEN, M. C. L. et al. Late Pleistocene glacial forest of Humaitá-Western Amazonia. **Palaeogeography, Palaeoclimatology, Palaeoecology**, v. 415, p. 37–47, 2014.

COLINVAUX, P. A. et al. A long pollen record from lowland Amazonia, forest cooling in Glacial times.pdf. **Science**, v. 274, p. 85–88, 1996.

COLINVAUX, P. A.; DE OLIVEIRA, P. E. Palaeoecology and climate of the amazon basin during the last glacial cycle. **Journal of Quaternary Science**, v. 15, n. 4, p. 347–356, 2000.

COLINVAUX, P.; OLIVEIRA, P. E. DE; PATIÑO, J. E. M. . **Amazon Pollen Manual and Atlas**. Reading: Harwood Academic Publishers, 1999.

CORDEIRO, R. C. et al. Acumulação de carbono em Lagos Amazônicos como indicador de eventos paleoclimáticos e antrópicos. **Oecologia Brasiliensis**, v. 12, n. 1, p. 130–154, 2008a. CORDEIRO, R. C. et al. Holocene fires in East Amazonia (Carajás), new evidences, chronology and relation with paleoclimate. **Global and Planetary Change**, v. 61, n. 1–2, p. 49–62, 2008b.

CORDEIRO, R. C. et al. Biogeochemical indicators of environmental changes from 50 Ka to 10 Ka in a humid region of the Brazilian Amazon. **Palaeogeography, Palaeoclimatology, Palaeoecology**, v. 299, p. 426–436, 2011.

COWLING, S. A.; MASLIN, M. A.; SYKES, M. T. Paleovegetation Simulations of Lowland Amazonia and Implications for Neotropical Allopatry and Speciation. **Quaternary Research**, v. 55, p. 140–149, 2001.

CRUZ, F. C. et al. Insolatio*n*-driven changes in atmospheric circulation over the past 116,000 years in subtropical Brazil. **Nature**, v. 434, p. 63–66, 2005.

CRUZ, F. W. et al. Orbitally driven east-west antiphasing of South American precipitation. **Nature Geoscience**, v. 2, n. 3, p. 210–214, 2009.

DA SILVA, M. S. et al. Morphology and morphometry of upland lakes over lateritic crust, Serra dos Carajás, southeastern Amazon region. **Annals of the Brazilian Academy of Sciences**, v. 90, n. 902, p. 1309–1325, 2018.

DE FREITAS, H. A. et al. Late Quaternary vegetation dynamics in the southern Amazon Basin inferred from carbon isotopes in soil organic matter. **Quaternary Research**, v. 55, n. 1, p. 39–46, 2001.

DUBOIS, N. et al. Millennial-scale Atlantic/East Pacific sea surface temperature linkages during the last 100,000 years. **Earth and Planetary Science Letters**, v. 396, p. 134–142, 2014.

EGGLESTON, S. et al. Evolution of the stable carbon isotope composition of atmospheric CO2 over the last glacial cycle. **Paleoceanography**, v. 31, n. 3, p. 434–452, 2016.

FISCH, G.; MARENGO, J. A.; NOBRE, C. A. Uma Revisão Geral sobre o Clima da Amazônia. **Acta Amazonica**, v. 28, n. 2, p. 101–126, 1998.

FLORA DO BRASIL. **Jardim Botânico do Rio de Janeiro**. Rio de Janeiro, 2020. Disponível em: <http://floradobrasil.jbrj.gov.br/reflora/listaBrasil/ConsultaPublicaUC/ResultadoDaConsultaNovaConsulta.do#CondicaoTaxonCP>. Acesso em: 24 maio 2019.

FONTES, D. et al. Paleoenvironmental dynamics in South Amazonia, Brazil, during the last 35,000 years inferred from pollen and geochemical records of Lago do Saci. **Quaternary Science Reviews**, v. 173, p. 161-180, 2017.

FRANÇOIS, L. M. et al. Carbon stocks and isotopic budgets of the terrestrial biosphere at mid-Holocene and last glacial maximum times. **Chemical Geology**, v. 159, n. 1-4, p. 163-189, 1999.

FREITAS, H. A. D. et al. Florestas x savanas: no passado a Amazônia. **Ciência Hoje**, v. 32, n. 189, p. 40–46, 2002.

FRIEDLINGSTEIN, P. et al. Carbo*n*-biosphere-climate interactions in the last glacial maximum climate vegetation distributions simulated by two bioclimatic schemes are attributable. **Journal of Geophysical Research. Atmospheres**, v. 100, n. 94, p. 7203–7221, 1995.

GARCIA FERESIN, E. et al. Primary productivity of the phytoplankton in a tropical Brazilian shallow lake: experiments in the lake and in mesocosms Produtividade primária em um lago tropical raso brasileiro: experimentos no lago e em mesocosmos. **Acta Limnologica Brasiliensia**, v. 22, n. 4, p. 384–396, 2010.

GASTMANS, D. et al. Controls over spatial and seasonal variations on isotopic composition of the precipitation along the central and eastern portion of Brazil. **Isotopes in Environmental and Health Studies**, v. 53, n. 5, p. 518–538, 2017.

GBIF.ORG. **GBIF home page**. Copenhagen, DK, 2019. Disponível em: <https://www.gbif.org/>. Acesso em: 27 maio. 2019.

GRIEPINK, B.; TOLG, G. Sample Digestion for the Determination of Elemental Traces in Matrices of Environmental Concern. **International Union of Pure and Applied Chemistry**, v. 61, n. 6, p. 1139–1, 1989.

GRIMM, A. M.; BARROS, V. R.; DOYLE, M. E. Climate Variability in Southern South America Associated with El Niño and La Niña Events. **Journal of Climate**, v. 13, p. 35–58, 2000.

GRIMM, E. C. CONISS: a FORTRAN 77 program for stratigraphically constrained cluster analysis by the method of incremental sum of squares. **Computers & Geosciences**, v. 13, n. 1, p. 13–35, 1987.

GUIMARÃES, J. T. F. et al. Mid- and late-Holocene sedimentary process and palaeovegetation changes near the mouth of the Amazon River. **The Holocene**, v. 22, n. 3, p. 359–370, 2011.

GUIMARÃES, J. T. F. et al. Source and distribution of pollen and spores in surface sediments of a plateau lake in southeastern Amazonia. **Quaternary International**, v. 352, p. 181-196, 2014.

GUIMARÃES, J. T. F. et al. Late Quaternary environmental and climate changes registered in lacustrine sediments of the Serra Sul de Carajás, south-east Amazonia. **Journal of**

Quaternary Science, v. 31, n. 2, p. 61–74, 2016.

GUIMARÃES, J. T. F. et al. Modern pollen rain as a background for palaeoenvironmental studies in the Serra dos Carajás, southeastern Amazonia. **The Holocene**, v. 27, n. 8, p. 1055–1066, 2017a.

GUIMARÃES, J. T. F. et al. Holocene history of a lake filling and vegetation dynamics of the Serra Sul dos Carajás, southeast Amazonia. **Anais da Academia Brasileira de Ciências**, v. 91, n. 2, e20160916, 2017b.

HABERLE, S. G.; MASLIN, M. Late Quaternary vegetation and climate history of the Amazon Basin based on a 50,000-years pollen record from the Amazon Fan. **Quaternary Research**, v. 51, n. 1999, p. 27–38, 1999.

HAMMER, D. A. T. et al. Past: Paleontological Statistics Software Package for Education and Data Analysis. **Palaeontologia Electronica**, v. 4, n.1, art. 4, 9 p. 2001. Disponível em: <http://palaeo-electronica.orghttp//palaeo-electronica.org/2001_1/past/issue1_01.htm.>. Acesso em: 13 dez. 2018.

HAUG, G. H. et al. Southward penetration of the intertropical convergence zonce through the Holocene. **Science**, v. 293, p. 1304–1308, 2001.

HERMANOWSKI, B. et al. Palaeoenvironmental dynamics and underlying climatic changes in southeast Amazonia (Serra Sul dos Carajás, Brazil) during the late Pleistocene and Holocene. **Palaeogeography, Palaeoclimatology, Palaeoecology**, v. 365–366, p. 227–246, 2012.

HERMANOWSKI, B.; DA COSTA, M. L.; BEHLING, H. Possible linkages of palaeofires in southeast Amazonia to a changing climate since the Last Glacial Maximum. **Vegetation History and Archaeobotany**, v. 24, n. 2, p. 279–292, 2015.

HOOGHIEMSTRA, H.; VAN DER HAMMEN, T. Quaternary Ice-Age dynamics in the Colombian Andes: developing an understanding of our legacy. **Philosophical Transactions of the Royal Society B**, v. 359, p. 173–181, 2004.

HUBBELL, S. P. et al. How many tree species are there in the Amazon and how many of them will go extinct? **Proceedings of the National Academy of Sciences of the USA**, v. 105, p. 11498–11504, 2008.

JACOB, J. et al. Paleohydrological changes during the last deglaciation in Northern Brazil. **Quaternary Science Reviews**, v. 26, n. 7–8, p. 1004–1015, 2007.

JOUZEL, J. et al. Orbital and Millennial Antarctic Climate Variability over the Past 800,000 Years. **Science**, v. 317, p. 793–796, 2007.

KANE, R. P. El Niño effects on rainfall in South America: comparison with rainfalls in India and other parts of the world. **Advances in Geosciences**, v. 6, p. 35-41, 2006. doi: 10.5194/adgeo-6-35-2006.

LABEYRIE, L. et al. The History of climate dynamics in the Late Quaternary. In: ALVERSON, K. D.; BRADLEY, R.; PEDERSEN, T. F. (Ed.). **Paleoclimate, global change and the future**. Heidelberg: Springer, 2003. p. 33–71.

LEA, D. W.; PAK, D. K.; SPERO, H. J. Climate impact of Late Quaternary Equatorial Pacific sea surface temperature variations. **Science**, v. 289, p. 1719–1724, 2000.

LEMOS, V. P. et al. Vivianite and siderite in lateritic iron crust: an example of bioreduction. **Química Nova**, v. 30, n. 1, p. 36–40, 2007.

LENG, M. J. et al. Isotopes in Lake Sediments. In: LENG, M. J. (Ed.). **Isotopes in Palaeoenvironmental Research**. Dordrecht: Kluwer Academic Publishers, 2006. p. 147–184:

LENG, M. J. et al. Understanding past climatic and hydrological variability in the Mediterranean from Lake Prespa sediment isotope and geochemical record over the Last Glacial cycle. **Quaternary Science Reviews**, v. 66, p. 123–136, 2013.

LI, W. et al. Impact of two different types of El Niño events on the Amazon climate and ecosystem productivity. **Journal of Plant Ecology**, v. 4, n. 2, p. 91–99, 2011.

LIEBMANN, B.; MARENGO, J. . Interannual variability of the rainy season and rainfall in the Brazilian Amazon Basin. **Journal of Climate**, v. 14, n. 22, p. 4308–4318, 2001.

LIEBMANN, B.; MECHOSO, C. R. **The South American Monsoon System**. 2. ed. Singapure: World Scientific Series on Asia-Pacific Weather and Climate, 2011. p. 137-157. doi: 10.1142/9789814343411_0009.

LIM, D. I. et al. Sequential growth of early diagenetic freshwater siderites in the Holocene coastal deposits, Korea. **Sedimentary Geology**, v. 169, p. 107–120, 2004.

LOPES, M. N. G.; DE SOUZA, E. B.; FERREIRA, D. B. DA S. Climatologia Regional da precipitação no estado do Pará. **Revista Brasileira de Climatologia**, v. 12, p. 84–102, 2013.

MACAMBIRA, M. J. B.; LAFON, J.-M. Geocronologia da Província Mineral de Carajás; Síntese dos dados e novos desafios. **Boletim do Museu Paraense Emílio Goeldi**, v. 7, p. 263–288, 1995.

MARENGO, J. A. Interannual variability of surface climate in the Amazon basin. **International Journal of Climatology**, v. 12, n. 8, p. 853–863, 1992.

MARENGO, J. A. et al. Climatology of the Low-Level Jet East of the Andes as Derived from the NCEP–NCAR Reanalyses: Characteristics and Temporal Variability. **Journal of Climate**, v. 17, n. 12, p. 2261–2280, 2004.

MARENGO, J. A.; HASTENRATH, S. Case Studies of Extreme Climatic Events in the Amazon Basin. **Journal of Climate**, v. 6, n. 4, p. 617–627, 1993.

MARLON, J.; BARTLEIN, P. J.; WHITLOCK, C. Fire-fuel-climate linkages in the northwestern USA during the Holocene. **The Holocene**, v. 16,8, p. 1059–1071, 2006.

MARTINELLI, L. A. et al. Isotopic Composition of Majors Carbon Reservoirs in the Amazon Floodplain. **International Journal of Ecology and Environmental Sciences**, v. 20, p. 31–46, 1994.

MARTINELLI, L. A. et al. Stable carbon isotope ratio of tree leaves, boles and tree litter in a tropical forest in Rondônia, Brazil. **Oecologia**, v. 114, p. 170–179, 1998.

MARTINELLI, L. A. et al. **Desvendando questões ambientais com isótopos estáveis**. 1. ed. São Paulo: Oficina de Textos, 2009.

MAURITY, C. W.; KOTSCHOUBEY, B. Evolução recente da cobertura de alteração no platô N1 - serra dos Carajás-PA. Degradação, pseudocarstificação, espeleotemas. **Boletim do Museu Paraense Emílio Goeldi**, v. 7, p. 331–362, 1995.

MAYLE, F. E.; BURBRIDGE, R.; KILLEEN, T. J. Millennial-scale dynamics of southern Amazonian rain forests. **Science**, v. 290, n. 5500, p. 2291–2294, 2000.

MEYERS, P. A. Preservation of elemental and isotopic source identification of sedimentary organic matter. **Chemical Geology**, v. 114, n. 3–4, p. 289–302, 1994.

MEYERS, P. A. Organic geochemical proxies of paleoceanographic, paleolimnologic, and paleoclimatic processes. **Organic Geochemistry**, v. 27, n. 5–6, p. 213–250, 1997.

MEYERS, P. A.; EADIE, B. J. Sources, degradation and recycling of organic matter associated with sinking particles in Lake Michigan. **Organic Geochemistry**, v. 20, n. 1, p. 47–56, 1993.

MILLSPAUGH, S. H.; WHITLOCK, C.; BARTLEIN, P. J. Variations in fire frequency and climate over the past 17,000 years in central Yellowstone National Park. **Geology**, v. 28, n. 3, p. 211–214, 2000.

MOREIRA, L. S. et al. Holocene paleoenvironmental reconstruction in the Eastern Amazonian Basin: Comprido Lake. **Journal of South American Earth Sciences**, v. 44, p. 55–62, 2013.

MOSBLECH, N. A. S. et al. North Atlantic forcing of Amazonian precipitation during the last ice age. **Nature Geoscience**, v. 5, p. 817–820, 2012.

NESBITT, H. W. et al. Effects of Chemical Weathering and Sorting on the Petrogenesis of Siliciclastic Sediments, with Implications for Provenance Studies. **The Journal of Geology**, v. 104, n. 5, p. 525–542, 1996.

NOBRE, P. et al. Coupled ocea*n*-atmosphere variations over the South Atlantic Ocean. **Journal of Climate**, v. 25, n. 18, p. 6349–6358, 2012.

NOBRE; SHUKLA, P. AND J. Variations of sea surface temperature, wind stress, and rainfall over the Tropical Atlantic and South America. **Journal of Climate**, v. 9, p. 2464–2479, 1996.

NOGUEIRA, A. C. R.; TRUCKENBROD, W.; PINHEIRO, R. V. L. Formação Águas

Claras, Pré-Cambriano da Serra dos Carajás: Redescrição e redefinição litoestratigráfica. **Boletim do Museu Paraense Emílio Goeldi**, v. 7, p. 177–207, 1995.

NORTH, R. L. et al. Evidence for phosphorus, nitrogen, and iron colimitation of phytoplankton communities in Lake Erie. **Limnology and Oceanography**, v. 52, n. 1, p. 315–328, 2007.

NUNES, G. L. et al. Quillworts from the Amazon: A multidisciplinary populational study on Isoetes serracarajensis and Isoetes cangae. **Plos One**, v. 13, n. 8, p. e0201417, 2018.

NUNES, J. A. et al. Soil-vegetation relationships on a banded ironstone 'island', Carajás Plateau, Brazilian Eastern Amazonia. **Anais da Academia Brasileira de Ciencias**, v. 87, n. 4, p. 2097–2110, 2015.

OLSZEWSKI, W. J. et al. The age, origin, and tectonics of the Grão Pará Group and associated rocks, Serra dos Carajás, Brazil: Archean continental volcanism and rifting. **Precambrian Research**, v. 42, n. 3–4, p. 229–254, 1989.

PADUANO, G. M. et al. A Vegetation and Fire History of Lake Titicaca since the Last Glacial Maximum. **Palaeogeography, Palaeoclimatology, Palaeoecology**, v. 194, p. 259–279, 2003.

PENA, L. D. et al. EI Niño-Southern Oscillatio*n*-like variability during glacial terminations and interlatitudinal teleconnections. **Paleoceanography**, v. 23, n. 3, p. 1–8, 2008.

PEREIRA, J. B. D. S. et al. Two New Species of Isoetes (Isoetaceae) from northern Brazil. **Phytotaxa**, v. 272, n. 2, p. 141–148, 2016.

PESSENDA, L. C. R. et al. The carbon isotope record in soils along a forest-cerrado ecosytem transect: implications for vegetation changes in the Rondonia state, southwestern Brazilian Amazon region. **The Holocene**, v. 8, n. 5, p. 599–603, 1998a.

PESSENDA, L. C. R. et al. 14 C Dating and Stable Carbon Isotopes of Soil Organic Matter in Forest–Savanna Boundary Areas in the Southern Brazilian Amazon Region. **Radiocarbon**, v. 40, n. 2, p. 1013–1022, 1998b.

PESSENDA, L. C. R. et al. The evolution of a tropical rainforest/grassland mosaic in southeastern Brazil since 28,000 14C yr BP based on carbon isotopes and pollen records. **Quaternary Research**, v. 71, n. 3, p. 437–452, 2009.

PETERSON, L. C. et al. Rapid Changes in the Hydrologic Cycle of the Tropical Atlantic During the Last Glacial. **Science**, v. 290, n. 5498, p. 1947–1951, 2000.

PETIT, J. R. et al. Climate and atmospheric history of the past 420,000 years from the Vostok ice core, Antarctica The recent completion of drilling at Vostok station in East. **Nature**, v. 399, p. 429–436, 1999.

PEZZI, L. P.; CAVALCANTI, I. F. A. The relative importance of ENSO and tropical Atlantic sea surface temperature anomalies for seasonal precipitation over South America: a numerical study. **Climate Dynamics**, v. 17, n. 2–3, p. 205–212, 2001.

PHILANDER, S. G. H. El Nino Southern Oscillation phenomena. **Nature**, v. 302, p. 295–301, 1983.

POWER, M. J. et al. Changes in fire regimes since the last glacial maximum: An assessment based on a global synthesis and analysis of charcoal data. **Climate Dynamics**, v. 30, n. 7–8, p. 887–907, 2008.

PYNE, S. J.; ANDREWS, P. L.; LAVEN, R. D. **Introduction to wildland fire**. New York: Wiley, 1996.

RACZKA, M. F.; BUSH, M. B.; DE OLIVEIRA, P. E. The collapse of megafaunal populations in southeastern Brazil. **Quaternary Research**, v. 89, p. 103–118, 2018.

RÄMÖ, O. T. et al. 1.88 Ga Oxidized A-Type Granites of the Rio Maria Region, Eastern Amazonian Craton, Brazil: Positively Anorogenic! **The Journal of Geology**, v. 110, n. 5, p. 603–610, 2002.

REIMER, P. J. et al. IntCal13 and Marine13 Radiocarbon Age Calibration Curves 0–50,000 Years cal BP. **Radiocarbon**, v. 55, n. 4, p. 1869–1887, 2013.

REIS, L. S. et al. Environmental and vegetation changes in southeastern Amazonia during the late Pleistocene and Holocene. **Quaternary International**, v. 449, p. 83–105, 2017.

ROBINSON, C. Lago Grande di Monticchio, southern Italy: a long record of environmental change illustrated by sediment geochemistry. **Chemical Geology**, v. 118, n. 1-4, p. 235-254, 1994.

ROUBIK, D. W.; MORENO, J. E. **Pollen and spores of Barro Colorado Island**. St. Louis: Missouri Botanical Garden, 1991.

SADORI, L.; GIARDINI, M. Charcoal analysis, a method to study vegetation and climate of the Holocene: The case of Lago di Pergusa (Sicily, Italy). **Geobios**, v. 40, n. 2, p. 173–180, 2007.

SAHOO, P. K. et al. Use of multi-proxy approaches to determine the origin and depositional processes in modern lacustrine sediments: Carajás Plateau, Southeastern Amazon, Brazil. **Applied Geochemistry**, v. 52, p. 130–146, 2015.

SAHOO, P. K. et al. Geochemistry of upland lacustrine sediments from Serra dos Carajás Southeastern Amazon , Brazil : Implications for catchment weathering , provenance , and sedimentary processes. **Journal of South American Earth Science**, v. 72, p. 178–190, 2016a.

SAHOO, P. K. et al. Influence of seasonal variation on the hydro-biogeochemical characteristics of two upland lakes in the Southeastern Amazon, Brazil. **Anais da Academia Brasileira de Ciências**, v. 88, n. 4, p. 2211–2227, 2016b.

SAHOO, P. K. et al. Limnological characteristics and planktonic diversity of five tropical upland lakes from Brazilian Amazon. **Annales de Limnologie - International Journal of Limnology**, v. 53, p. 467–483, 2017.

SAHOO, P. K. et al. Statistical analysis of lake sediment geochemical data for understanding surface geological factors and processes: An example from Amazonian upland lakes, Brazil. **Catena**, v. 175, p. 47–62, 2019.

SALATI, E. et al. Recycling of water in the Amazon Basin: An isotopic study. **Water Resources Research**, v. 15, n. 5, p. 1250–1258, 1979.

SCHNEIDER, T.; BISCHOFF, T.; HAUG, G. H. Migrations and dynamics of the intertropical convergence zone. **Nature**, v. 513, p. 45-53, 2014.

SCHNURRENBERGER, D.; RUSSELL, J.; KELTS, K. Classification of lacustrine sediments based on sedimentary components. **Journal of Paleolimnology**, v. 29, n. 2, p. 141–154, 2003.

SIFEDDINE, A. et al. La sédimentation lacustre indicateur de changements des paléoenvironnements au cours des 30 O00 dernières années (Caraias, Amazonie, Brésil). **Académie des Sciences de Paris**, v. 318, p. 1645–1652, 1994.

SIFEDDINE, A. et al. Variations of the Amazonian rainforest environment: A sedimentological record covering 30,000 years. **Palaeogeography, Palaeoclimatology, Palaeoecology**, v. 168, n. 3–4, p. 221–235, 2001.

SILVA JÚNIOR, R. O. DA et al. Three decades of reference evapotranspiration estimates for a tropical watershed in the eastern Amazon. **Anais da Academia Brasileira de Ciências**, v. 89, n. 3, p. 1985–2002, 2017. Suplemento.

SILVA, M. F. F. Análise florística da vegetação que cresce sobre canga hematítica em Carajás - Pará (Brasil). **Boletim do Museu Paraense Emílio Goeldi**, v. 7, n. 1, p. 79–105, 1991.

SKIRYCZ, A. et al. Canga biodiversity, a matter of mining. **Frontiers in Plant Science**, v. 5, p. 653-6661, 2014.

SOUZA, E. B. DE et al. Precipitação sazonal sobre a Amazônia oriental no período chuvoso: observações e simulações regionais com o RegCM3. **Revista Brasileira de Meteorologia**, v. 24, n. 2, p. 111–124, 2009.

STEVENSON, J.; HABERLE, S. **Macro Charcoal Analysis**: A modified technique used by the Department of Archaeology and Natural History. Canberra, ACT: PalaeoWorks, Department of Archaeology & Natural History, 2005. (PalaeoWorks Technical Report, 5). Disponível em: <http://palaeoworks.anu.edu.au/paltr05.pdf>. Acesso em: 29 jan. 2018.

STOCKMARR, J. Tablets with spores used in absolute pollen analysis. **Pollen et Spores**, v. 13, p. 615–621, 1971.

STUIVER, M.; POLACH, H. A. Discussion: Reporting and calibration of 14C data. **Radiocarbon**, v. 19, n. 3, p. 355–363, 1977.

STUTE, M. et al. Cooling of Tropical Brazil (5° C) during the Last Glacial Maximum. **Science**, v. 269, n. 5222, p. 379–383, 1995.

TAKIGIKU, R. et al. Primary and secondary controls on carbon-isotopic compositions of sedimentary organic matter. **Developments in Geochemistry**, v. 6, p. 3–14, 1991.

TAVARES, A. L. et al. Climate indicators for a watershed in the eastern Amazon. **Revista Brasileira de Climatologia**, v. 23, n. 6, p. 389-410, 2018.

TOLU, J. et al. Spatial variability of organic matter molecular composition and elemental geochemistry in surface sediments of a small boreal Swedish lake. **Biogeosciences**, v. 14, p. 1773–1792, 2017.

TURCQ, B. et al. Amazonia Rainforest Fires: A Lacustrine Record of 7000 Years. **Ambio**, v. 27, n. 2, p. 139–142, 1998.

VAN DER HAMMEN, T.; HOOGHIEMSTRA, H. Neogene and Quaternary history of vegetation, climate, and plant diversity in Amazonia. **Quaternary Science Reviews**, v. 19, p. 725–742, 2000.

VAN LOON, J. C. et al. **Analytical methods for geochemical exploration**. New York: Elsevier, 1989. chap. 9, p. 292–317: Biogeochemical analysis.

VON DEIMLING, T. S. et al. How cold was the last Glacial maximum? **Geophysical Research Letters**, v. 33, n. 14, p. 1–5, 2006.

WAGNER, B. et al. Understanding past climatic and hydrological variability in the Mediterranean from Lake Prespa sediment isotope and geochemical record over the Last Glacial cycle. **Quaternary Science Reviews**, v. 66, p. 123–136, 2013.

WALKER, R. G.; JAMES, N. P. **Facies models**: response to sea level change. Newfoundland St. John's: Geological Association of Canada, 1992.

WANG, X. et al. Wet periods in northeastern Brazil over the past 210 kyr linked to distant climate anomalies. **Nature**, v. 432, p. 740–743, 2004.

WANG, X. et al. Interhemispheric anti-phasing of rainfall during the last glacial period. **Quaternary Science Reviews**, v. 25, p. 3391–3403, 2006.

WANG, X. et al. Millennial-scale precipitation changes in southern Brazil over the past 90,000 years. **Geophysical Research Letters**, v. 34, n. 23, p. 1–5, 2007.

WANG, X. et al. Hydroclimate changes across the Amazon lowlands over the past 45,000 years. **Nature**, v. 541, n. 7636, p. 204–207, 2017.

WANG, Y. J. et al. A high-resolution absolute-dated late Pleistocene Monsoon record from Hulu Cave, China. **Science**, v. 294, n. 5550, p. 2345–2348, 2001.

YOON, J.-H.; ZENG, N. An Atlantic influence on Amazon rainfall. **Climate Dynamics**, v. 34, p. 249–264, 2010.

ZANIOLO, S. R. **Ecologia de Hedyosmum brasiliense Mart. ex Miq. (Chloranthaceae):** subsídio para cultivo e manejo sustentável. 2002. 99 p. Tese (Doutorado em Ciências) –

Departamento de Fitotecnia e Fitossanitarismo, Universidade Federal do Paraná, Curitiba, 2002.

3. MOLECULAR AND ISOTOPIC ($\delta^{13}C$, δD) COMPOSITION OF PLANT WAXES RECORDS HYDROCLIMATE AND VEGETATION CHANGES IN THE SOUTHEASTERN AMAZONIA

Abstract

Qualitative data based on pollen data have been widely applied in environmental reconstruction studies with climate inferences within the Amazon Basin, meanwhile, detailed information regarding hydroclimate changes is quite scarce. Based on molecular (plant wax lipids), carbon and hydrogen isotopic records of *n*-fatty acids from Lake Amendoim, we show no replacement of the forest by savanna, although relevant hydrological changes took place in the study site over the last ~22 ka. Enriched plant wax $\delta^{13}C$ and δD values together with the high abundance of montane savanna and cool-adapted taxa indicate mixed C_3/C_4 community between the Last Glacial Maximum (LGM, ~22-18 ka) and Late Glacial, under cooler and less humid conditions compared to modern levels. Within the Holocene, depleted δD values and progressive increase in the C_3-dominated forest community points to increased humidity and warmer conditions. The low correlation between plant wax $\delta^{13}C$ and δD from Lake Amendoim reveals the minor influence of vegetation composition on δD signature, being highly influenced by rainfall amount and moisture source instead. Overall, our study highlights that beyond changes in precipitation amount, fluctuations in regional temperature have played an important role in plant community composition and distribution in the Serra dos Carajás, southeastern Amazonia.

Keywords: Amazon basin, Paleohydroclimate, Plant-wax biomarkers, Pollen data

3.1. Introduction

The relevance of the Amazon rainforest to global environmental and climate issues is linked to its ability to retain large amounts of carbon from the atmosphere – one of its greatest contributions to mitigate climate change – and due to its enormous biodiversity, between 6,000 and 16,000 species (CARDOSO et al., 2017), that provides important ecosystem services such as water availability, cycling nutrients, protecting and reducing soil erosion, regulating the temperature, and maintaining the water cycle by returning water to the atmosphere via evapotranspiration (ELLISON et al., 2017; KUNERT et al., 2017; PONTES et al., 2019). Evapotranspiration from the Amazon Basin contributes between 25% and 40% of the annual precipitation in the eastern and western sub-regions (ELTAHIR; BRAS, 1994; VAN DER ENT et al., 2010), and up to 20% of the total annual precipitation over the La Plata Basin, (MARTINEZ; DOMINGUEZ, 2014; ZEMP et al., 2014).

Over the past 60,000 years, glacial and interglacial cycles led to considerable hydroclimate changes over the globe associated with fluctuations in atmospheric CO_2 levels (BARNOLA et al., 1987), ice-sheet cover (CLARK et al., 2009; CLARK; MIX, 2002), sea surface temperature (SST) (RAHMSTORF, 2002) as well as summer insolation (CRUZ et al., 2005). In the Amazon Basin, paleoclimatic studies reported a cooling of 3 to 5°C (COLINVAUX et al., 1996; PADUANO et al., 2003; STUTE et al., 1995; and references therein) during the Last Glacial Maximum (LGM) (26-18 ka; CLARK et al., 2009), which caused changes in plant community distribution such as the incursion of cool-adapted species (e.g. *Podocarpus*, *Alnus*, *Hedyosmum*) from Andean highlands into Amazonian lowland (COHEN et al., 2014; COLINVAUX et al., 1996; REIS et al., 2017).

In the eastern Amazonia, some studies mostly based on pollen records reported the replacement of ombrophylous forest by savanna in response to lower precipitation amount during LGM (ABSY et al., 1991; HERMANOWSKI et al., 2012). Similarly, speleothem records from Paraíso cave, southeastern Amazonia, indicated drier conditions in the eastern edge marked by a decrease in rainfall amount of 58% compared to modern levels (WANG et al., 2017). Although there was a decrease in convective activity and probably plant transpiration due to lower temperature (REIS et al., 2017), previous studies suggested that the rainforest persisted throughout the time (BUSH et al., 2004; COLINVAUX; OLIVEIRA, 2000; WANG et al., 2017).

Over the last decades, several studies have been conducted across Amazon basin in order to assess information about past environmental and vegetation cover changes during the Late Quaternary (BURBRIDGE; MAYLE; KILLEEN, 2004; BUSH et al., 2004; COHEN et al., 2014; COLINVAUX et al., 1996; D'APOLITO; ABSY; LATRUBESSE, 2013; PESSENDA et al., 2009; VAN DER HAMMEN; ABSY, 1994; and references therein). However, there is no broad consensus about climatic conditions over Amazonian lowlands, and robust data regarding changes in precipitation amount throughout the most relevant climate events in the northern hemisphere such as LGM, Heinrich Stadial (HS), and Holocene Thermal Maximum (HTM). Understanding past climate change and identifying its effects on environmental dynamics as well as on the distribution of vegetation is of great importance in the development of future projections. Thus, assessing such environmental changes has major implications for decision-making and the establishment of public policies.

In order to address the question of humidity variation in South America (CRIVELLARI et al., 2018; HÄGGI et al., 2017; JACOB et al., 2007), compound-specific deuterium/hydrogen (D/H) ratios of sedimentary biomarkers have been increasingly used as palaeohydrological proxies over a range of geological timescales (SACHSE et al., 2012; SCHEFUSS; SCHOUTEN; SCHNEIDER, 2005).

Lipid compounds derived from leaf waxes of vascular land plants such as *n*-alkanes and *n*-fatty acids, especially those with long-chain of carbons (e.g. $>C_{20}$), are slightly modified in natural archives (KUNST; SAMUELS, 2003). This makes *n*-alkanes and *n*-fatty acids valuable tools for determining OM sources, i.e. terrestrial and/or aquatic plants (AZIZUDDIN et al., 2014; FICKEN et al., 2000; LAVRIEUX et al., 2012; MEYERS; ISHIWATARI, 1993; and references therein).

Nevertheless, hydrocarbons may undergo some selective diagenesis during and after sedimentation (KAWAMURA; ISHIWATARI; OGURA, 1987; MEYERS; LEENHEER; BOURBONNIERE, 1995) that can be used to infer general processes that may affect lacustrine OM deposits, e.g. diagenetic processes (MEYERS; ISHIWATARI, 1993), and their preservation level (BADEWIEN; VOGTS; RULLKÖTTER, 2015; HO; MEYERS, 1994; HOU et al., 2006).

The distribution of *n*-alkanes (primarily odd-numbered C_{15}-C_{35})/fatty acids (primarily even-numbered C_{16}-C_{34}) (CHIKARAISHI; NARAOKA; POULSON, 2004; MEYERS; TAKEUCHI, 1979) vary among vascular land plants, macrophytes, and algae (CRANWELL, 1973; DIEFENDORF et al., 2011; FICKEN et al., 2000). Terrestrial plants which include several C_4 and C_3 plants tend to have higher concentrations of longer chain *n*-alkanes/fatty

acids (>C_{23}) (CRANWELL, 1973; HOU et al., 2006; RIELEY; COLLIER; JONES, 1991; ROMMERSKIRCHEN et al., 2006; VOGTS et al., 2016), which provides greater protection against higher exposure to ultraviolet radiation and mechanical damage to leaf cells among other functions (EGLINTON; HAMILTON, 1967; KUNST; SAMUELS, 2003). Meanwhile, shorter (<C_{21}) and Mid- (C_{22}-C_{25}) chain *n*-alkanes/fatty acids have been reported to be mainly synthesized by algae and macrophytes, respectively (AZIZUDDIN et al., 2014; FICKEN et al., 2000).

The environmental water (e.g. precipitation, soil water) is the primary hydrogen source of photosynthesizing organisms and their biosynthetic products (SACHSE et al., 2012). Since precipitation is the most important source of hydrogen for most terrestrial plants, leaf waxes δD values of *n*-alkanes/fatty acids from soils and sediments are strongly correlated with precipitation δD values (CRAIG, 1961). Thus, the original isotopic composition of the water used during leaf waxes biosynthesis can be recorded and preserved for over millions of years, providing information about past hydrologic changes (LIU; LIU; AN, 2015).

Environmental and geological factors also control the hydrogen isotopic composition of the water (DANSGAARD, 1964). The rainfall δD for a given region is highly dependent on the δD of the source water (the ocean), isotopic effects due to temperature and latitude, continentality (Figure 1) and altitude as well as the amount of rainfall and its seasonality. Besides environmental factors such as precipitation, evapotranspiration, relative humidity (RH), and light intensity (FARQUHAR; EHLERINGER; HUBICK, 1989; LIU; LIU; AN, 2015 and references therein), physiological factors including plant life forms (e.g. trees, shrubs, and grasses) (DUAN; HE, 2011; VOGTS et al., 2009), photosynthetic and biosynthetic pathway also exert a strong control over leaf wax δD signature (COLLISTER et al., 1994; SMITH; FREEMAN, 2006).

In addition to these factors, recycling moisture which consists on the contribution of evaporation within a region to precipitation in that same region (ELTAHIR; BRAS, 1994), may exert certain influence on isotopic composition of precipitation (MAYR et al., 2018; SALATI et al., 1979). According to Van Der Ent (2010), it is estimated that about 50-60% of all the rain that falls into the Amazon basin is contributed by evaporation within the basin. The contribution of recycling increases westward and southward and can lead to heavier isotopic signature due to the presence of evapotranspirated water (KURITA; YAMADA, 2008). In the south-western region, more than 50% of the precipitation comes from moisture recycling, while in the eastern region it contributes with only 16% of the rainfall amount (ELTAHIR; BRAS, 1994; LETTAU; LETTAU; MOLION, 1979). Regarding the Amazon

basin, a large amount of its moisture comes from the Atlantic Ocean although an important part of the basin's precipitation consists of recycled moisture (GAT; MATSUI, 1991; SALATI et al., 1979) that will be recorded by plant waxes – leading to smaller continental gradients and more positive values.

Thus, considering the valuable potential of compound-specific $\delta^{13}C$ and δD isotope analysis (CSIA) as vegetation source and paleohydrological proxy, here we present the first molecular, carbon and hydrogen isotopic records of *n*-fatty acids combined with pollen data from Lake Amendoim. The combination of CSIA and pollen data will provide us valuable information to address questions about major control factors over leaf wax δD variability.

Figure 1 – Map of South American continent with sites cited in the text and the mean January precipitation (mm/month, using the 1981-2010 base period). The grey star indicates the location of Carajás (Lake Amendoim); 1- French Guiana (marine core GeoB16224-1) (HÄGGI et al., 2017); 2- Lake Pata (BUSH et al., 2004; D'APOLITO; ABSY; LATRUBESSE, 2013); 3- Paraíso Cave (WANG et al., 2017); 4- Lake Saci (FONTES et al., 2017); 5- Madre de Dios River (FEAKINS et al., 2018); 6- Lake Titicaca (FORNACE et al., 2014); 7,8- Laguna Chaplin/ Laguna Bella Vista (MAYLE; BURBRIDGE; KILLEEN, 2000); 9- Laguna La Gaiba (FORNACE et al., 2016); 10- Botuverá Cave (CRUZ et al., 2005); 11- Lake Caçó (JACOB et al., 2007). Color types refer to the marine core (blue), pollen (grey), stable isotope analysis of plant waxes (orange), and speleothem (yellow) records (Source: http://iridl.ldeo.columbia.edu/)

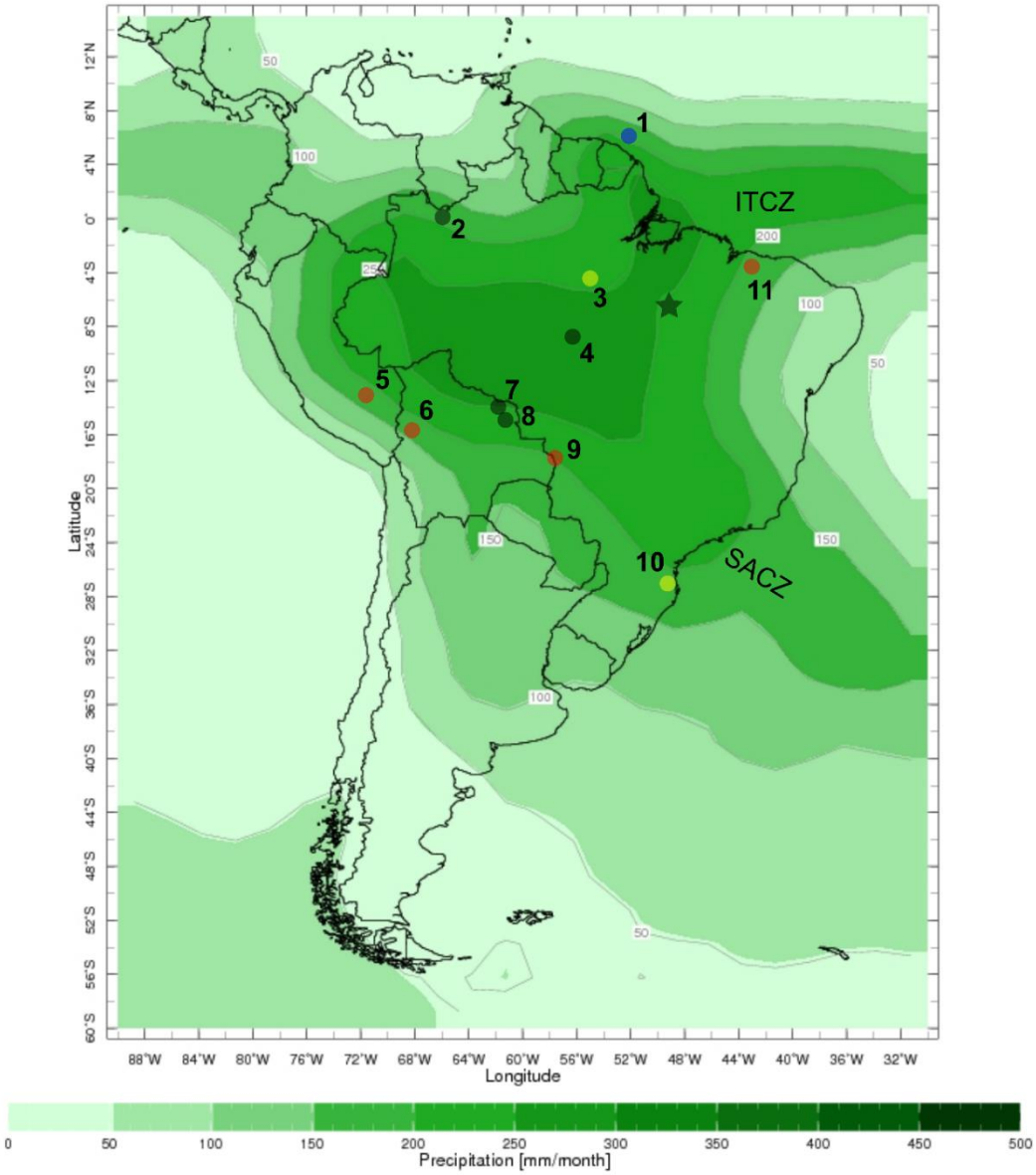

3.2. Study site

Lake Amendoim is an active lake located in Serra Sul de Carajás (Figure 2; 6°25'0" S – 6°20'0" S e 50°25'0" W - 50°17'30" W), southeastern Amazonia, formed by structural processes and degradation of the lateritic profile (MAURITY; KOTSCHOUBEY, 1995). It lies at an altitude of ca. 710-720 m above mean sea level (a.m.s.l.), with a surface area of 1.23 km^2, and a maximum water depth of ca. 8 m.

The lake level is controlled by precipitation, and can vary by ± 2 m (SAHOO et al., 2016). The water column remains throughout the year relatively homogeneous, poorly stratified (SAHOO et al., 2017). Lake Amendoim can be classified as ultra-oligotrophic to oligotrophic, with low chlorophyll content (<1 μg/L), low pH (4.02-6.71), dissolved oxygen between 7.05 and 7.6 mg/L, low total organic carbon (1.20-3.10 mg/L) and total phosphorus <20 μg/L (SAHOO et al., 2016).

Vegetation cover

Serra Sul plateau lies within the domain of the ombrophylous forest phytophysiognomies, subdivided into dense (montane, sub-montane) and open (sub-montane) ombrophylous forest. The dense ombrophylous forests are mainly represented by Fabaceae, Moraceae and Sapotaceae and occur on deeper soils at the slopes of the plateau. Meanwhile, the open ombrophylous forests occur on steep slopes, with a predominance of lianas and/or palms. Seasonal deciduous forests occur in the middle of the ombrophylous forest, merged into different communities. Over ferruginous crust at the top of the plateau, "*Campos rupestres*" (SILVA, 1991) occurs with a predominance of herbaceous-shrub species (NUNES et al., 2015; SKIRYCZ et al., 2014). The lake bottom in turn is largely colonized by macrophytes, including *Isoetes cangae* J.B.S. Pereira, Salino & Stützel (PEREIRA et al., 2016).

Climate

The regional climate is tropical monsoon (ALVARES et al., 2013), with rainy season from November to May, and dry season from June to October (LOPES; DE SOUZA; FERREIRA, 2013). The total mean annual rainfall range between 1310 and 1568 mm during the rainy season and from 159 to 321 mm during the dry season (SILVA JÚNIOR et al., 2017a; 2017b). Figure 3 shows monthly precipitation amount (mm/month) and its δ^2H signature throughout the year for Belém, the closest GNIP station to Carajás. The average

temperature is 27°C, with minimum (January) and maximum (September) mean temperatures of 26.6°C and 28.1°C, respectively (TAVARES et al., 2018).

Seasonal and annual rainfall variability in the Amazon basin is linked to the South American Summer Monsoon (SASM) (LIEBMANN; MECHOSO, 2011). The SASM is strongly influenced by two important meteorological systems, the South Atlantic Convergence Zone (SACZ) and the Intertropical Convergence Zone (ITCZ) (SCHNEIDER; BISCHOFF; HAUG, 2014). The migration of the ITCZ occurs seasonally over South America and the tropical Atlantic in response to changes in summer insolation and the southern SST gradient, reaching maximum latitude to the north (10°N) in August and the maximum latitude south of the equator (2°S) in March (NOBRE et al., 2012; NOBRE; SHUKLA, 1996). The SACZ, in turn, intensifies between November and February by the Low-Level Jets (LLJ) (MARENGO et al., 2004), which transports moisture from the tropical Atlantic Ocean to the western Amazon and the adjacent Andes, flowing along the eastern flank of the Andes. Humidity crosses the Bolivian Amazon and later, reaches the southeast of Brazil, where the SACZ begins to form. Thus, the southward migration of the ITCZ and the intensification of the SACZ (between November and February) both contribute to the strengthening of the SAMS and to increased precipitation in the Amazon basin.

Figure 2 - Location of the study site. (a) Aerial view of the Serra Sul Plateau; (b) Vegetation cover of the Lake Amendoim catchment basin; (c) Bathymetric map of the lake and the location of the core AM3 (black star) (Adapted from SAHOO et al., 2016a)

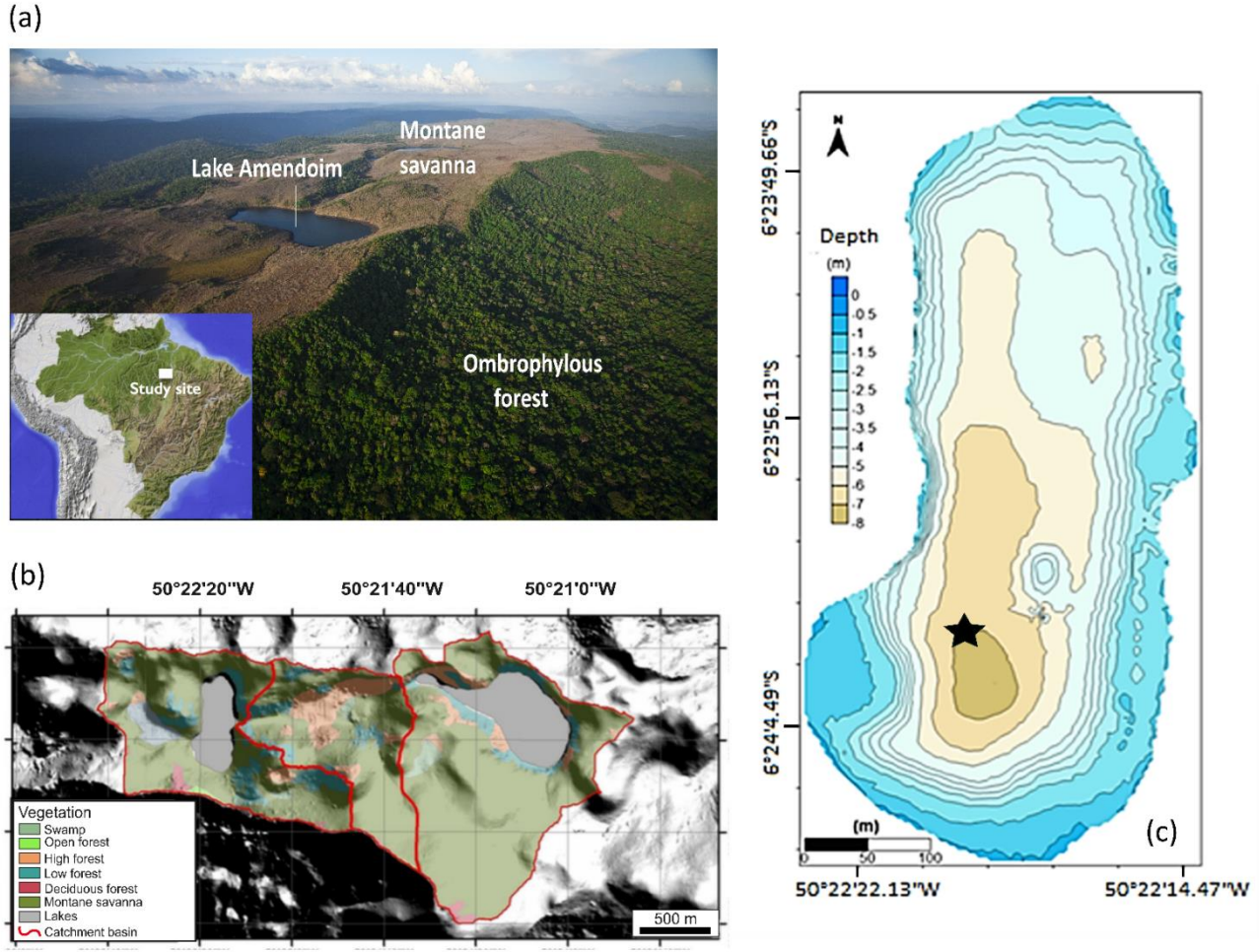

Figure 3 – Monthly average precipitation (mm, 1965-1987) and δ^2H signature (‰) for Belém station provided by Global Network of Isotopes in Precipitation (GNIP) (Source: https://nucleus.iaea.org/wiser/index.aspx).

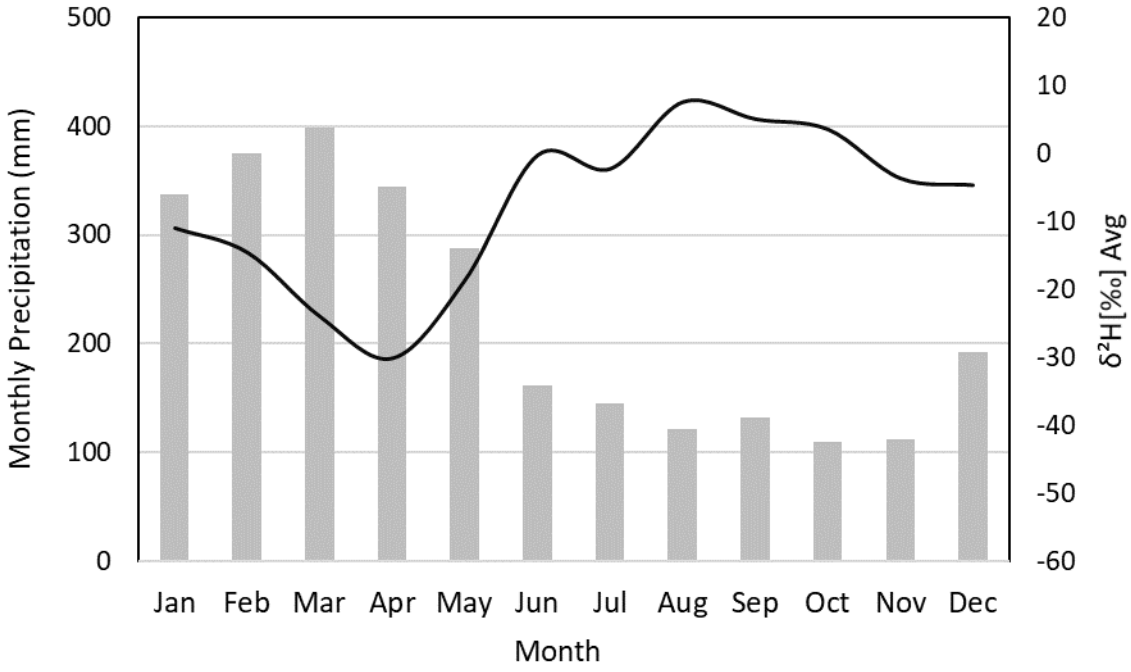

3.3. Material and Methods

Sampling

A 170 cm-long sedimentary core (AM3) was collected from Lake Amendoim (6°24'2.66"S/ 50°22'20.51"O) in July 2016 using a Livingstone sampler (LIVINGSTONE, 1955). Here we focus on the upper 82 cm, subsampled every 1 cm for molecular analysis. For Isotopic analysis, samples were chosen taking into account the periods of greatest interest, including climate events.

Sedimentary facies description

The description of sedimentary facies followed the proposal of Walker and James (1992), which includes descriptions of color, lithology, texture and sedimentary structures, besides the lake sediment classification system of the Global Lake Drilling Program (SCHNURRENBERGER; RUSSELL; KELTS, 2003).

Radiocarbon dating and age-depth model

Eleven bulk sediment samples (~2 g) were used for radiocarbon dating at the Beta Analytic facilities (Miami, FL, USA) by accelerator mass spectrometry (AMS). Radiocarbon ages are expressed as ^{14}C year BP normalized to a $\delta^{13}C$ of -25‰ VPDB (STUIVER; POLACH, 1977). The age-depth model was developed on Bacon (BLAAUW; CHRISTEN, 2011) using an R software package (R Development Core Team, 2013) as an interface and using the Intcal13.14c calibration dataset (REIMER et al., 2013).

Lipid extraction and purification

Approximately 2-3 g of freeze-dried sediments were mixed with an internal standard (5-α-Cholestane), and solvent extracted (three times) with a mixture of dichloromethane (DCM): methanol (MeOH) (9:1 *v/v*), under sonication (10 min) followed by centrifugation. Supernatants were gathered and the excess of solvent was removed under an N_2 stream. The total lipid extract (TLE) was transmethylated using BF_3 (Boron trifluoride): MeOH (2:1 *v/v*) at 80°C for 1 hour, in order to convert free fatty acids and esters into the corresponding fatty acids methyl esters (FAMEs) (LIU, 1994). The transmethylated TLE was recovered by partitioning with a Hexane: Ether (9:1 *v/v*) mixture and the elemental sulfur was removed with acid-activated copper (MECHLIŃSKA et al., 2012).

Fractionation

TLEs were fractionated by open silica gel (500 mg) column chromatography with solvent mixtures of increasing polarity. Elution with hexane, hexane: DCM (3:1 *v/v*) and DCM: MeOH (9:1 *v/v*) yielded a first fraction (F1) containing hydrocarbons, a second one (F2) containing FAMEs and a third fraction (F3) containing more polar compounds (e.g. hydroxylated compounds). Fractions 1 and 2 were dried and transferred to vials of 2 μL, and then kept frozen until further analyzes.

Instrumental analysis

FAMEs were analyzed on Agilent 6890 Plus gas chromatograph equipped with a CPSIL5 column (50 m length, 0.32 mm ID, 0.25 μm film thickness) and a flame ionization detector (GC-FID). The on-column injector was set to the "track column" mode of temperature and the detector was operated at 330°C. The oven temperature was maintained at 50°C (0 min), heated at 30 °C min^{-1} to 100°C, then raised to 310°C at a rate of 2°C min^{-1} and held at 310°C for 30 min. Helium was used as carrier gas at constant flow (2.5 mL min^{-1}).

Hydrocarbons, in turn, were analyzed on Agilent 6890N gas chromatography equipped with a DB5 column (30 m length, 0.32 mm ID, 0.25 μm film thickness) and flame ionization detector (GC-FID). The on-column injector was set to the "track column" mode of temperature and the detector was operated at 330°C. The oven temperature was maintained at 50°C (0 min), heated at 30°C min^{-1} to 120°C, then raised to 320°C at 5°C min^{-1} and held at 320°C for 20 min. Helium was used as carrier gas at constant flow (2.0 mL min^{-1}).

Identification and quantification

The identification of FAMEs and n-alkanes was based on GC retention time. Further verification was achieved by GC-MS analysis on Agilent 6890 gas chromatography coupled to an Agilent 5973N mass spectrometry detector (ionization energy = 70 eV, scanning mass range = m/z 50-800 at 3 scans/s). GC and GC-MS data were retrieved using the Agilent ChemStation software. The quantification of individual FAME and *n*-alkane compounds was performed by comparing their GC response (peak area) with that of an internal standard (5-α-Cholestane standard) added before analysis. Concentrations hereinafter are expressed in per gram of dry weight of sediment.

Isotopic analysis of hydrogen (δD) and carbon ($\delta^{13}C$)

Compound-specific stable carbon and hydrogen isotope composition of FAME were measured using an online continuous flow gas chromatograph Trace-GC-Ultra coupled with an Isotopic Ratio Mass Spectrometer Delta V Plus via combustion/Pyrolysis furnaces and conflow IV interface from Thermo Fischer Scientific (GC-HT/C-IRMS).

The GC was equipped with a split/splitless injector kept at 320°C, and fitted with a 60 m fused silica capillary column (DB-5MS, 0.25 mm inner diameter, 0.25 μm film thickness). The GC oven program starts at 80°C for 2 min and increases from 80 to 160°C at 10°C/min. The oven was kept at 160°C for 5 min and an increase from 160°C to 320°C at 3°C/min. Finally, the oven was kept at 320°C for 20 min. Helium was used as carrier gas at a constant flow of 2 $ml.min^{-1}$.

The accuracy and reproducibility of the GC-C/HT-IRMS measurements were accessed with a standard mixture of *n*-alkanes (C_{16} to C_{30}) purchase from Arndt Schimmelmann (Indiana University) of known $\delta^{13}C$ and δD isotopic composition. The *n*-alkane standard mixture (type A6) was injected three times at the beginning of each run and then once every three samples. Analytical mean standard deviation was of 0.4 ‰ (n = 62) and 4.2 ‰ (n = 62) for the ^{13}C and D/H measurements, respectively. The $\delta^{13}C$ are expressed in per mil (‰)

against the international standard VPDB (Vienna Pee Dee Belemnite) and the δD in per mil (‰) against VSMOW (Vienna Standard Mean Ocean Water) according to the equation 1. For D/H, the $H3^+$ factor was determined daily and the average value was 2.66 ± 0.02 ‰.

$$\delta D \text{ or } \delta^{13}C(R) = \left(\frac{R\ sample - R\ standard}{R\ standard}\right) \cdot 1000 \quad (1)$$

Where R is the ratio of $^2H/^1H$ or $^{13}C/^{12}C$ in the sample and standard.

The isotopic values of the samples were not corrected for the isotopic (H and C) values added by transmethylation. However, all samples were processed by reagent from the same batch, leading to a systematic error that enable to compare samples one to each other.

Data analysis

The odd-even feature of the carbon number from *n*-alkanes was evaluated by the Carbon Preference Index (CPI; BRAY; EVANS, 1961). This index is also a key parameter associated with *n*-alkanes sources (CRANWELL, 1973; EGLINTON et al., 1962) whether biogenic and/or petrogenic (COLLISTER et al., 1994; POYNTER et al., 1989). CPI values >3 indicates the predominance of terrestrial plant origin for *n*-alkanes, while low values (<3) may indicate degradation of the organic matter (CASTAÑEDA et al., 2009; HÄGGI et al., 2016; PANCOST; BOOT, 2004).

$$CPI_{25-33} = 1/2 \cdot ((\Sigma C_{25} - C_{33}/\Sigma C_{26} - C_{32}) + (\Sigma C_{25} - C_{33}/\Sigma C_{28} - C_{34}) \quad (2)$$

Average chain length (ACL) is the average number of carbon atoms of the *n*-alkanes (see Equation 3) and provides information regarding the dominant carbon chain (POYNTER et al., 1989). It can vary among different plant groups (e.g. C_3 and C_4), with longer chain lengths associated with savanna-dominated vegetation and shorter related to rainforest (BADEWIEN; VOGTS; RULLKÖTTER, 2015; ROMMERSKIRCHEN et al., 2006).

$$ACL_{25-33} = \frac{(25 \cdot nC_{25} + 27 \cdot nC_{27} + 29 \cdot nC_{29} + 31 \cdot nC_{31} + 33 \cdot nC_{33})}{(nC_{25} + nC_{27} + nC_{29} + nC_{31} + nC_{33})} \quad (3)$$

The ratio among long (C_{26}, C_{28}, C_{30}) and short-chain (C_{16}, C_{18}, C_{20}) *n*-fatty acids (Eq. 4) was applied to identify changes in terrestrial vs. aquatic contributions to lacustrine sediments (FANG et al., 2014)

$$TARfa = \frac{(C_{26} + C_{28} + C_{30})}{(C_{16} + C_{18} + C_{20})} \quad (4)$$

The composition diversity index (CDI) of *n*-fatty acids, which may represent changes in their sources was calculated following Equation 5. Higher (lower) values imply greater (reduced) diversity of plant-wax sources (MATSUDA; KOYAMA, 1977).

$$CDI = \frac{1}{\sqrt{\left(\left[\sum_{i=1}^{S}\left(\frac{X_i}{100}\right)^2\right]\right)}} \quad (5)$$

Where Xi is the percentage of each fatty acid based on total fatty acids isolated from the sediments and S is the number of varieties of fatty acids in a sample.

3.4. Results and Discussions

3.4.1. Facies descriptions and age-depth model

The ^{14}C dating and sedimentary facies descriptions are shown in Tables 1 and 2. Based on the age model (Figure 4), the upper ca 100 cm of the core AM3 records the last 35 ka. Sedimentation rates range from 0.01 to 0.08 mm $year^{-1}$. Lower sedimentation rates (0.01-0.03 mm $year^{-1}$) are observed between 35 and 23 ka, while higher sedimentation rates (0.03-0.08 mm $year^{-1}$) are recorded from 15 to 10,5 ka, except for a downward trend around 13 ka. After 10,5 ka, there is a gradual decrease in sedimentation rates, reaching minimum value (0.02 mm $year^{-1}$) around 7.4 ka.

The deeper part of the core, from 35 to 27 ka (100-85 cm), composed by laminated mud (M1), indicate deposition by suspension (GUIMARÃES et al., 2016); Between 100 and 85 cm a thick layer of siderite or iron carbonate ($FeCO_3$) nodules occurs. This marks a change in lake redox conditions around 27 ka, as these minerals precipitate under anaerobic conditions at the water-sediment interface (LEMOS et al., 2007). Between 15,8 and 14,7 ka (60-50 cm), mud and peat (P/M) intercalations occurred, which indicate variations in detrital input from the catchment basin to the lake basin. From 14,7 to 12 ka (50-35 cm), higher detrital input is evidenced by the laminated mud layer. This period is followed by another change in the redox conditions which led to another event of siderite precipitation around 12 ka, although less intense compared to the previous period. Finally, mud and peat (P/M) compose the upper part of the profile, which probably reflects alternations in the allochthonous and autochthonous OM input into the lake during the Holocene.

Table 1 - ^{14}C dating (AMS) and calibrated ages from core AM3 collected in the Lake Amendoim, Serra Sul de Carajás

Code	Sample ID	Pre-treatment material	$^{13}C/^{12}C$ (‰)	Age ^{14}C (yr BP*)	Cal. age, 2σ range (Cal yr. BP) **
LAB34700	AM3 4-5	Graphite	-25	1140 +/- 27	857-980 Cal AD***
LAB34699	AM3 7-8	Graphite	-25	1511 +/- 28	529-619 Cal AD
BETA445932	AM3 9-10	(organic sediment): acid washes	-26.8	6010 +/- 30	6940-6779
BETA445933	AM3 24-25	(organic sediment): acid washes	-24.5	9350 +/- 30	10665-10496
BETA445934	AM3 53-54	(organic sediment): acid washes	-20.5	12500 +/- 40	15057-14359
LAB41321	AM3 71-72	Graphite	-25	14510 +/- 47	15937-15562
LAB41322	AM3 86-87	Graphite	-25	25488 +/- 106	28041-27284
BETA445935	AM3 99-100	(organic sediment): acid washes	-22.3	31740 +/- 170	36077-35184

* BP – before present; ** Cal yr. BP – calibrated years before present; *** AD – Anno Domini

Table 2 - Summary of facies descriptions and sedimentary processes from core AM3

Facies	Description	Formation/Process	Sedimentation rate (mm yr^{-1})
Mud and peat (M/P)	Dark grayish brown (2.5Y 4/1) to black (5Y 2.5/1) mud. Some Yellow (5Y 7/8) to olive-yellow (5Y 6/8) spots are also present, besides clasts.	Equal periods of mud inflow from suspension and input of autochthonous organic matter under reduced conditions, which favored a higher degree of organic matter preservation.	0.02-0.08
Laminated mud (Ml)	Dark gray (5Y 4/1) to olive-gray (5R 5/2) mud.	Low energy flows with mud input from suspension into the lake basin and high preservation of organic matter.	0.01-0.08
Siderite mud (Ms)	Olive yellow (5Y 6/6) to Olive (5Y 5/4) mud, massive, oxidized, with yellow (5Y 7/8) to olive-yellow (5Y 6/8) spots. Besides, nodules of siderite and clasts are present. Mud is also a present forming an incipient matrix.	Siderite or $FeCO_3$ is an early diagenetic mineral, forming in pore waters close to the sediment-water boundary layer.	0.01-0.03

Figure 4 - Lithological profile of the core AM3 with the age model as a function of the depth calculated from the ^{14}C dating in R program

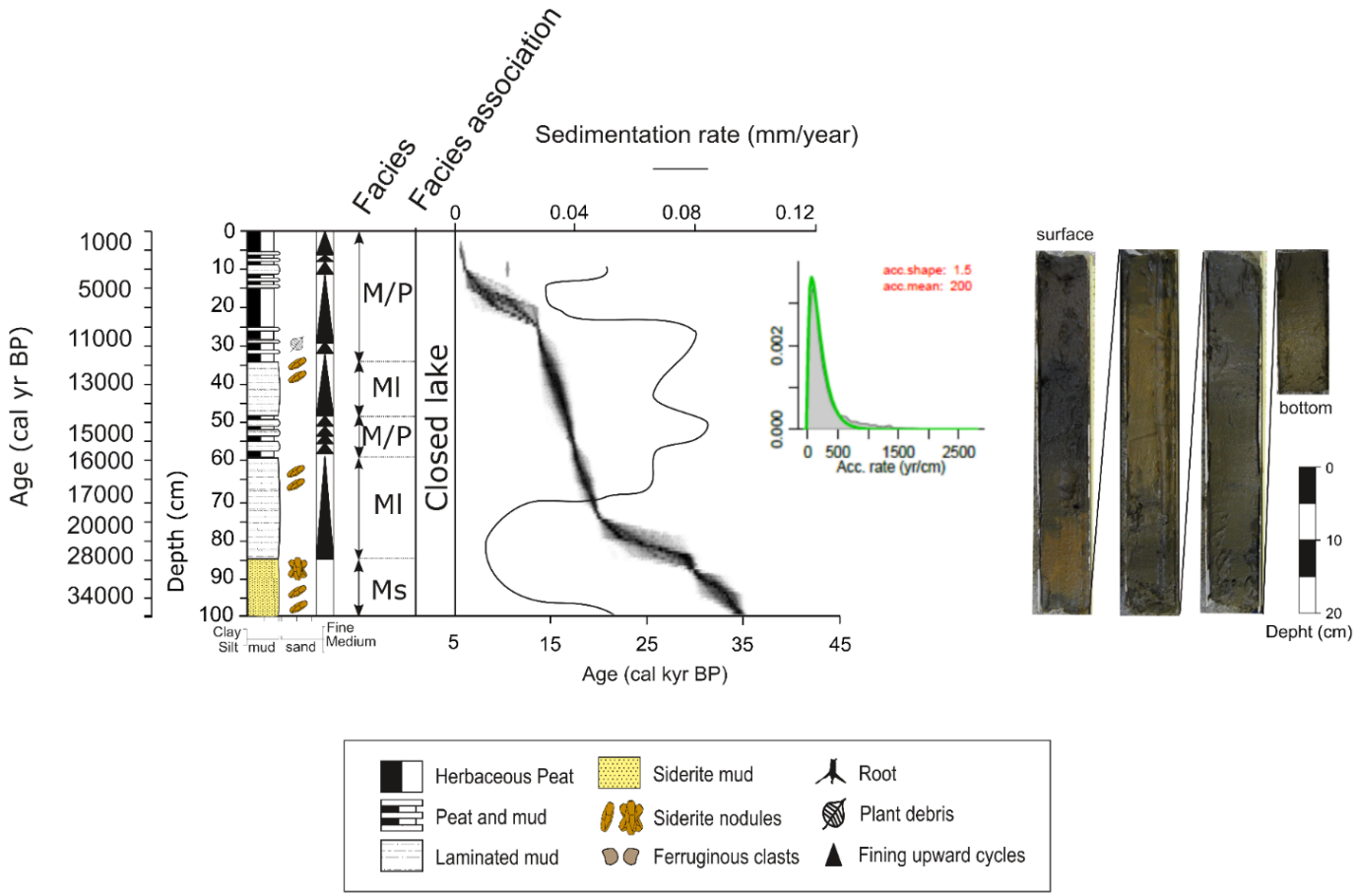

3.4.2. Plant waxes distribution and abundance

In core AM3, the *n*-alkane distributions range from C_{25} to C_{35} and show a strong odd-over-even-carbon-number predominance (Figure 5). Most of the samples showed similar distribution, maximizing at *n*-C_{31} or *n*-C_{29} (Table 3). The fatty acids methyl esters (FAME) distribution in turn range from C_{16} to C_{34} and are characterized by a clear even-carbon-number predominance (Figure 5), with *n*-C_{28} as the most abundant homologue. This distributional pattern remains unchanged throughout the core.

Total concentration of odd-numbered long-chain *n*-alkanes (ΣC_{25}-C_{35}) varies from 0.6 to 42 µg g^{-1} dry weight (DW) sediment (Table A.1). Short to Mid--chain (C_{17-23}) *n*-alkanes were not detected in samples. The total concentration of even-numbered (C_{16}-C_{34}) FAME ranges from 1.8 to 194 µg g^{-1} DW (Table A.2). The sum of the total concentration of short (C_{16}-C_{20}), Mid- (C_{22}-$_{24}$) and long-chain (C_{26}-C_{34}) *n*-fatty acids ranges from 0.5 to 22 µg g^{-1} DW, 0.2 to 16 ng g^{-1} DW, 1.0 to 155 µg g^{-1} DW, respectively.

Long-chain odd-carbon numbered *n*-alkanes (>C_{25}) and long-chain even-carbon numbered FAME (>C_{26}) are major components of epicuticular waxes from terrestrial plants (KOLATTUKUDY; WALTON, 1972; MEYERS; ISHIWATARI, 1993; RIELEY; COLLIER; JONES, 1991), while shorter-chain *n*-alkanes (C_{17}, $C_{19,}$ and C_{21}) and FAME (C_{16}, $C_{18,}$ and C_{20}) have been reported to mainly derived from algae and macrophytes (FICKEN et al., 2000), although short chain FAMEs are ubiquitous in living organisms (HUANG et al., 2004).

The CPI values for *n*-alkanes in sediment samples range from 2.9 to 4.6. The TARfa index can approximate changes in the terrestrial vs aquatic contributions to the sedimentary organic matter inside the lake. In core AM3, TARfa varies between1.2 and 8.8 (Table 3; Figure 6), stressing the predominance of terrestrial over aquatic sources during period with higher values.

Overall, the *n*-alkanes and FAME occurrence and distribution in core AM3 point to plant waxes as their primary sources. Thus, the sum of C_{25}-C_{33} *n*-alkanes (odd) and/or C_{26}-C_{34} FAME (even) can be used to infer temporal variations of terrestrial, higher plants input.

The chain length distribution, expressed by the ACL values (Table 3) for the plant wax *n*-alkanes (C_{25} to C_{33}) ranges from 29.4 to 30.6. Similar ranges were also reported for sediments from Amazon River tributaries (ACL 28.8-30.5) (HÄGGI et al., 2016) and for marine sediments from Amazon shelf (ACL 29.8-30.4) (HÄGGI et al., 2017). In soil sediments from Amazonian highlands, ACL (C_{27}-C_{33}) values ranged between 27.2 and 32.6 (FEAKINS et al., 2016, 2018). High minimum ACL values recorded in the Lake Amendoim

and river/marine sediments compared to highland soils may be explained by a tendency to longer chain length at a lower elevation (FEAKINS et al., 2016), while high maximum ACL values can be related to higher temperatures and/or greater contribution of C_4 plants.

Previous studies performed in ecotones (transition forest-savanna) from tropical Africa have reported that ACL values may increase from rainforest (29.8) to wood- and shrubland (30.4-31.0), and savanna (30.5-31.3) (BADEWIEN; VOGTS; RULLKÖTTER, 2015; ROMMERSKIRCHEN et al., 2006; VOGTS et al., 2012). This was also evidenced by Zhang et al. (2017) based on molecular analysis of modern plants from Tibetan Plateau, which showed lower ACL values for trees (26.7-26.8) than grasses (28.1-28.7). The ACL range found in core AM3 is consistent with pollen records from the same lake (core AM2) that show a greater abundance of montane savanna and forest formation (Figure 6).

Figure 5 –Total average concentration (µg g^{-1} DW) of odd-numbered (C_{17}-C_{35}) *n*-alkanes and even-numbered (C_{16}-C_{34}) FAME in all samples from core AM3

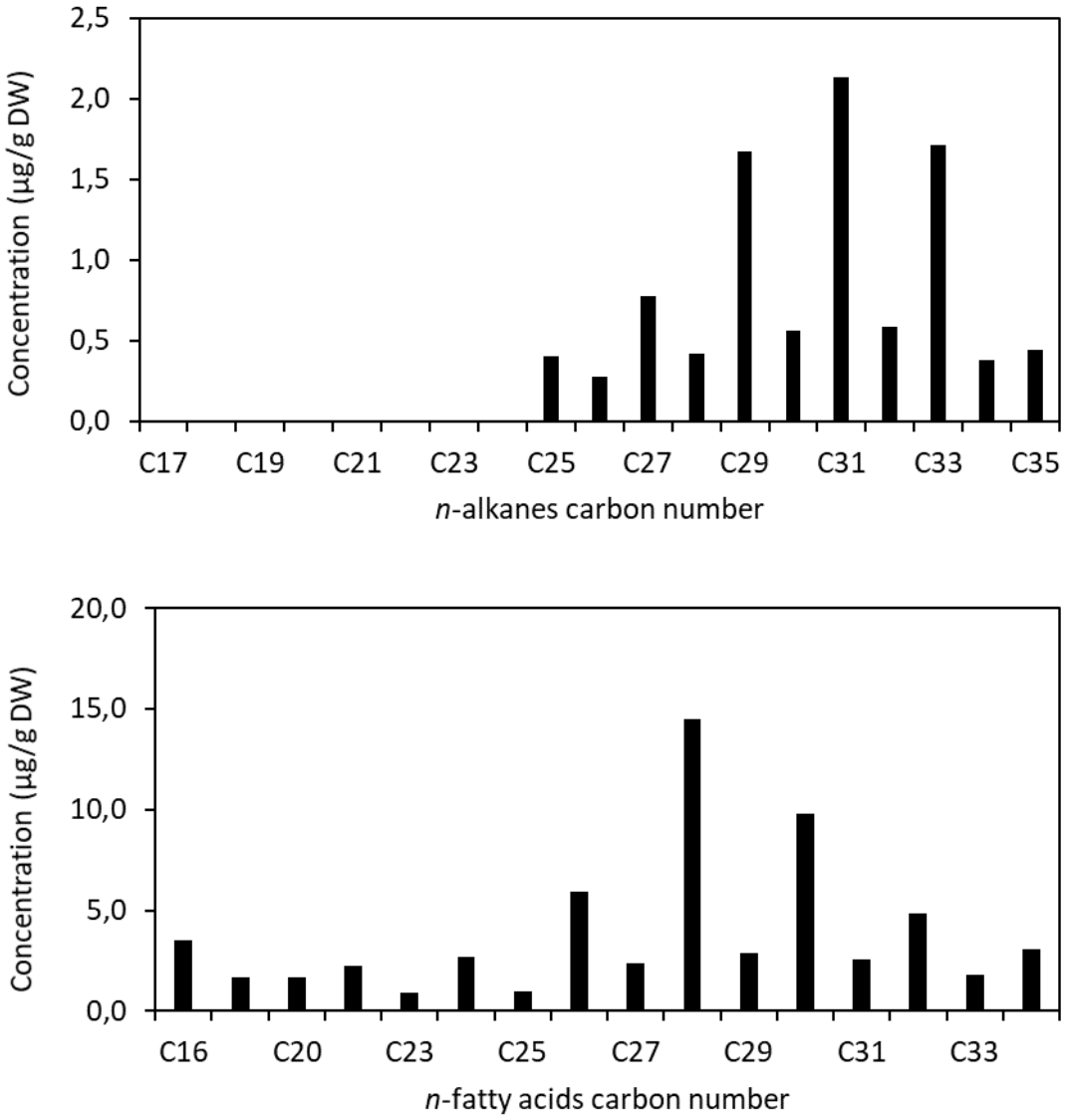

Table 3 – *n*-Alkanes and FAME distribution, Average Chain Length (ACL; C_{25}-C_{33}), Carbon Preference Index (CPI; C_{25}-C_{33}), Odd over even preference index (OEP; C_{27}-C_{33}), carbon number maximum (C_{max}) of *n*-alkanes, Terrestrial and aquatic ratio (TARfa), Composition Diversity Index (CDI) and C_{max} of *n*-fatty acids.

		n-alkanes			FAME			
AM3 ID Sample	Age (Cal yr. BP)	ACL C_{25}-C_{33}	CPI C_{25}-C_{33}	Cmax C_{25}-C_{33}	ACL C_{24}-C_{34}	TARfa	CDI	Cmax C_{16}-C_{34}
9	6846	29.8	3.1	C_{31}	28.8	2.9	3.4	C_{28}
10	7055	29.7	3.3	C_{31}	28.8	3.2	3.3	C_{28}
12	7453	29.7	3.2	C_{31}	28.8	2.7	3.3	C_{28}
13	7651	29.6	3.0	C_{31}	28.8	3.6	3.2	C_{28}
14	7849	30.2	3.2	C_{31}	29.0	4.4	3.1	C_{28}
15	8145	30.1	3.2	C_{31}	28.8	4.9	3.1	C_{28}
16	8463	30.2	3.3	C_{31}	28.8	5.6	2.9	C_{28}
17	8800	30.3	3.1	C_{31}	28.7	5.1	2.9	C_{28}
18	9096	30.4	3.4	C_{31}	28.8	5.3	2.8	C_{28}
19	9364	30.4	3.4	C_{31}	28.7	5.0	2.8	C_{28}
20	9611	30.4	3.4	C_{31}	28.8	4.7	2.8	C_{28}
21	9859	30.4	3.2	C_{31}	28.6	4.3	2.8	C_{28}
22	10107	30.5	3.4	C_{31}	29.0	5.3	2.9	C_{28}
23	10358	30.4	3.3	C_{31}	28.7	4.9	2.8	C_{28}
24	10612	30.4	3.6	C_{31}	28.8	5.4	2.8	C_{28}
25	10757	30.0	3.6	C_{31}	28.3	3.2	2.9	C_{28}
26	10887	29.8	4.6	C_{31}	28.8	6.2	2.6	C_{28}
27	11013	29.9	3.8	C_{29}	28.8	7.8	2.6	C_{28}
28	11139	29.6	4.5	C_{29}	28.8	6.8	2.6	C_{30}
29	11263	29.8	3.7	C_{29}	28.9	7.7	2.6	C_{30}
30	11413	29.8	3.8	C_{29}	28.9	5.6	2.8	C_{30}
31	11575	29.5	3.7	C_{29}	29.0	8.8	2.6	C_{30}
32	11733	29.8	3.9	C_{29}	29.0	6.4	2.8	C_{30}
33	11878	29.6	3.6	C_{29}	28.9	4.6	2.8	C_{30}
34	12006	29.9	4.1	C_{31}	28.9	5.9	2.8	C_{30}
35	12146	29.8	3.6	C_{31}	28.9	5.7	2.9	C_{28}
36	12307	30.0	3.9	C_{31}	29.0	4.5	3.0	C_{28}
37	12468	29.9	3.5	C_{31}	29.0	5.1	3.0	C_{28}
38	12620	30.1	3.5	C_{31}	28.9	4.1	3.2	C_{28}
39	12761	29.9	3.4	C_{31}	28.9	3.3	3.2	C_{28}
40	12915	30.0	3.5	C_{31}	28.9	3.3	3.3	C_{28}
41	13085	30.1	3.1	C_{31}	29.0	2.6	3.3	C_{28}
42	13246	30.1	3.5	C_{31}	28.9	3.3	3.3	C_{28}
43	13415	30.2	3.4	C_{31}	29.1	4.1	3.2	C_{28}
44	13563	30.4	3.9	C_{31}	29.0	3.9	3.3	C_{28}
45	13702	30.4	3.7	C_{31}	29.4	4.6	3.3	C_{28}

46	13845	30.6	3.9	C_{31}	29.4	2.7	3.4	C_{28}
47	13996	30.5	3.5	C_{31}	28.9	2.0	3.5	C_{28}
50	14426	30.4	3.5	C_{31}	29.3	2.6	3.3	C_{28}
52	14661	30.3	3.8	C_{31}	29.1	2.3	3.4	C_{28}
53	14794	30.4	3.7	C_{31}	29.3	4.1	3.2	C_{28}
54	14932	30.4	4.0	C_{31}	29.0	2.8	3.4	C_{28}
55	15094	30.4	3.8	C_{31}	29.2	3.5	3.2	C_{28}
56	15250	30.3	3.8	C_{31}	28.9	2.0	3.4	C_{28}
57	15387	30.4	3.6	C_{31}	29.3	3.0	3.2	C_{28}
58	15514	30.3	3.9	C_{31}	29.0	2.7	3.3	C_{28}
59	15649	30.3	3.7	C_{31}	29.2	2.9	3.2	C_{28}
60	15816	30.3	3.7	C_{31}	29.0	1.7	3.4	C_{28}
61	15998	30.2	3.3	C_{31}	29.3	1.5	3.3	C_{28}
62	16180	30.1	3.6	C_{31}	28.9	1.4	3.4	C_{30}
64	16521	30.3	3.4	C_{31}	29.0	1.7	3.4	C_{30}
65	16688	30.3	3.3	C_{31}	29.4	1.3	3.3	C_{30}
66	16857	30.0	3.7	C_{31}	28.9	1.6	3.4	C_{30}
67	17034	30.2	3.3	C_{31}	29.1	1.2	3.3	C_{16}
68	17209	30.1	3.7	C_{31}	28.8	1.5	3.4	C_{30}
69	17369	30.1	3.1	C_{31}	29.1	1.4	3.4	C_{30}
70	17535	29.8	3.9	C_{31}	29.1	1.3	3.4	C_{30}
71	17703	30.1	3.5	C_{31}	29.2	1.4	3.4	C_{30}
73	18061	30.1	3.7	C_{31}	29.1	1.6	3.3	C_{30}
74	18252	30.0	3.9	C_{31}	29.4	2.0	3.1	C_{30}
75	18993	30.0	3.8	C_{31}	29.2	1.7	3.3	C_{28}
76	19717	30.0	3.9	C_{31}	29.1	2.6	3.2	C_{28}
77	20447	30.0	3.4	C_{31}	29.3	1.9	3.2	C_{28}
78	21172	30.0	3.6	C_{31}	29.4	2.6	3.2	C_{28}
79	21901	30.1	3.2	C_{31}	29.4	2.8	3.2	C_{28}
80	22826	30.0	3.6	C_{31}	29.5	4.5	3.2	C_{28}
81	23763	30.1	3.1	C_{31}	29.3	2.8	3.1	C_{28}
82	24761	30.0	3.2	C_{31}	29.5	4.4	3.1	C_{28}

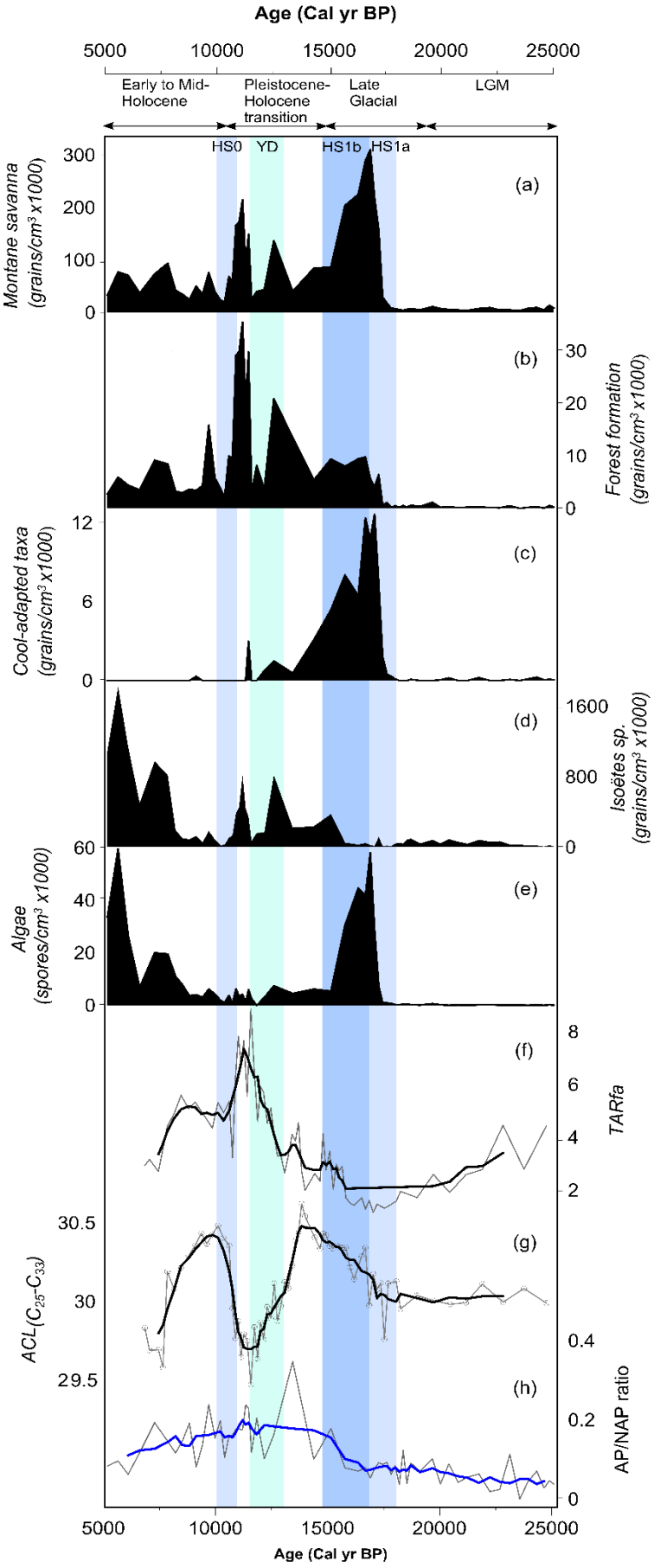

Figure 6 – Comparison between different ecological groups concentrations obtained from core AM2 (25 ka) in the Lake Amendoim and compound-specific indexes. (a) Montane savanna; (b) Forest formation; (c) Cool-adapted taxa; (d) Macrophytes; (e) Algae; (f) Terrestrial and aquatic ratio (TARfa); (g) ACL (*n*-C_{25}-C_{33}); (h) Arboreal pollen and non-arboreal pollen (AP/NAP) ratio from core AM2; Blue and gray bars delimit the range of the Heinrich Stadial and Younger Dryas Events. Filled lines in blue and black represent weighted-average values

Downcore distribution of plant wax lipids

Plant wax *n*-alkanes concentrations show a clear trend to higher values from LGM (0.8-2.2 µg g^{-1} DW) to Early Holocene (4.6-42 µg g^{-1} DW), followed by a considerable decrease from Early to Mid-Holocene (4.4-11 µg g^{-1} DW). Similarly, plant wax FAME concentrations reveal minimum and maximum values during the Late Glacial (2.9-12 ng g^{-1} DW) and Early Holocene (47-194 µg g^{-1} DW), respectively (Table A.1; Figure 7).

Regarding CPI values, a trend to higher values (3.1-3.9) is observed throughout the LGM, between 24 and 17,5 ka (Figure 8). This interval is followed by a sharp decrease in CPI values, reaching a minimum value of 3.1 during the Late Glacial, between 17,5 and 16,1 ka. From 16,1 ka, higher values (<3.3) are recorded with maximum (4.0) around 14,9 ka. Another decrease in CPI values occurs between 13,5 and 12,7 ka, which followed by a period (12,7-10,8 ka) with the highest values (3.5-4.6) of the core at the beginning of the Early Holocene. Finally, lower CPI values are observed from 10,8 ka to the Mid-Holocene.

The lowest TARfa (by 2.19 on average) are found between the LGM and Late Glacial, which correspond to the intervals with the lowest total concentration of wax lipids. A remarkable increase in TARfa is observed from Late Glacial (1.16-3.48) to the beginning of the Early Holocene (2.0-8.8), displaying a similar pattern observed in the CPI values along with the higher total concentration of plant wax *n*-alkanes. From the beginning of the Early Holocene, TARfa presents a gradual decrease, reaching a minimum value of 2.70 around 6,8 ka. This is highly associated with a decrease in the total concentration of *n*-alkanes and FAME, suggesting a lower contribution of plant waxes from terrestrial plants during this period.

The CDI index, in turn, vary from 2.58 to 3.53 (Table 3; Figure 8) with higher values (greater source diversity) from Late Glacial to the Pleistocene-Holocene transition, between 18 and 12,7 ka. Consistently, pollen data for this period show high concentrations of montane savanna, forest formation, cool-adapted taxa, and algae. Higher CDI values recorded between 17 and 16 ka may be also associated with the occurrence of post-depositional diagenetic processes (MATSUDA; KOYAMA, 1977) that led to siderite precipitation in Lake Amendoim, although less likely when considering pollen data.

Figure 7 – Boxplot with total concentrations (µg g^{-1} DW) of (a) odd-numbered *n*-alkanes (C_{25}-C_{35}) and (b) even-numbered FAME (C_{16}-C_{34}) through the last ~25 ka. Mid-_H: Mid-Holocene; Early_H: Early Holocene; P_H_trans: Pleistocene-Holocene transition; Late_G: Late Glacial; LGM: Last Glacial Maximum

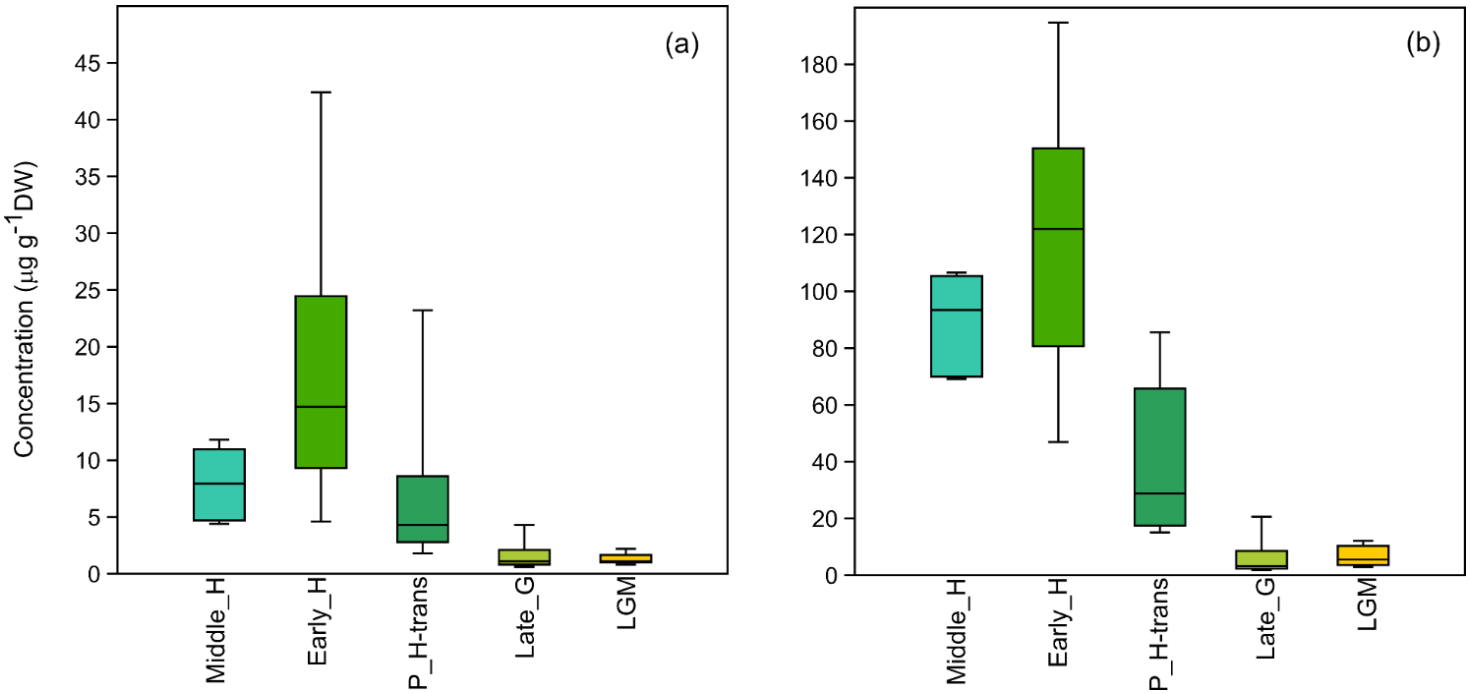

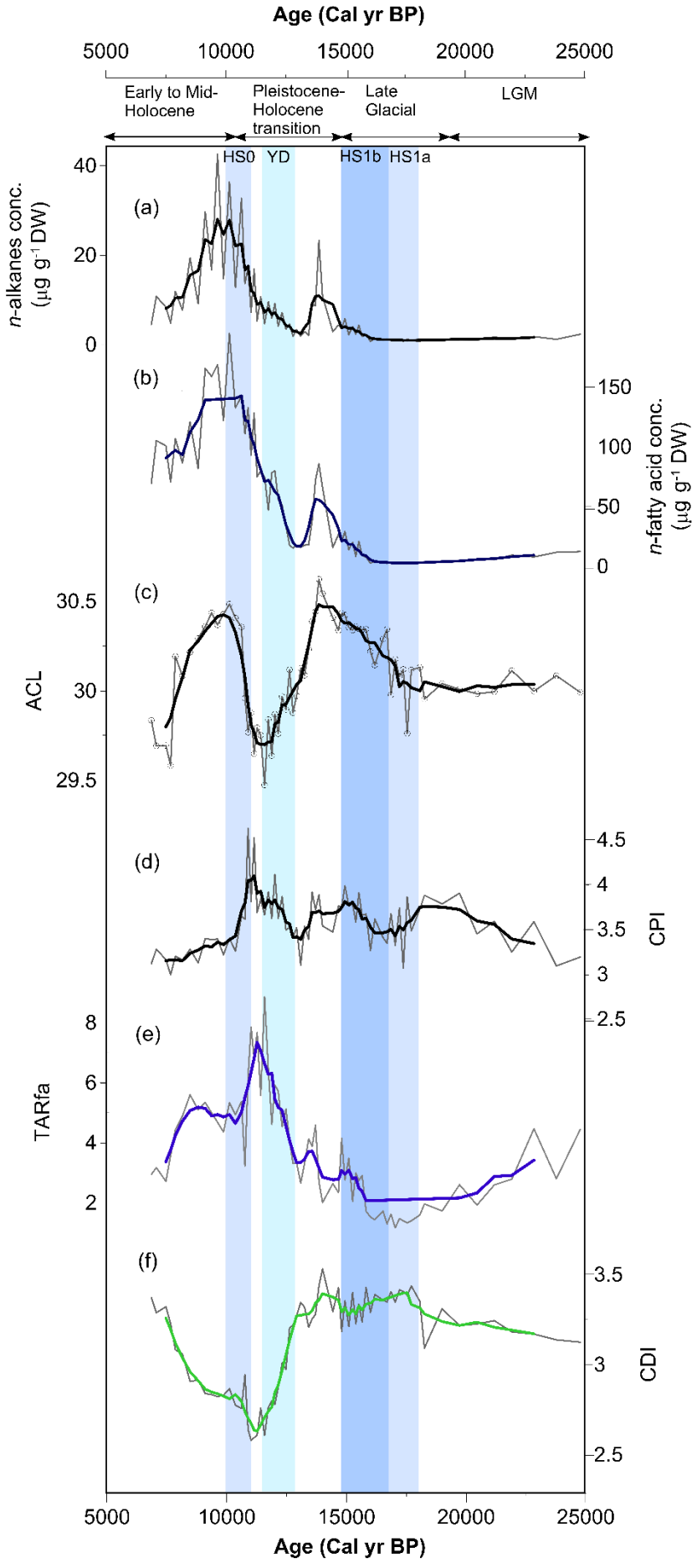

Figure 8 – Downcore variations of plant wax concentrations of (a) *n*-alkanes, (b) *n*-fatty-acids, (c) Average Chain Length (ACL, C_{25}-C_{33}); (d) Carbon Preference Index (CPI); (e) Terrestrial and aquatic ratio (TARfa) and; (f) Composition Diversity Index (CDI) of fatty acids. Columns in green and blue colors delimit the occurrence range of the Heinrich Stadial and Younger Dryas Events. Filled lines in blue and black represent weighted mean average values

A sharp decrease in CDI values occurs from Pleistocene-Holocene transition to the beginning of the Early Holocene and reaches the lowest value (2.6) around 11 ka. This is coeval with the strong increase of plant wax (FAME) concentrations and TARfa index, and marks the greater dominance of terrestrial inputs as compared with others (aquatic sources). Consistently, pollen data show that this period is marked by high abundance of montane savanna and forest formation. From 11 ka, CDI values increase continuously and maximize around the Mid-Holocene (6,8 ka), suggesting greater diversity of FAME sources. Indeed, the concomitant decrease of plant wax FAME, the increase in TAR and the pollen data point to contributions from aquatic sources (albeit not predominant) to the FAME (Figure 5).

Regarding ACL values, during the LGM, the ACL remains relatively constant around 30.0 and then increase up to 30.6 at 13,8 ka. From 13,8 ka, ACL values show a decrease in lowest values (<29.8) followed by a substantial increase during the HS0. After that, there is a new trend of decrease from Early to Mid-Holocene, reaching minimum values around 7,8 ka.

From Late Glacial to the Mid-Holocene, a considerable increase (>0.4) in ACL values is observed and may be considered quite relevant since variations in ACL among different phytophysiognomies such as rainforest, wood- and shrubland and savanna can be around 0.2 (BADEWIEN; VOGTS; RULLKÖTTER, 2015). The gradual increase in ACL values from LGM to Late Glacial is correlated with greater TARfa, CPI values and a high abundance of montane savanna which suggest a greater contribution of C_4 plants (ROMMERSKIRCHEN et al., 2006; VOGTS et al., 2009). However, although individual terrestrial lipids are highly used to discriminate potential plant sources and to reconstruct spatial and temporal changes in C_3/C_4 vegetation, in particular, the relative abundance of tree and shrub-dominated vegetation compared to grasslands (BADEWIEN; VOGTS; RULLKÖTTER, 2015; COLLISTER et al., 1994; GARCIN et al., 2012; HOLTVOETH et al., 2019; HUANG et al., 1996; VOGTS et al., 2012); a potential connection between climatic parameters and chain length has been widely debated (BADEWIEN; VOGTS; RULLKÖTTER, 2015; BUSH; MCINERNEY, 2015; CARR et al., 2014; VOGTS et al., 2009a). It is suggested that spatial and temporal variation in chain length distribution may be strongly driven by growing season temperature and/or aridity. In response to water stress, the plants increase the *n*-alkane chain length to maintain the hardness of their leaf surface and control the evapotranspiration (COLLISTER et al., 1994; ROMMERSKIRCHEN et al., 2006).

Considering that, a second explanation for the increase in ACL values from LGM to Pleistocene-Holocene transitions can be major biosynthesis of longer-chain *n*-alkanes – to

maintain the protective waxy coating on their leaves – due to the increasing trend of global temperature from the end of the glacial period. During the Pleistocene-Holocene transition, in turn, lower ACL values correspond to greater concentrations of forest formation, as shown by pollen data, which led to a decrease in ACL values due to enhanced contribution of leaf waxes from C_3 plants (VOGTS et al., 2012; ZHANG et al., 2017).

Higher ACL values around 10 ka are possibly associated with the elongation of *n*-alkanes in response to warmer conditions throughout the Holocene Thermal Maximum (11-5 ka; RENSSEN et al., 2009) since there is no substantial contribution of C_4 plants compared to previous periods. From 10 to 6.8 ka, a decrease in ACL values corresponds to enhanced concentration of non-terrestrial spores such as algae and Isoëtes, while terrestrial (arboreal and non-arboreal) pollen show no major changes. Thus, lower ACL is possibly associated with greater aquatic plant input rather than terrestrial C_3 plants, which is evidenced by a low AP/NAP ratio (<0.2).

3.4.3. Carbon and hydrogen isotope signature of plant waxes

CSIA ($\delta^{13}C$ and δD) of plant waxes were performed on *n*-fatty acids because of their greater abundance throughout the core AM3 and better GC resolution compared to *n*-alkanes. We focus on C_{28} *n*-fatty acids as the most abundant long-chain homologue and commonly applied in paleoclimate studies (FORNACE et al., 2014; HOU; D'ANDREA; HUANG, 2008).

The $\delta^{13}C_{wax}$ values range from –37‰ to –30‰ (Figure 9; Table 4), in agreement with plant waxes $\delta^{13}C$ values reported by previous studies from modern sediments on Amazon basin (from –36‰ to –30‰; FEAKINS et al., 2018; HÄGGI et al., 2016). The carbon isotopic signatures of leaf waxes from plants with C_3 and C_4 photosynthetic pathways differ considerably among them (COLLISTER et al., 1994). C_3 plants are relatively ^{13}C-depleted ($\delta^{13}C$= –39‰ to –32‰), while C4 plants are ^{13}C-enriched ($\delta^{13}C$= – 25‰ to –18‰) (CHIKARAISHI; NARAOKA; POULSON, 2004; COLLISTER et al., 1994; RIELEY; COLLIER; JONES, 1991). Based on carbon isotopic signatures of *n*-fatty acids from modern plants, Ballentine et al. (1998) also revealed depleted $\delta^{13}C$ values for C_3 plants (–32‰ to –38‰), and enriched $\delta^{13}C$ values for C_4 plants (– 21‰ to –28‰). Thus, the $\delta^{13}C_{wax}$ values in the Lake Amendoim record indicate the presence of C_3-dominated vegetation in the drainage basin during the last ~22 ka, with some contribution of C_4 plants.

This pattern resembles the one found in present days at Serra Sul, with a stronger signal of the ombrophylous forest relative to montane savanna (GUIMARÃES et al., 2017).

A trend to depleted $\delta^{13}C_{wax}$ values is observed from LGM to the Mid-Holocene, representing a C-depletion of approximately 6‰ in $\delta^{13}C_{wax}$ values, which points to a continuous increase in the contribution of C_3 plants throughout the last ~22 ka. Between the Late Glacial and Early Holocene, small fluctuations in $\delta^{13}C_{wax}$ values are observed.

Measured δD values for long-chain FAME over the past ~22 ka is shown in Table 4. Here we focus on *n*-C_{28} FAME δD (hereafter referred to as δD_{wax}) as the more abundant compound with the more robust signal during δD measurement. δD_{wax} values range from –135‰ to –93‰. Compound-specific δD *n*-$C_{29–31}$ analyses in modern sediments from Amazon river tributaries reported values between –142‰ and –168‰ (HÄGGI et al., 2016). Moreover, Lake Titicaca δD *n*-C_{28} FAME analysis yielded values ranging from –236‰ and –114‰, with a D-depletion of approximately 100‰ compared to values reported for the Lake Amendoim. Depleted δD signatures of *n*-C_{30} FAME were recorded across an Andes-Amazon elevation, with values between –236‰ and –114‰. These differences reflect the variation in the isotopic composition of precipitation, influenced by continental (rainout) and altitude effects, which lead to more depleted δD values of precipitation in the western Amazon basin and more enriched values in the eastern portion of the basin (FORNACE et al., 2014; HÄGGI et al., 2016).

The mean isotopic composition of hydrogen in the hydrological cycle around the globe became more D-enriched (by 8‰ on average) during the last glacial period compared to present-day conditions due to the accumulation of the lighter hydrogen isotope (^1H) in continental ice sheets (BINTANJA; VAN DE WAL; OERLEMANS, 2005). Thus, in order to remove the ice volume effect, we applied the ice volume correction (IVC; TIERNEY; DEMENOCAL, 2013) in δD_{wax} values, using the formula:

$$\delta D_{wax-IVC} = \frac{1000 + \delta D_{wax}}{8 \cdot 0.001 \cdot \delta^{18}O_{isoice} + 1} - 1000$$

Where $\delta D_{wax\text{-}IVC}$ represents the ice volume corrected isotope values, δD_{wax} the measured δD of fatty acids and $\delta^{18}O_{isoice}$ (1.05‰) the effect of ice volume on the benthic $\delta^{18}O$ variation (BINTANJA; VAN DE WAL; OERLEMANS, 2005).

Thus, from now on we focus on the ice volume corrected δD_{wax} values for *n*-C_{28} FAME ($\delta D_{wax\text{-}IVC}$). The $\delta D_{wax\text{-}IVC}$ values are shown in Figure 9, and range from –142‰ to –101‰ (Table 4). From LGM to the Late Glacial, between ~22 and 15,9 ka, the most

enriched $\delta D_{wax\text{-}IVC}$ values (– 117‰ and –101‰) are observed. Throughout the Pleistocene-Holocene transition, the values decrease down to –127‰ at 14,7 ka before slightly increasing up to – 120‰ at 13 ka. A decrease in $\delta D_{wax\text{-}IVC}$ (–127‰) around 12,7 ka is followed by a sharp increase at the beginning of the Early Holocene, between 11,7 and 11,2 ka, reaching values up to –111‰.

Table 4 – Sampled depth (cm), age model of core AM3, Carbon ($\delta^{13}C$) and Hydrogen (δD) isotopic composition (per mil, ‰) of *n*-C_{28} fatty acids, the weighted mean ($\delta^{13}C$, δD) values of long-chain (C_{26}-C_{30}) *n*-fatty acids, and D/H isotopic ratio of leaf waxes with Ice Volume Correction ($\delta D_{wax\text{-}IVC}$)

Depth (cm)	Age (years BP)	$\delta^{13}C$ and δD data of *n*-fatty acids				
		[a] $\delta^{13}C_{28}$	[b] $\delta^{13}C_{WM26\text{-}30}$	[c] δD_{28}	[d] $\delta D_{WM26\text{-}30}$	[e] $\delta D_{wax\text{-}IVC}$
9	6846	-37	-36	-135	-143	-142
13	7651	-36	-35	-124	-136	-131
15	8145	-35	-35	-122	-130	-129
17	8800	-35	-35	-120	-132	-127
19	9364	-34	-33	-105	-120	-113
21	9859	-33	-33	-134	-140	-141
23	10358	-33	-33	-124	-129	-131
26	10887	-33	-33	-129	-120	-136
29	11263	-34	-33	-103	-99	-111
31	11575	-33	-33	-114	-108	-121
32	11733	-33	-32	-111	-105	-119
39	12761	-33	-32	-120	-127	-128
41	13085	-33	-33	-112	-121	-120
45	13702	-31	-31	-116	-130	-124
47	13996	-32	-31	-117	-129	-124
53	14794	-32	-31	-119	-133	-127
57	15387	-31	-30	-110	-121	-118
61	15998	-31	-30	-93	-104	-101
65	16688	-31	-31	-101	-108	-109
69	17369	n.d.	n.d.	-96	-97	-103
73	18061	-30	-30	-107	n.d.	-115
76	19717	-30	-30	-99	n.d.	-107
79	21901	-31	-30	-109	-117	-117

n.d.: not determined

[a] $\delta^{13}C$: Molecular stable carbon isotopic composition of *n*-C_{28} fatty acids

[b] Weighted mean values for molecular stable carbon/hydrogen isotopic composition of even-carbon-numbered *n*-fatty acids = $(\Sigma[Ci] \times \delta i)/\Sigma[Ci]$; for i = n-$C_{28}$

[c] δD: Molecular stable hydrogen isotopic composition of *n*-C_{28} fatty acids

[d] $\delta D_{wax\text{-}IVC}$: Molecular stable hydrogen isotopic composition of *n*-C_{28} fatty acids with Ice Volume Correction (IVC)30; ‰ vs. SMOW).

Figure 9 – Comparison between (a) Arboreal pollen and non-arboreal pollen (AP/NAP) ratio from core AM2, (b) Composition Diversity Index (CDI) of *n*-fatty acids, (c) $\delta^{13}C_{wax}$, and (d) $\delta D_{wax\text{-}IVC}$ values of *n*-C_{28} fatty acid along the Last Glacial Maximum (LGM) to Mid-Holocene for Lake Amendoim, southeastern Amazonia. Blue bars delimit the range of the Heinrich Stadials (HS)

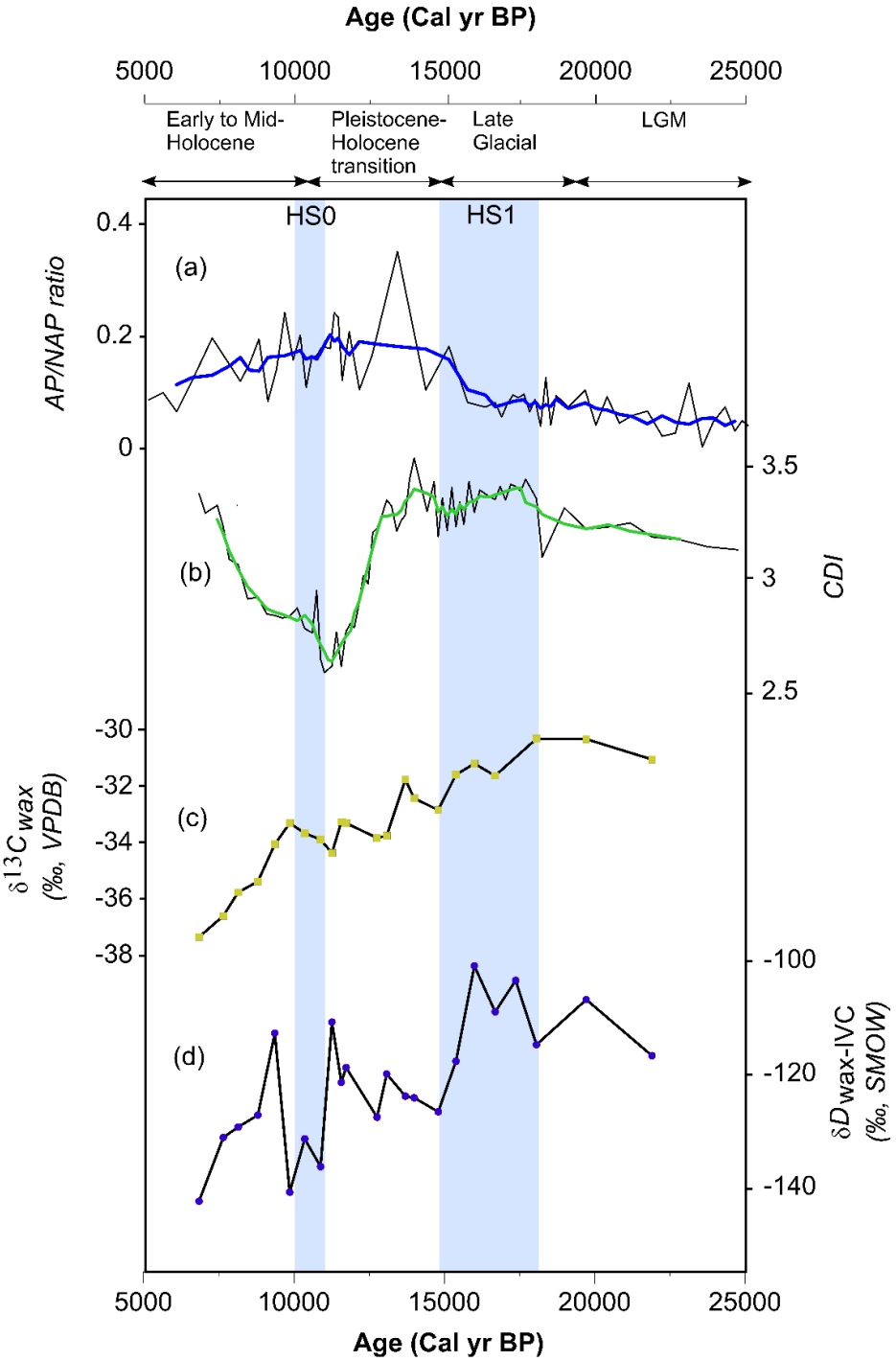

This period is followed by minimum $\delta D_{wax\text{-}IVC}$ values (–141‰) around 10 ka, representing a D-depletion of approximately 30‰. Then, $\delta D_{wax\text{-}IVC}$ values increase again and reach maximum (– 113‰) at 9.3 ka. From 9.3 ka, the values progressively decrease from –113‰ down to –142‰ with mean enrichment of ~30‰. The most remarkable aspect of the AM3 record is the large shift in $\delta D_{wax\text{-}IVC}$ values – around – 40‰ – from the glacial period to the Holocene.

3.4.4. Controls on $^{13}C/^{12}C$ and D/H ratios of n-fatty acids from plant waxes

The carbon isotopic composition of plant waxes has been primarily used to assess organic matter sources and distinguish between C_3 and C_4 plants – assuming minor contribution of waxes from Crassulacean acid metabolism (CAM) plants – hence it can reflect the vegetation associated with a particular phytophysiognomy such as forest formation (trees) and savanna (herbs and grasses) (ALEWELL et al., 2016; HOLTVOETH et al., 2019; MEYERS; ISHIWATARI, 1993; and references therein). However, environmental factors may also affect the natural variability of compound-specific isotopic signature (REIFFARTH et al., 2016). For instance, the increase in humidity may lead to an increase in stomatal conductance and thus depleted $\delta^{13}C$ values. Whereas, low humidity and consequently water availability induces stomatal closure to reduce water loss via transpiration which results in a lower rate of CO_2 influx. As stomatal conductance decreases, the pool of CO_2 inside the leaf becomes progressively enriched, resulting in ^{13}C enrichment (AMESBURY et al., 2015; FARQUHAR; EHLERINGER; HUBICK, 1989; REIFFARTH et al., 2016).

Although a low AP/NAP ratio indicates enhanced C_4 plant input during the glacial period, it is important to take into account the degradation of pollen grains as a result of diagenetic processes. This may have led to selective preservation, i.e. the permanence of pollen-resistant often produced in large numbers, i.e. anemophilous plants (e.g. herbs and grasses), rather than fragile and less-produced pollen grains, i.e. zoophilic plants (e.g. trees). Therefore, higher $\delta^{13}C_{wax}$ values recorded from ~22 to 18 ka, can be possibly linked to lower stomatal conductance due to reduced humidity rather than changes in the overlying vegetation. Meanwhile, ^{13}C enriched values between 18 and 15 ka indicate a higher contribution of C_4 over C_3 plants as shown by low AP/NAP ratio and pollen data. From 15 ka, depleted $\delta^{13}C_{wax}$ values correspond to greater AP/NAP ratio and high concentration of pollen from forest formation which reinforces that $\delta^{13}C_{wax}$ signature of the plant waxes from Lake Amendoim reflects the catchment vegetation.

The non-similarity between the Lake Amendoim δD and $\delta^{13}C$ records, i.e. distinct shifts in δD signature compared to $\delta^{13}C$ values across all time periods, points to low influence of vegetation over δD signal. The correlation between measured δD and $\delta^{13}C$ values for *n*-C_{28} fatty acid is shown in Figure 10. Plant wax δD and $\delta^{13}C$ values show a positive relationship (R^2=0.42) throughout the core AM3, in line with the expected association of low δD values (i.e. greater precipitation amount/higher humidity) and low $\delta^{13}C$ values (i.e. C_3-dominated community) when climatic factors are the main control on δD signature. However, periods (e.g. Pleistocene-Holocene transition, Early Holocene) with important changes in the floristic composition, as shown by pollen data and TAR, CPI and CDI indexes, correspond to considerable variations in δD. Thus, although much of the variability in Lake Amendoim δD values can be explained by changes in the hydrological cycle, including source water, relative humidity, and rainfall amount, shifts in vegetation cover seems to exert a considerable influence on plant wax δD signal at the study site.

3.4.5. Past vegetation dynamics

The range of $\delta^{13}C_{wax}$ values (–37‰ to –30‰; Figure 9) in the core AM3 evidenced a wide spectrum of C_3-dominated plant communities over the past ~22 ka. A comparison of $\delta^{13}C_{wax}$ signal to detailed pollen data also reveals the contribution of OM from macrophytes and algae to the lake basin.

From LGM (~22-20 ka) to Late Glacial (18-15 ka), plant wax $\delta^{13}C$ values indicate a mixed C_3/C_4 vegetation community, which was mainly composed of montane savanna, rainforest, and cool-adapted taxa according to pollen data and supported by high CDI values. The presence of highland tree species has been widely reported throughout Amazon basin (COHEN et al., 2014; COLINVAUX et al., 1996; VAN DER HAMMEN; HOOGHIEMSTRA, 2000 and references therein), and evidences the migration of these taxa to Carajás Plateau in response to cooler temperatures (~3°C; REIS et al., 2017) during the glacial period as had been proposed by previous studies (HERMANOWSKI et al., 2012; VAN DER HAMMEN; ABSY, 1994). Higher ACL show a strong correlation to an increase in the concentration of plant wax lipids, and montane savanna pollen abundance, indicating ACL was also highly influenced by *n*-alkanes and FAME from C_4 plants.

In contrast to the LGM and Late Glacial, *n*-fatty acids $\delta^{13}C$ values show a steady decrease during the Pleistocene-Holocene transition which points to increased C_3 plants contribution. This period is also marked by a sharp decrease in ACL values, indicating a greater contribution of forest-like vegetation, which is consistent with a considerable increase

in forest formation pollen abundance. An upward trend in long-chain *n*-alkanes concentrations, as well as TARfa and CPI values, reinforce the predominantly terrestrial input, which is also supported by lower CDI values. Our data are consistent with a forest expansion after the glacial period, favored by trend warming plus increased atmospheric CO_2 levels and greater humidity, in agreement with previous studies performed in the Serra Sul de Carajás (HERMANOWSKI; DA COSTA; BEHLING, 2015; REIS et al., 2017; and references therein) and southern Amazonia (FONTES et al., 2017).

At the beginning of the Holocene, between 11 and 10 ka, a slight increase in $\delta^{13}C_{wax}$ values coincides with the rise of ACL values, in line with a slight increase in montane savanna abundance, although forest abundance (AP/NAP ratio) remains high. Thus, $\delta^{13}C_{wax}$ variability may be linked to changes in the floristic composition of the vegetation around the Lake Amendoim.

After the slight increase at the beginning of the Holocene, $\delta^{13}C_{wax}$ values show a steady decrease until the Mid-Holocene (6.8 ka). During this interval, all *n*-fatty acids $\delta^{13}C$ values are less than –34‰, indicating a progressive increase in the C_3-dominated community. This is supported by a continuous decrease in ACL values. Meanwhile, lower TARfa and CPI values suggest enhanced contribution of OM from aquatic sources to the lacustrine deposits as shown by pollen data. The predominance of autochthonous organic matter as shown by sedimentary facies, is possibly linked to lower transport of plant waxes from land plants to the lake basin in response to a phase of reduced surface runoff. This can be further supported by evidence of (1) lower sedimentation rates and a drop in lake level during the Mid-Holocene in Carajás (CORDEIRO et al., 2008; GUIMARÃES et al., 2016; HERMANOWSKI et al., 2012), (2) expansion of seasonal forest elements in Lake Saci, between 7.5 and 5 ka (FONTES et al., 2017), besides high frequency of fire events in Rondônia/Amazonas border, southern Amazonia, between 7 and 6 ka (DE FREITAS et al., 2001; PESSENDA et al., 1998a, 1998b). Since modern limnological characteristics of the Lake Amendoim are associated with algae bloom under lower lake levels during dry seasons (SAHOO et al., 2017), this suggests more seasonal conditions during the Mid-Holocene.

Figure 10 – Correlation (a) and (b) binary diagram with measured $\delta^{13}C$ vs. δD (per mil, ‰) values of *n*-C_{28} fatty acids from Lake Amendoim (core AM3) across all time periods. LGM- Last Glacial Maximum; Late_G – Late Glacial; P_H-trans – Pleistocene-Holocene transition; Early_H – Early Holocene; Middle_Hol – Mid-Holocene

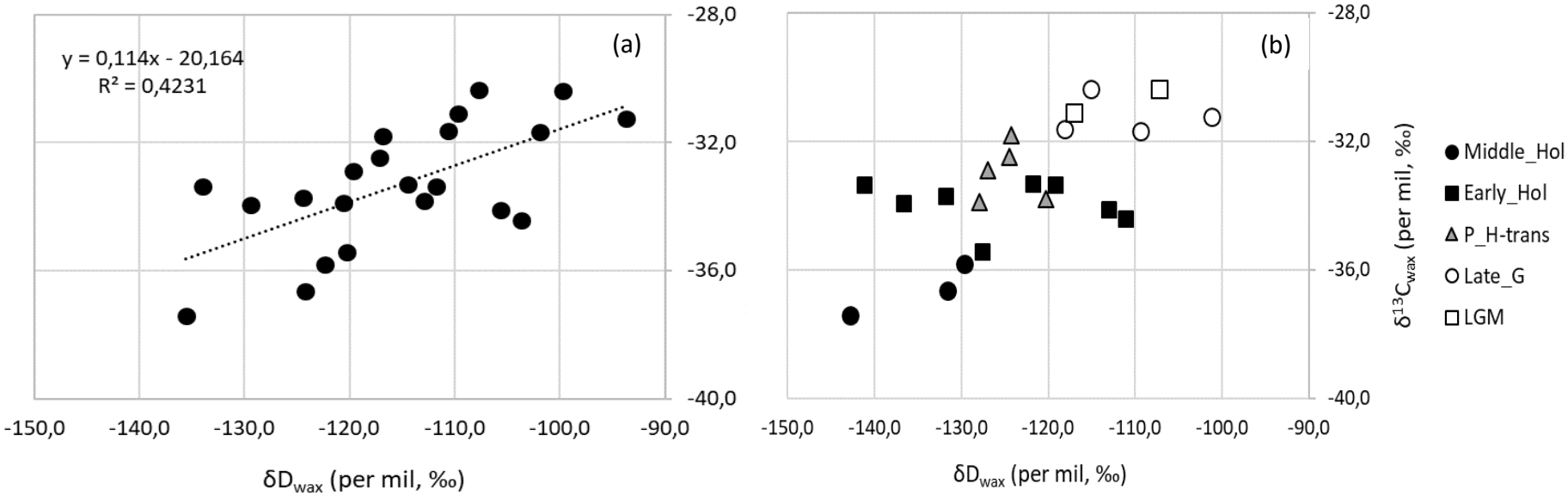

3.4.6. Paleohydroclimatic interpretation

δD values in the Lake Amendoim record shows relevant fluctuations (up to 30‰) suggesting changes in the regional hydroclimate over the past ~22 ka. Major shifts are observed at the end of the glacial period and from Early to Mid-Holocene.

During the LGM and Late Glacial period (~22-15 ka), δD_{wax} values reflect isotopically heavier signature (Figure 9). This period is marked by a pronounced cooling in the Northern Hemisphere (by 4.3°C on average; BUSH; GEORGE; PHILANDER, 1999) among other regions of the globe. In Serra dos Carajás, an estimated cooling of 3°C has been inferred from pollen data, based on the occurrence of cool-adapted taxa (REIS et al., 2017). Meanwhile, lower pCO_2 (BARNOLA et al., 1987; STREET-PERROTT et al., 1997), and reduced humidity compared to the modern levels possibly promoted the growth of C_4 vegetation, which led to a mixed C_3/C_4 community as shown by $\delta^{13}C_{wax}$ values and pollen data. Thus, higher δD_{wax} values recorded during this interval are probably related to cooler conditions and reduced humidity at the study site. Reduced rainfall and increased C_4 vegetation community during the last glacial period were also reported by previous studies in Carajás (HERMANOWSKI et al., 2012; SIFEDDINE et al., 2001; VAN DER HAMMEN; ABSY, 1994), as well as in southern Amazon sites (FORNACE et al., 2016; MAYLE et al., 2004), and northeastern Brazil (JACOB et al., 2007). Also, in agreement with speleothem data from Paraíso Cave that showed reduced precipitation amount relative to modern levels, possibly due to suppressed moisture supply from the ocean and reduced convection within the Amazon basin (WANG et al., 2017).

The Pleistocene-Holocene transition (15-11 ka) is marked by a steep decrease in δD_{wax} by 20‰, indicating a shift to more humid conditions. This corresponds to a rise in TARfa and AP/NAP ratios, as well as a greater concentration of tree pollen, indicating rainforest expansion over the Serra Sul Plateau. According to Whitney et al., (2011), the growth of tropical rainforest can be attributed to deglacial warming which possibly led to increased humidity and along with higher pCO_2 levels fostered the development of C_3-dominated community under wetter conditions compared to glacial period.

At the beginning of the Holocene (11 ka), a trend to heavier δD_{wax} values is observed, which in first approximation based on the amount affect interpretation of rainfall isotopes, would imply in less humid conditions as previously proposed by pollen records at the study site (CORDEIRO et al., 2008; HERMANOWSKI et al., 2015). However, this period is marked by the highest concentrations of forest formation, followed by high TARfa and minimum ACL values, which evidence the pronounced expansion of the rainforest at Serra

Sul. Thus, a likely explanation for higher δD values may be an enhanced contribution of evapotranspirated water from trees that is enriched in heavier isotopes relative to atmospheric vapor from Atlantic Ocean (GAT; MATSUI, 1991; SALATI et al., 1979). Greater evaporated moisture, in turn, can be linked to a warm climatic phase (11 and 5 ka), known as Holocene Thermal Maximum (RENSSEN et al., 2012), which probably induced higher evapotranspiration within Amazon basin. This period is followed by a large shift to more depleted δD_{wax} values between 11 and 9.8 ka, reflecting a phase of increased humidity. Wetter conditions at Serra Sul are related to Heinrich Stadial 0 (VEIGA-PIRES; HILLAIRE-MARCEL, 1999), which possibly led to increased precipitation throughout tropical South America in response to the southward migration of the ITCZ (FONTES et al., 2017; FORNACE et al., 2016; JACOB et al., 2007).

From Early to Mid-Holocene, an abrupt increase in δD_{wax} values coincides with a forest peak around 9.3 ka, probably associated with moisture recycling, i.e. enhanced contribution of evaporated vapor from land surface to precipitation (VAN DER ENT et al., 2010). After 9.3 ka, a steady decrease in δD_{wax} signal corresponds to depleted $\delta^{13}C_{wax}$ values, suggesting predominantly wet conditions in agreement with speleothem record from Paraíso Cave that revealed abundant precipitation during the Mid-Holocene as a result of enhanced upward motion of moisture (WANG et al., 2017). However, greater contribution of aquatic over terrestrial OM as shown by lower TARfa and increased concentration of macrophytes and algae indicate fluctuations in the lake level, which are possibly related to periodic droughts. Previous studies have also reported an increasingly seasonal condition in Carajás marked by phases of reduced sedimentation rate, variation in lake level, and large biomass burning events (CORDEIRO et al., 2008; HERMANOWSKI et al., 2012; REIS et al., 2017; and references therein). The effects of the Mid-Holocene dry episodes were also recorded on lacustrine sediments in western (BUSH et al., 2004) and southern Amazonia (BURBRIDGE; MAYLE; KILLEEN, 2004; FONTES et al., 2017), as well as in the Bolivian Altiplano (BAKER et al., 2001).

3.5. Conclusions

Here we applied molecular (*n*-alkanes and *n*-fatty acids) techniques and isotope analysis (δD and $\delta^{13}C$) of *n*-C_{28} fatty acid in sedimentary archives from Lake Amendoim, southeastern Amazonia. Combined with existing pollen data and paleoenvironmental reconstitution studies, we identified remarkable changes in the vegetation composition over the last ~22 ka.

Molecular (*n*-alkanes and *n*-fatty acids) and pollen data showed terrestrial plants as the primary source of OM to lacustrine sediments. Also, no large vegetation changes have occurred within the catchment basin of the lake over the last ~22 ka, except for the incursion of cool-adapted taxa in response to cooler conditions during the LGM. Moreover, we reaffirm that there was no replacement of the rainforest by savanna. Such phytophysiognomies contributed concomitantly as sources of allochthonous organic material for Lake Amendoim, which evidences their presence at Serra dos Carajás across all time periods.

Regarding ACL and TARfa indexes, our records showed high agreement with pollen data when compared to the abundance of the different phytophysiognomies. Fluctuations in terrestrial and aquatic plants registered by pollen and spore data were also evidenced by both indexes as well, which reinforces the use of ACL and TARfa as suitable proxies to distinguish between different organic matter sources, i.e. terrestrial vs. aquatic plants. Additionally, we observed a potential effect of temperature over ACL values evidenced by strong variations in the ACL index during intervals with considerable changes in global temperature such as LGM and Holocene Thermal Maximum. Nevertheless, local and/or regional calibration studies with modern plants are indispensable for a robust interpretation of plant wax origin and distribution in sedimentary archives besides their response to environmental changes.

The CSIA of *n*-fatty acids from Lake Amendoim, in turn, revealed a relevant influence of vegetation change on plant wax δD signature. Additionally, the coherence among the δD_{wax} (core AM3) and previous studies performed in the study site and within the Amazon basin demonstrates that precipitation amount and moisture source exert a strong control on the δD_{wax} signature, reaffirming the value of δD_{wax} as a paleoclimate proxy. Moreover, the hydroclimatic changes over tropical South America are strongly linked to climatic events in the Northern Hemisphere, including LGM and HS. However, changes in precipitation appear to influence the environment more intensely, e.g. lake level, while

vegetation responds faster to cooling and/or heating. Finally, we conclude that the rainfall amount was not the only factor influencing vegetation cover in the study site. Temperature changes have also played an important role in plant community composition and distribution in the Serra dos Carajás.

References

ABSY, M. et al. Mise en évidence de quatre phases d'ouverture de la forêt dense dans le sud-est de l'Amazonie au cours des 60 000 dernières années. Première comparaison avec d'autres régions tropicales. **Comptes rendus de l'Académie des sciences. Série 2, Mécanique, Physique, Chimie, Sciences de l'univers, Sciences de la Terre**, v. 312, n. 6, p. 673–678, 1991.

ABSY, M. L. et al. Palynological differentiation of savanna types in Carajás, Brazil (Southeastern Amazonia). **Palynology**, v. 38, n. 1, p. 78–89, 2014.

ALEWELL, C. et al. Quantitative sediment source attribution with compound-specific isotope analysis in a C3 plant-dominated catchment (Central Switzerland). **Biogeosciences**, v. 13, p. 1587–1596, 2016.

ALVARES, C. A. et al. Köppen's climate classification map for Brazil. **Meteorologische Zeitschrift**, v. 22, n. 6, p. 711–728, 2013.

AMESBURY, M. J. et al. Carbon stable isotopes as a palaeoclimate proxy in vascular plant dominated peatlands. **Geochimica et Cosmochimica Acta**, v. 164, p. 161–174, 2015.

AZIZUDDIN, A. D. et al. Characterization and sources of extractable organic matter from sediment cores of an urban lake (Tasik Perdana), Kuala Lumpur, Malaysia. **Environmental Earth Sciences**, v. 71, p. 4363–4377, 2014.

BADEWIEN, T.; VOGTS, A.; RULLKÖTTER, J. n-Alkane distribution and carbon stable isotope composition in leaf waxes of C 3 and C 4 plants from Angola. **Organic Geochemistry**, v. 89–90, p. 71–79, 2015.

BAKER, P. A. et al. The History of South American Tropical Precipitation for the Past 25 , 000 Years. **Science**, v. 291, p. 640–643, 2001.

BALLENTINE, D. C.; MACKO, S. A.; TUREKIAN, V. C. Variability of stable carbon isotopic compositions in individual fatty acids from combustion of C4 and C3 plants: Implications for biomass burning. **Chemical Geology**, v. 152, n. 1–2, p. 151–161, 1998.

BARNOLA, J.-M. et al. Vostok ice core provides 160,000-years record of atmospheric CO2. **Nature**, v. 329, p. 408–414, 1987.

BINTANJA, R.; VAN DE WAL, R. S. W.; OERLEMANS, J. Modelled atmospheric temperatures and global sea levels over the past million years. **Nature**, v. 437, n. 125–128, 2005.

BLAAUW, M.; CHRISTEN, J. A. Radiocarbon peat chronologies and environmental change. **Journal of the Royal Statistical Society**, v. 54, n. 4, p. 805–816, 2005.

BLAAUW, M.; CHRISTEN, J. A. Flexible paleoclimate age-depth models using an autoregressive gamma process. **Bayesian Analysis**, v. 6, n. 3, p. 457–474, 2011.

BRAY, E. E.; EVANS, E. D. Distribution of n-paraffins as a clue to recognition of source beds. **Geochimica et Cosmochimica Acta**, v. 22, n. 1, p. 2–15, 1961.

BURBRIDGE, R. E.; MAYLE, F. E.; KILLEEN, T. J. Fifty-thousand-year vegetation and climate history of Noel Kempff Mercado National Park, Bolivian Amazon. **Quaternary Research**, v. 61, n. 2, p. 215–230, 2004.

BUSH, M. B. et al. Amazonian paleoecological histories: one hill, three watersheds. **Palaeogeography, Palaeoclimatology, Palaeoecology**, v. 214, n. 4, p. 359–393, 2004.

BUSH, R. T.; MCINERNEY, F. A. Influence of temperature and C 4 abundance on n-alkane chain length distributions across the central USA. **Organic Geochemistry**, v. 79, p. 65–73, 2015.

CARDOSO, D. et al. Amazon plant diversity revealed by a taxonomically verified species list. **Proceedings of the National Academy of Sciences of the USA**, v. 114, n. 40, p. 10695–10700, 2017.

CARR, A. S. et al. Leaf wax n-alkane distributions in arid zone South African flora: Environmental controls, chemotaxonomy and palaeoecological implications. **Organic Geochemistry**, v. 67, p. 72–84, 2014.

CASTAÑEDA, I. S. et al. Late Quaternary vegetation history of southeast Africa: The molecular isotopic record from Lake Malawi. **Palaeogeography, Palaeoclimatology, Palaeoecology**, v. 275, p. 100–112, 2009.

CHIKARAISHI, Y.; NARAOKA, H.; POULSON, S. R. Hydrogen and carbon isotopic fractionations of lipid biosynthesis among terrestrial (C3, C4 and CAM) and aquatic plants. **Phytochemistry**, v. 65, p. 1369–1381, 2004.

CLARK, P. U. et al. The Last Glacial Maximum. **Science**, v. 325, n. 5941, p. 710–714, 2009.

CLARK, P. U.; MIX, A. L. Ice sheets and sea level of the Last Glacial Maximum. **Quaternary Science Reviews**, v. 21, n. 1-3, p. 1–7, 2002.

COHEN, M. C. L. et al. Late Pleistocene glacial forest of Humaitá-Western Amazonia. **Palaeogeography, Palaeoclimatology, Palaeoecology**, v. 415, p. 37–47, 2014.

COLINVAUX, P. A. et al. A long pollen record from lowland Amazonia, forest cooling in Glacial times.pdf. **Science**, v. 274, p. 85–88, 1996.

COLINVAUX, P. A.; OLIVEIRA, P. E. DE. Palaeoecology and climate of the Amazon basin during the last glacial cycle. **Journal of Quaternary Science**, v. 15, n. 4, p. 347–356, 2000.

COLLISTER, J. W. et al. Compound-specific d13C analyses of leaf lipids from plants with differing carbon dioxide metabolisms. **Organic Geochemistry**, v. 21, n. 93, p. 619–627, 1994.

CORDEIRO, R. C. et al. Holocene fires in East Amazonia (Carajás), new evidences, chronology and relation with paleoclimate. **Global and Planetary Change**, v. 61, n. 1–2, p. 49–62, 2008.

CRAIG, H. Isotopic Variations in Meteoric Waters. **Science**, v. 133, n. 3465, p. 1702–1703, 1961.

CRANWELL, P. A. Chain-length distribution of n-alkanes from lake sediments in relation to post-glacial environmental change. **Freshwater Biology**, v. 3, p. 259–265, 1973.

CRIVELLARI, S. et al. Increased Amazon freshwater discharge during late Heinrich Stadial 1. **Quaternary Science Reviews**, v. 181, p. 144–155, 2018.

CRUZ, F. C. et al. Insolation-driven changes in atmospheric circulation over the past 116,000 years in subtropical Brazil. **Nature**, v. 434, p. 63–66, 2005.

D'APOLITO, C.; ABSY, M. L.; LATRUBESSE, E. M. The Hill of Six Lakes revisited: New data and re-evaluation of a key Pleistocene Amazon site. **Quaternary Science Reviews**, v. 76, p. 140–155, 2013.

DA SILVA, M. S. et al. Morphology and morphometry of upland lakes over lateritic crust, Serra dos Carajás, southeastern Amazon region. **Annals of the Brazilian Academy of Sciences**, v. 90, n. 902, p. 1309–1325, 2018.

DANSGAARD, W. Stable isotopes in precipitation. **Tellus**, v. 16, n. 4, p. 436–468, 1964.

DE FREITAS, H. A. et al. Late Quaternary vegetation dynamics in the southern Amazon Basin inferred from carbon isotopes in soil organic matter. **Quaternary Research**, v. 55, n. 1, p. 39–46, 2001.

DIEFENDORF, A. F. et al. Production of n-alkyl lipids in living plants and implications for the geologic past. **Geochimica et Cosmochimica Acta**, v. 75, p. 7472–7485, 2011.

DUAN, Y. I.; HE, J. Distribution and isotopic composition of n-alkanes from grass, reed and tree leaves along a latitudinal gradient in China. **Geochemical Journal**, v. 45, p. 199–207, 2011.

EGLINTON, G. et al. Hydrocarbon constituents of the wax coatings of plant leaves: a taxonomic survey. **Phytochemistry**, v. 1, n. 2, p. 89–102, 1962.

EGLINTON, G.; HAMILTON, R. J. Leaf Epicuticular Waxes. **Science**, v. 156, p. 1322–1335, 1967.

ELLISON, D. et al. Trees, forests and water: Cool insights for a hot world. **Global Environmental Change**, v. 43, p. 51–61, 2017.

ELTAHIR, E. A. B.; BRAS, R. L. Precipitation recycling in the Amazon basin. **Quarterly Journal of the Royal Meteorological Society**, v. 120, n. 518, p. 861–880, 1994.

FANG, J. et al. Source characterization of sedimentary organic matter using molecular and stable carbon isotopic composition of n-alkanes and fatty acids in sediment core from Lake Dianchi, China. **Science of the Total Environment**, v. 473–474, p. 410–421, 2014.

FARQUHAR, G. D.; EHLERINGER, R.; HUBICK, K. T. Carbon Isotope Discrimination and Photosynthesis. **Annual Review of Plant Physiology and Plant Molecular Biology**, v. 40, p. 503–537, 1989.

FEAKINS, S. J. et al. Production of leaf wax n-alkanes across a tropical forest elevation transect. **Organic Geochemistry**, v. 100, p. 89–100, 2016.

FEAKINS, S. J. et al. Dual isotope evidence for sedimentary integration of plant wax biomarkers across an Andes-Amazon elevation transect. **Geochimica et Cosmochimica Acta**, v. 242, p. 64–81, 2018.

FICKEN, K. J. et al. An n-alkane proxy for the sedimentary input of submerged/ floating freshwater aquatic macrophytes. **Organic Geochemistry**, v. 31, p. 745–749, 2000.

FONTES, D. et al. Paleoenvironmental dynamics in South Amazonia, Brazil, during the last 35,000 years inferred from pollen and geochemical records of Lago do Saci. **Quaternary Science Reviews**, v. 173, p. 161-180, 2017.

FORNACE, K. L. et al. A 60,000-year Record of Hydrologic Variability in the Central Andes from the Hydrogen Isotopic Composition of Leaf Waxes in Lake Titicaca Sediments. **Earth and Planetary Science Letters**, v. 408, p. 263–271, 2014.

FORNACE, K. L. et al. Late Quaternary environmental change in the interior South American tropics: New insight from leaf wax stable isotopes. **Earth and Planetary Science Letters**, v. 438, p. 75–85, 2016.

GARCIN, Y. et al. Hydrogen isotope ratios of lacustrine sedimentary n-alkanes as proxies of tropical African hydrology: Insights from a calibration transect across Cameroon. **Geochimica et Cosmochimica Acta**, v. 79, p. 106–126, 2012.

GAT, J. R.; MATSUI, E. Atmospheric water balance in the Amazon basin: An isotopic evapotranspiration model. **Journal of Geophysical Research**, v. 96, n. D7, p. 13179, 1991.

GUIMARÃES, J. T. F. et al. Late Quaternary environmental and climate changes registered in lacustrine sediments of the Serra Sul de Carajás, south-east Amazonia. **Journal of Quaternary Science**, v. 31, n. 2, p. 61–74, 2016.

HÄGGI, C. et al. Origin, transport and deposition of leaf-wax biomarkers in the Amazon Basin and the adjacent Atlantic. **Geochimica et Cosmochimica Acta**, v. 192, p. 149–165, 2016.

HÄGGI, C. et al. Response of the Amazon rainforest to late Pleistocene climate variability. **Earth and Planetary Science Letters**, v. 479, p. 50–59, 2017.

HASLETT, J.; PARNELL, A. A simple monotone process with application to radiocarbon-dated depth chronologies. **Journal of the Royal Statistical Society**, v. 57, n. 4, p. 399–418, 2008.

HERMANOWSKI, B. et al. Palaeoenvironmental dynamics and underlying climatic changes in southeast Amazonia (Serra Sul dos Carajás, Brazil) during the late Pleistocene and Holocene. **Palaeogeography, Palaeoclimatology, Palaeoecology**, v. 365–366, p. 227–246, 2012.

HERMANOWSKI, B.; DA COSTA, M. L.; BEHLING, H. Possible linkages of palaeofires in southeast Amazonia to a changing climate since the Last Glacial Maximum. **Vegetation History and Archaeobotany**, v. 24, n. 2, p. 279–292, 2015.

HO, E. S.; MEYERS, P. A. Variability of early diagenesis in lake sediments: Evidence from the sedimentary geolipid record in an isolated tarn. **Chemical Geology**, v. 112, n. 3–4, p. 309-324, 1994.

HOLTVOETH, J. et al. The paleolimnologist's guide to compound-specific stable isotope analysis – An introduction to principles and applications of CSIA for Quaternary lake sediments. **Quaternary Science Reviews**, v. 207, p. 101–133, 1 mar. 2019.

HOU, J. et al. Postglacial climate reconstruction based on compound- specific D/H ratios of fatty acids from Blood Pond, New England. **Geochemistry, Geophysics, Geosystems**, v. 7, n. 3, p. 1–11, 2006.

HOU, J.; D'ANDREA, W. J.; HUANG, Y. Can sedimentary leaf waxes record D/H ratios of continental precipitation? Field, model, and experimental assessments. **Geochimica et Cosmochimica Acta**, v. 72, n. 14, p. 3503–3517, 2008.

HUANG, Y. et al. Post-glacial variations in distributions, 13C and 14C contents of aliphatic hydrocarbons and bulk organic matter in three types of British acid upland soils. **Organic Geochemistry**, v. 24, n. 3, p. 273–287, 1996.

HUANG, Y. et al. Hydrogen isotope ratios of individual lipids in lake sediments as novel tracers of climatic and environmental change: A surface sediment test. **Journal of Paleolimnology**, v. 31, n. 3, p. 363–375, 2004.

JACOB, J. et al. Paleohydrological changes during the last deglaciation in Northern Brazil. **Quaternary Science Reviews**, v. 26, n. 7–8, p. 1004–1015, 2007.

KAWAMURA, K.; ISHIWATARI, R.; OGURA, K. Early diagenesis of organic matter in the water column and sediments: Microbial degradation and resynthesis of lipids in Lake Haruna. **Organic Geochemistry**, v. 11, n. 4, p. 251–264, 1987.

KOLATTUKUDY, P. E.; WALTON, T. J. The biochemistry of plant cuticular lipids. **Progress in the Chemistry of Fats and Other Lipids**, v. 13, n. 3, p. 119-175, 1972.

KUNERT, N. et al. A revised hydrological model for the Central Amazon: The importance of emergent canopy trees in the forest water budget. **Agricultural and Forest Meteorology**, v. 239, p. 47–57, 2017.

KUNST, L.; SAMUELS, A. L. Biosynthesis and secretion of plant cuticular wax. **Progress in Lipid Research**, v. 42, p. 51–80, 2003.

KURITA, N.; YAMADA, H. The Role of Local Moisture Recycling Evaluated Using Stable Isotope Data from over the Middle of the Tibetan Plateau during the Monsoon Season. **Journal of Hydrometeorology**, v. 9, p. 760–775, 2008.

LAVRIEUX, M. et al. Preservation of an ancient grassland biomarker signature in a forest soil from the French Massif Central. **Organic Geochemistry**, v. 51, p. 1–10, 2012.

LEMOS, V. P. et al. Vivianite and siderite in lateritic iron crust: an example of bioreduction. **Química Nova**, v. 30, n. 1, p. 36–40, 2007.

LETTAU, H.; LETTAU, K.; MOLION, L. C. Amazonia's hydrological cycle and the role of atmospheric recycling in assessing deforestation effects. **Montly Weather Review**, v. 107, n. 3, p. 227-238, 1979.

LIEBMANN, B.; MECHOSO, C. R. **The South American Monsoon System**. 2. ed. Singapure: World Scientific Series on Asia-Pacific Weather and Climate, 2011. p. 137-157. doi: 10.1142/9789814343411_0009.

LIU, J.; LIU, W.; AN, Z. Insight into the reasons of leaf wax δDn-alkane values between grasses and woods. **Science Bulletin**, v. 60, n. 5, p. 549–555, 2015.

LIU, K.-S. Preparation of fatty acid methyl esters for gas-chromatographic analysis of lipids in biological materials. **Journal of the American Oil Chemists' Society**, v. 71, n. 11, p. 1179–1187, 1994.

LIVINGSTONE, D. A. A Lightweight piston sampler for lake deposits. **Ecology**, v. 36, n. 1, p. 137–139, 1955.

LOPES, M. N. G.; DE SOUZA, E. B.; FERREIRA, D. B. DA S. Climatologia Regional da precipitação no estado do Pará. **Revista Brasileira de Climatologia**, v. 12, p. 84–102, 2013.

MARENGO, J. A. et al. Climatology of the Low-Level Jet East of the Andes as Derived from the NCEP–NCAR Reanalyses: Characteristics and Temporal Variability. **Journal of Climate**, v. 17, n. 12, p. 2261–2280, 2004.

MARTINEZ, A. J.; DOMINGUEZ, F. Sources of atmospheric moisture for the La Plata River Basin. **Journal of Climate**, v. 27, n. 17, p. 6737–6753, 2014.

MATSUDA, H.; KOYAMA, T. Early diagenesis of fatty acids in lacustrine sediments-II. A statistical approach to changes in fatty acid composition from recent sediments and some source materials. **Geochimica et Cosmochimica Acta**, v. 41, n. 12, p. 1825–1834, 1977.

MAURITY, C. W.; KOTSCHOUBEY, B. Evolução recente da cobertura de alteração no platô N1 - serra dos Carajás-PA. Degradação, pseudocarstificação, espeleotemas. **Boletim do Museu Paraense Emílio Goeldi**, v. 7, p. 331–362, 1995.

MAYLE, F. E. et al. Responses of Amazonian ecosystems to climatic and atmospheric carbon dioxide changes since the last glacial maximum. **Philosophical Transactions of the Royal Society. B – Biological Sciences**, v. 359, p. 499–514, 2004. doi: 10.1098/rstb.2003.1434.

MAYLE, F. E.; BURBRIDGE, R.; KILLEEN, T. J. Millennial-scale dynamics of southern Amazonian rain forests. **Science**, v. 290, n. 5500, p. 2291–2294, 2000.

MAYR, C. et al. Atmospheric controls on hydrogen and oxygen isotope composition of meteoric and surface waters in Patagonia. **Hydrology and Earth System Sciences**, v. 1–22, 2018. doi: 10.5194/hess-2018-431.

MECHLIŃSKA, A. et al. Removal of sulfur from a solvent extract. **Trends in Analytical Chemistry**, v. 31, p. 129–133, 2012.

MEYERS, P. A.; ISHIWATARI, R. Lacustrine organic geochemistryman overview of indicators of organic matter sources and diagenesis in lake sediments. **Organic Geochemistry**, v. 20, n. 7, p. 867–900, 1993.

MEYERS, P. A.; LEENHEER, M. J.; BOURBONNIERE, R. A. Diagenesis of vascular plant organic matter components during burial in lake sediments. **Aquatic Geochemistry**, v. 1, n. 1, p. 35–52, 1995.

MEYERS, P. A.; TAKEUCHI, N. Fatty acids and hydrocarbons in surficial sediments of Lake Huron. **Organic Geochemistry**, v. 1, p. 127–138, 1979.

NOBRE, P. et al. Coupled ocean-atmosphere variations over the South Atlantic Ocean. **Journal of Climate**, v. 25, n. 18, p. 6349–6358, 2012.

NOBRE; SHUKLA, P. AND J. Variations of sea surface temperature, wind stress, and rainfall over the Tropical Atlantic and South America. **Journal of Climate**, v. 9, p. 2464–2479, 1996.

NUNES, J. A. et al. Soil-vegetation relationships on a banded ironstone ‘island’, Carajás Plateau, Brazilian Eastern Amazonia. **Anais da Academia Brasileira de Ciencias**, v. 87, n. 4, p. 2097–2110, 2015.

PADUANO, G. M. et al. A Vegetation and Fire History of Lake Titicaca since the Last Glacial Maximum. **Palaeogeography, Palaeoclimatology, Palaeoecology**, v. 194, p. 259–279, 2003.

PANCOST, R. D.; BOOT, C. S. The palaeoclimatic utility of terrestrial biomarkers in marine sediments. **Marine Chemistry**, v. 92, n. 1- 4, p. 239–261, 2004. Special issue.

PEARSON, E. J.; FARRIMOND, P.; JUGGINS, S. Lipid geochemistry of lake sediments from semi-arid Spain: Relationships with source inputs and environmental factors. **Organic Geochemistry**, v. 38, p. 1169–1195, 2007.

PEREIRA, J. B. D. S. et al. Two New Species of Isoetes (Isoetaceae) from northern Brazil. **Phytotaxa**, v. 272, n. 2, p. 141–148, 2016.

PESSENDA, L. C. R. et al. ^{14}C Dating and Stable Carbon Isotopes of Soil Organic Matter in Forest–Savanna Boundary Areas in the Southern Brazilian Amazon Region. **Radiocarbon**, v. 40, n. 2, p. 1013–1022, 1998a.

PESSENDA, L. C. R. et al. The carbon isotope record in soils along a forest-cerrado ecosystem transect: implications for vegetation changes in the Rondonia state, southwestern Brazilian Amazon region. **The Holocene**, v. 8, n. 5, p. 599–603, 1998b.

PESSENDA, L. C. R. et al. The evolution of a tropical rainforest/grassland mosaic in southeastern Brazil since 28,000 14C yr BP based on carbon isotopes and pollen records. **Quaternary Research**, v. 71, n. 3, p. 437–452, 2009.

PONTES, P. R. M. et al. The role of protected and deforested areas in the hydrological processes of Itacaiúnas River Basin, eastern Amazonia. **Journal of Environmental Management**, v. 235, p. 489–499, 2019.

POYNTER, J. G. et al. Aeolian-derived higher plant lipids in the marine sedimentary record: links with paleoclimate. In: LEINEN, M.; SARNTHEIN, M. (Ed.). **Paleoclimatology and paleometeorology**: Modern and past patterns of global atmospheric transport. 1. ed. Dordrecht: Springer Netherlands, 1989. p. 435–462.

RAHMSTORF, S. Ocean circulation and climate during the past 120,000 years. **Nature**, v. 419, p. 207–214, 2002.

REIFFARTH, D. G. et al. Sources of variability in fatty acid (FA) biomarkers in the application of compound-specific stable isotopes (CSSIs) to soil and sediment fingerprinting and tracing: A review. **Science of the Total Environment**, v. 565, p. 8-27, 2016.

REIMER, P. J. et al. IntCal13 and Marine13 Radiocarbon Age Calibration Curves 0–50,000 Years cal BP. **Radiocarbon**, v. 55, n. 4, p. 1869–1887, 2013.

REIS, L. S. et al. Environmental and vegetation changes in southeastern Amazonia during the late Pleistocene and Holocene. **Quaternary International**, v. 449, p. 83–105, 2017.

RENSSEN, H. et al. The spatial and temporal complexity of the Holocene thermal maximum. **Nature Geoscience**, v. 2, p. 411-414, 2009.

RENSSEN, H. et al. Global characterization of the Holocene Thermal Maximum. **Quaternary Science Reviews**, v. 48, p. 7–19, 2012.

RIELEY, G. et al. Source of sedimentary lipids deduced from stable carbon-isotope analyses of individual compounds. **Nature**, v. 352, p. 425–427, 1991.

RIELEY, G.; COLLIER, R. J.; JONES, D. M. et al. Sources of sedimentary lipids deduced from stable carbon-isotope analyses of individual compounds. **Nature**, v. 352, p. 425–427, 1991.

ROMMERSKIRCHEN, F. et al. Chemotaxonomic significance of distribution and stable carbon isotopic composition of long-chain alkanes and alkan-1-ols in C 4 grass waxes. **Organic Geochemistry**, v. 37, p. 1303–1332, 2006.

SACHSE, D. et al. Molecular Paleohydrology: Interpreting the Hydrogen-Isotopic Composition of Lipid Biomarkers from Photosynthesizing Organisms. **Annual Review of Earth and Planetary Science**, v. 40, p. 221–249, 2012.

SAHOO, P. K. et al. Influence of seasonal variation on the hydro-biogeochemical characteristics of two upland lakes in the Southeastern Amazon, Brazil. **Anais da Academia Brasileira de Ciências**, v. 88, n. 4, p. 2211–2227, 2016.

SAHOO, P. K. et al. Limnological characteristics and planktonic diversity of five tropical upland lakes from Brazilian Amazon. **Annales de Limnologie - International Journal of Limnology**, v. 53, p. 467–483, 2017.

SALATI, E. et al. Recycling of water in the Amazon Basin: An isotopic study. **Water Resources Research**, v. 15, n. 5, p. 1250–1258, 1979.

SCHAEFER, C. E. et al. Solos desenvolvidos sobre canga ferruginosa no Brasil: uma revisão crítica e papel ecológico de termiteiros. In: CARMO, F. F.; KAMINO, L. H. Y. (Org.). **Geossistemas ferruginosos do Brasil**: áreas prioritárias para conservação da diversidade geológica e biológica, patrimônio cultural e serviços ambientais. Belo Hrizonte: 3i Editora, 2015. p. 77–102.

SCHEFUSS, E.; SCHOUTEN, S.; SCHNEIDER, R. R. Climatic controls on central African hydrology during the past 20,000 years. **Nature**, v. 437, n. 7061, p. 1003–1006, 2005.

SCHNEIDER, T.; BISCHOFF, T.; HAUG, G. H. Migrations and dynamics of the intertropical convergence zone. **Nature**, v. 513, p. 45-53, 2014.

SCHNURRENBERGER, D.; RUSSELL, J.; KELTS, K. Classification of lacustrine sediments based on sedimentary components. **Journal of Paleolimnology**, v. 29, n. 2, p. 141–154, 2003.

SIFEDDINE, A. et al. Variations of the Amazonian rainforest environment: A sedimentological record covering 30,000 years. **Palaeogeography, Palaeoclimatology, Palaeoecology**, v. 168, n. 3–4, p. 221–235, 2001.

SILVA, M. F. F. Análise florística da vegetação que cresce sobre canga hematítica em Carajás - Pará (Brasil). **Boletim do Museu Paraense Emílio Goeldi**, v. 7, n. 1, p. 79–105, 1991.

SILVA JÚNIOR, R. O. DA et al. Three decades of reference evapotranspiration estimates for a tropical watershed in the eastern Amazon. **Anais da Academia Brasileira de Ciências**, v. 89, n. 3, p. 1985–2002, 2017a. Suplemento.

SILVA JÚNIOR, R. O. et al. Estimativa de precipitação e vazões médias para a bacia hidrográfica do rio Itacaiúnas (BHRI), Amazônia Oriental, Brasil. **Revista Brasileira de Geografia Física**, v. 10, n. 5, p. 1638–1654, 2017b.

SKIRYCZ, A. et al. Canga biodiversity, a matter of mining. **Frontiers in Plant Science**, v. 5, p. 1–9, 2014.

SMITH, F. A.; FREEMAN, K. H. Influence of physiology and climate on δD of leaf wax n-alkanes from C3 and C4 grasses. **Geochimica et Cosmochimica Acta**, v. 70, n. 5, p. 1172–1187, 2006.

STUIVER, M.; POLACH, H. A. Discussion: Reporting and Calibration of 14C Data. **Radiocarbon**, v. 19, n. 3, p. 355–363, 1977.

STUTE, M. et al. Cooling of Tropical Brazil (5 ° C) during the Last Glacial Maximum. **Science**, v. 269, n. 5222, p. 379–383, 1995.

TAVARES, A. L. et al. Climate indicators for a watershed in the eastern Amazon. **Revista Brasileira de Climatologia**, v. 23, n. 6, p. 389-410, 2018.

TIERNEY, J. E.; DEMENOCAL, P. B. Abrupt Shifts in Horn of Africa Hydroclimate Since the Last Glacial Maximum. **Science**, v. 342, p. 843–846, 2013.

VAN DER ENT, R. J. et al. Origin and fate of atmospheric moisture over continents. **Water Resources Research**, v. 46, n. 9, p. 1–12, 2010.

VAN DER HAMMEN, T.; ABSY, M. L. Amazonia during the last glacial. **Palaeogeography, Palaeoclimatology, Palaeoecology**, v. 109, n. 2–4, p. 247–261, 1994.

VAN DER HAMMEN, T.; HOOGHIEMSTRA, H. Neogene and Quaternary history of vegetation, climate, and plant diversity in Amazonia. **Quaternary Science Reviews**, v. 19, n. 8, p. 725–742, 2000.

VEIGA-PIRES, C.; HILLAIRE-MARCEL, C. U and Th isotope constraints on the duration of Heinrich events H0-H4 in the southeastern Labrador Sea. **Paleoceanography**, v. 14, n. 2, p. 187–199, 1999.

VOGTS, A. et al. Distribution patterns and stable carbon isotopic composition of alkanes and alkan-1-ols from plant waxes of African rain forest and savanna C3 species. **Organic Geochemistry**, v. 40, p. 1037–1054, 2009.

VOGTS, A. et al. n-Alkane parameters from a deep sea sediment transect off southwest Africa reflect continental vegetation and climate conditions. **Organic Geochemistry**, v. 47, p. 109–119, 2012.

VOGTS, A. et al. Near-constant apparent hydrogen isotope fractionation between leaf wax n-alkanes and precipitation in tropical regions: Evidence from a marine sediment transect off SW Africa. **Organic Geochemistry**, v. 96, p. 18-27, 2016.

WALKER, R. G.; JAMES, N. P. **Facies models**: response to sea level change. Newfoundland St. John's: Geological Association of Canada, 1992.

WANG, X. et al. Hydroclimate changes across the Amazon lowlands over the past 45,000 years. **Nature**, v. 541, n. 7636, p. 204–207, 2017.

WHITNEY, B. S. et al. A 45kyr palaeoclimate record from the lowland interior of tropical South America. **Palaeogeography, Palaeoclimatology, Palaeoecology**, v. 307, n. 1–4, p. 177–192, 2011.

ZEMP, D. C. et al. On the importance of cascading moisture recycling in South America. **Atmospheric Chemistry and Physics**, v. 14, p. 13337–13359, 2014.

ZHANG, X. et al. Hydrogen isotope ratios of terrestrial leaf wax n -alkanes from the Tibetan Plateau: Controls on apparent enrichment factors, effect of vapor sources and implication for altimetry. **Geochimica et Cosmochimica Acta**, v. 211, p. 10–27, 2017.

4. FINAL REMARKS AND CONCLUSION

The multi-proxy approach applied to two sedimentary cores (AM2 and AM3) from Lake Amendoim revealed important changes in the climate conditions and vegetation composition in the Serra dos Carajás, southeastern Amazonia. Moreover, our study attested to the complexity regarding the climatic configuration active in the Amazon basin and the controls on rainfall variability over the last 22,000 years.

Unlike earlier studies performed in Carajás, our study evidenced the permanence of the tropical forest in the study site even under reduced precipitation during the LGM and Late Glacial. Cooler conditions during this interval also promoted one of the most relevant changes in the vegetation composition, characterized by the incursion cool-adapted taxa from highlands to Amazonian lowlands, which evidence that changes in global temperature played an important role in vegetation dynamics over the Amazon basin.

During the Pleistocene-Holocene transition, a rise in atmospheric CO_2 levels together with an increase in Atlantic SST marked a shift to warm and wetter conditions at Carajás compared to the glacial period, which led to the expansion of C_3-dominated forest community. Within the Holocene, major shifts in hydroclimate and vegetation cover were highly associated with the climate events in the Northern Hemisphere, e.g. Heinrich Stadial 0 and Holocene Thermal Maximum. Furthermore, our data also pointed to a greater influence of orbital forcing on precessional timescale at rainfall patterns in Serra dos Carajás and throughout the Amazon basin.

Finally, our results also provided an important development for reconstructions of past vegetation dynamics and hydrologic conditions using plant wax $\delta^{13}C$ and δD, respectively, combined with molecular and pollen data. This combination, therefore, provided a more robust interpretation and reaffirmed plant wax δD as a valuable climate proxy. Nevertheless, local and/or regional calibration studies with modern plants are indispensable for a robust interpretation of plant wax origin and distribution in sedimentary archives besides their response to environmental changes.

APPENDIX

Appendix A - Figure A.1: Distribution of geochemical components (major and traces elements) throughout the core AM2

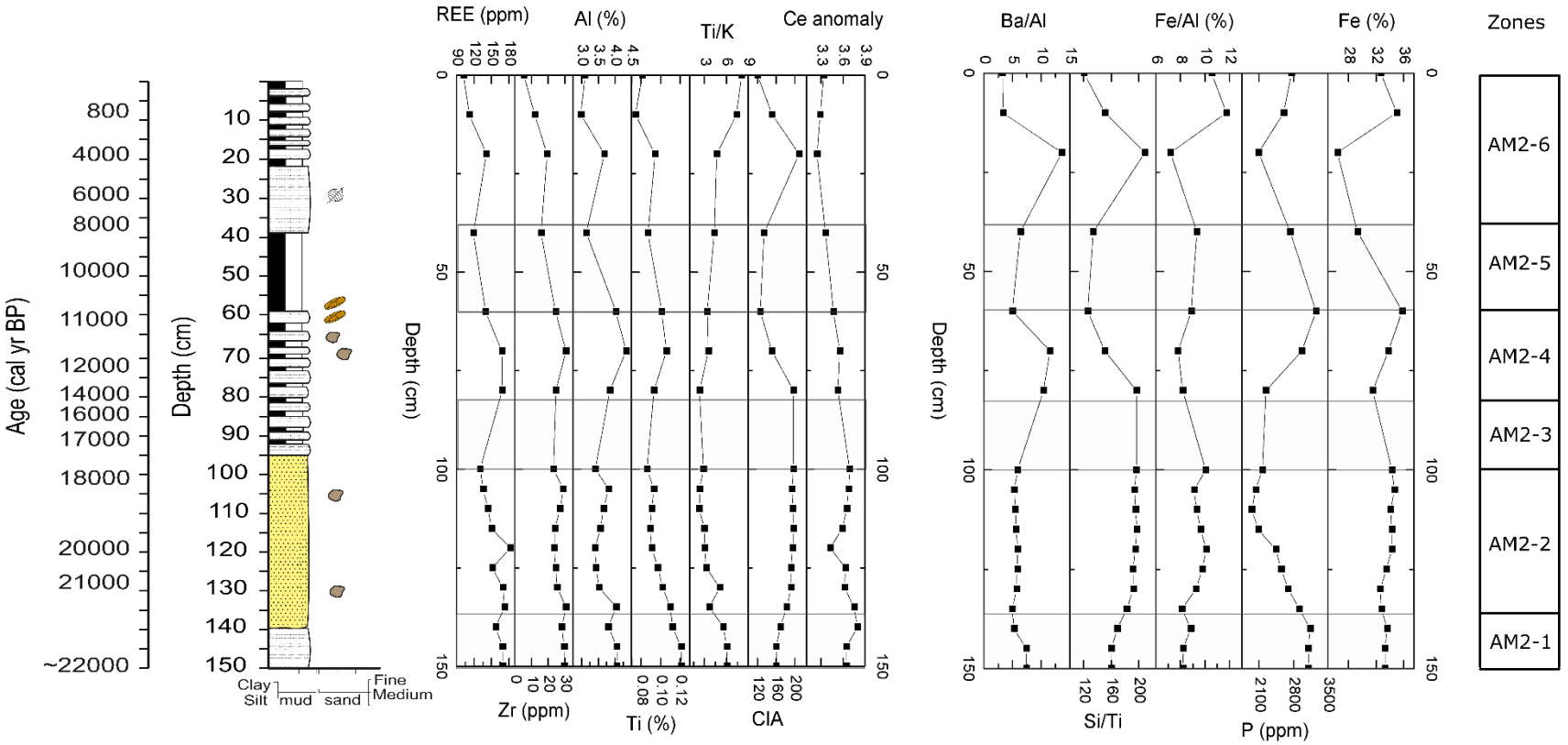

Table A.1 – Individual and total concentration (µg g^{-1} dry weight) of odd-numbered *n*-alkanes (C_{25}-C_{35}) along the core AM3 from Lake Amendoim

AM3 ID Sample	Age (cal yr BP)	n-alkane concentration (µg g^{-1} DW)						
		C_{25}	C_{27}	C_{29}	C_{31}	C_{33}	C_{35}	ΣC_{25}-C_{35}
9	6846	0,3	0,6	1,1	1,4	0,8	0,3	4,4
10	7055	1,1	1,4	2,5	3,1	2,0	0,5	10,7
12	7453	0,6	1,4	2,0	2,5	1,5	0,3	8,3
13	7651	0,6	0,7	1,0	1,3	0,9	0,4	4,8
14	7849	0,7	1,3	2,8	3,5	2,9	0,5	11,8
15	8145	0,6	0,8	1,6	2,2	1,7	0,8	7,6
16	8463	1,2	2,0	4,4	5,8	4,8	1,1	19,3
17	8800	0,5	0,8	1,9	2,6	2,2	1,0	9,1
18	9096	1,5	2,9	6,6	9,1	7,9	1,6	29,6
19	9364	0,7	1,4	3,4	5,0	4,2	1,9	16,6
20	9611	2,3	4,0	9,2	13,1	11,4	2,5	42,4
21	9859	0,6	1,3	3,1	4,5	3,7	1,5	14,7
22	10107	1,6	3,3	7,7	11,3	10,3	2,1	36,3
23	10358	0,5	1,1	2,8	3,9	3,1	1,3	12,7
24	10612	1,5	3,2	7,4	9,9	8,6	1,9	32,6
25	10757	0,7	1,8	3,5	3,8	2,7	1,0	13,6
26	10887	1,1	2,5	4,9	4,3	3,3	1,0	17,2
27	11013	0,3	1,0	2,0	1,8	1,4	0,6	7,1
28	11139	1,2	2,6	5,2	4,1	3,0	0,9	16,9
29	11263	0,3	0,7	1,5	1,3	1,0	0,4	5,2
30	11413	0,7	1,6	3,1	2,8	2,0	0,4	10,7
31	11575	0,4	0,8	1,4	1,1	0,7	0,3	4,6
32	11733	0,6	1,3	2,8	2,5	1,9	0,4	9,5
33	11878	0,4	0,9	1,8	1,4	1,0	0,5	5,9
34	12006	0,5	1,2	2,7	2,4	1,9	0,3	9,1
35	12146	0,3	0,5	1,1	1,1	0,7	0,3	4,0
36	12307	0,4	0,9	1,9	2,0	1,6	0,2	7,1
37	12468	0,2	0,4	0,9	0,9	0,7	0,3	3,4
38	12620	0,3	0,5	1,1	1,4	1,1	0,1	4,5
39	12761	0,2	0,2	0,4	0,5	0,4	0,2	1,8
40	12915	0,2	0,5	0,7	0,9	0,8	0,1	3,2
41	13085	0,1	0,2	0,4	0,5	0,4	0,2	1,8
42	13246	0,2	0,4	0,6	0,9	0,7	0,1	2,8
43	13415	0,1	0,2	0,4	0,6	0,5	0,2	2,0
44	13563	0,5	0,8	2,0	3,1	2,4	0,2	9,0
45	13702	0,4	0,7	1,7	2,8	2,2	0,8	8,6
46	13845	1,1	1,7	4,6	8,2	6,9	0,7	23,2
47	13996	0,5	0,9	2,1	3,4	2,9	1,1	10,8
50	14426	0,2	0,2	0,5	0,9	0,7	0,3	2,8

52	14661	0,2	0,4	0,9	1,4	1,1	0,1	4,3
53	14794	0,2	0,3	0,7	1,1	0,9	0,3	3,5
54	14932	0,3	0,5	1,3	2,0	1,6	0,1	5,7
55	15094	0,1	0,2	0,4	0,7	0,5	0,2	2,1
56	15250	0,2	0,4	0,9	1,3	1,0	0,1	4,0
57	15387	0,1	0,2	0,4	0,7	0,6	0,2	2,3
58	15514	0,2	0,4	1,0	1,5	1,1	0,1	4,3
59	15649	0,1	0,2	0,3	0,6	0,4	0,2	1,7
60	15816	0,1	0,2	0,5	0,7	0,6	0,0	2,1
61	15998	0,0	0,1	0,1	0,2	0,2	0,1	0,7
62	16180	0,1	0,2	0,3	0,4	0,3	0,0	1,3
64	16521	0,0	0,1	0,3	0,4	0,3	0,0	1,1
65	16688	0,1	0,1	0,2	0,3	0,2	0,1	0,9
66	16857	0,1	0,1	0,3	0,3	0,3	0,0	1,1
67	17034	0,0	0,1	0,2	0,2	0,2	0,1	0,8
68	17209	0,1	0,1	0,3	0,3	0,2	0,0	1,0
69	17369	0,0	0,1	0,1	0,2	0,1	0,1	0,6
70	17535	0,1	0,2	0,3	0,3	0,2	0,0	1,2
71	17703	0,1	0,1	0,2	0,2	0,2	0,1	0,8
73	18061	0,0	0,1	0,1	0,2	0,2	0,1	0,6
74	18252	0,1	0,1	0,3	0,3	0,3	0,0	1,1
75	18993	0,1	0,1	0,2	0,2	0,2	0,1	0,8
76	19717	0,1	0,2	0,3	0,4	0,3	0,0	1,3
77	20447	0,1	0,1	0,2	0,3	0,2	0,1	0,9
78	21172	0,1	0,2	0,4	0,5	0,4	0,0	1,6
79	21901	0,1	0,1	0,2	0,3	0,3	0,1	1,1
80	22826	0,1	0,2	0,4	0,5	0,4	0,0	1,7
81	23763	0,1	0,1	0,2	0,3	0,2	0,1	1,1
82	24761	0,2	0,3	0,6	0,7	0,5	0,1	2,2

Table A.2 – Individual and total concentration (µg g^{-1} dry weight) of even-numbered *n*-fatty acids (C_{16}-C_{34}) along the core AM3, from Lake Amendoim

AM3	Age	*n*-fatty acids concentration (µg g^{-1})										
ID Sample	(cal yr BP)	C_{16}	C_{18}	C_{20}	C_{22}	C_{24}	C_{26}	C_{28}	C_{30}	C_{32}	C_{34}	ΣC_{16}-C_{34}
9	6846	6,5	3,0	2,5	4,2	4,8	9,6	15,6	10,3	8,1	4,4	69
10	7055	9,5	4,7	3,5	6,0	6,2	14,6	25,2	16,2	12,4	6,6	105
12	7453	10,2	5,2	4,0	5,0	5,9	14,0	24,1	14,6	10,9	6,6	101
13	7651	5,6	3,1	2,5	3,3	4,1	10,1	19,0	10,5	7,5	4,6	70
14	7849	7,5	4,0	2,8	4,6	5,0	13,5	31,0	18,9	11,5	7,9	107
15	8145	5,5	2,7	2,4	4,0	5,2	11,4	26,0	14,6	8,7	5,8	86
16	8463	7,1	3,6	2,8	4,6	6,1	15,4	39,4	20,8	12,0	8,6	121
17	8800	5,7	2,4	1,9	3,5	4,6	10,7	27,0	13,2	7,5	5,0	82
18	9096	11,0	4,8	3,7	6,2	8,3	19,8	55,9	28,1	15,8	11,7	165
19	9364	11,3	4,9	3,8	6,6	8,7	19,5	54,5	25,5	14,3	9,5	159
20	9611	12,8	5,5	4,1	6,8	9,2	19,1	56,9	28,6	15,4	10,1	169
21	9859	10,1	3,9	3,4	5,5	7,4	14,9	41,4	19,3	10,0	6,1	122
22	10107	12,5	5,5	4,7	7,1	9,5	21,5	63,3	36,3	20,1	14,2	195
23	10358	9,7	4,1	3,4	5,3	7,2	15,5	46,0	23,2	11,2	6,8	133
24	10612	9,8	3,9	3,5	5,2	6,8	15,6	46,3	30,2	12,8	8,0	142
25	10757	11,6	4,6	4,3	6,4	7,9	14,3	32,8	19,1	6,0	3,7	111
26	10887	7,7	3,7	3,3	4,9	6,1	14,5	40,7	36,3	9,6	5,9	133
27	11013	4,3	2,1	2,1	3,1	4,1	10,7	30,1	25,7	6,6	4,0	93
28	11139	6,9	3,1	3,3	4,5	6,1	14,5	37,0	38,6	8,6	5,3	128
29	11263	3,5	2,0	1,5	2,3	3,0	8,8	22,8	22,0	5,6	3,4	75

30	11413	4,6	2,6	2,4	3,0	4,1	9,3	21,1	22,7	6,0	3,8	80
31	11575	2,7	1,5	1,7	2,1	3,1	8,5	21,1	23,5	6,3	4,0	75
32	11733	2,1	1,1	1,6	1,7	2,5	5,4	12,3	13,5	3,9	2,8	47
33	11878	6,2	2,5	2,3	2,7	3,7	9,1	21,3	20,5	6,1	3,8	78
34	12006	4,2	2,1	2,7	2,9	4,0	9,6	21,6	21,7	6,4	4,5	80
35	12146	2,7	1,4	2,1	2,3	3,0	6,8	15,8	13,3	5,1	3,2	56
36	12307	3,0	1,8	2,0	2,2	2,8	6,0	13,7	11,1	4,9	3,5	51
37	12468	1,8	1,0	1,2	1,4	1,7	3,8	9,3	7,3	3,6	2,3	33
38	12620	0,8	0,6	0,9	0,9	1,2	2,1	4,6	2,9	2,0	1,3	17
39	12761	1,1	0,7	0,7	0,8	1,0	1,7	4,0	2,4	1,7	1,0	15
40	12915	1,1	0,9	0,8	1,2	1,1	2,0	4,4	2,7	1,9	1,3	17
41	13085	1,4	0,8	0,8	1,0	1,0	1,7	3,8	2,3	1,7	1,2	16
42	13246	1,0	0,8	0,9	1,1	1,2	2,1	4,2	2,7	2,1	1,3	18
43	13415	1,0	0,7	0,7	0,9	1,0	2,1	4,7	2,9	2,4	1,4	18
44	13563	1,9	1,4	2,0	1,9	2,4	4,7	9,8	5,9	5,0	3,1	38
45	13702	3,2	1,8	3,3	2,9	3,9	8,2	17,2	12,4	11,6	7,4	72
46	13845	6,4	3,2	5,2	3,9	5,0	8,7	17,8	13,6	13,1	8,7	86
47	13996	5,8	3,2	5,5	4,5	5,4	7,2	13,1	8,8	7,7	4,7	66
50	14426	1,5	0,7	0,7	0,7	0,7	1,5	3,8	2,4	2,2	1,3	16
52	14661	1,9	1,2	2,2	1,6	1,8	2,7	5,8	3,8	3,3	2,1	26
53	14794	1,2	0,7	0,8	0,8	0,9	2,2	5,4	3,4	3,1	1,8	20
54	14932	1,8	1,2	2,1	1,6	1,9	3,1	6,7	4,4	3,6	2,2	29
55	15094	0,9	0,5	0,7	0,6	0,6	1,4	3,6	2,2	1,9	1,1	14
56	15250	2,0	1,1	1,5	1,2	1,3	2,0	4,4	2,8	2,3	1,3	20
57	15387	0,7	0,4	0,3	0,3	0,4	0,8	2,1	1,3	1,2	0,7	8
58	15514	1,4	0,9	1,5	1,2	1,4	2,2	4,9	3,1	2,6	1,5	21
59	15649	0,8	0,4	0,4	0,4	0,4	0,9	2,3	1,5	1,2	0,7	9
60	15816	0,9	0,5	0,5	0,5	0,5	0,7	1,5	1,1	0,7	0,5	7
61	15998	0,4	0,2	0,1	0,2	0,1	0,2	0,4	0,4	0,3	0,1	2

62	16180	0,5	0,3	0,3	0,4	0,3	0,3	0,6	0,7	0,3	0,2	4
64	16521	0,4	0,2	0,2	0,3	0,2	0,3	0,6	0,6	0,3	0,2	3
65	16688	0,4	0,2	0,1	0,2	0,1	0,2	0,4	0,4	0,2	0,1	2
66	16857	0,4	0,2	0,3	0,3	0,2	0,3	0,5	0,6	0,3	0,2	3
67	17034	0,4	0,2	0,2	0,2	0,1	0,1	0,4	0,4	0,2	0,1	2
68	17209	0,3	0,2	0,2	0,3	0,2	0,3	0,4	0,4	0,3	0,1	3
69	17369	0,3	0,1	0,1	0,1	0,1	0,1	0,3	0,3	0,2	0,1	2
70	17535	0,4	0,3	0,2	0,3	0,2	0,2	0,4	0,5	0,3	0,1	3
71	17703	0,3	0,2	0,2	0,2	0,1	0,2	0,4	0,4	0,2	0,1	2
73	18061	0,3	0,2	0,1	0,2	0,1	0,2	0,4	0,4	0,3	0,1	2
74	18252	0,4	0,0	0,2	0,8	0,0	0,2	0,5	0,5	0,3	0,1	3
75	18993	0,5	0,3	0,2	0,2	0,2	0,3	0,7	0,7	0,4	0,2	4
76	19717	0,5	0,0	0,3	0,0	0,2	0,3	0,8	0,7	0,4	0,2	4
77	20447	0,8	0,4	0,2	0,3	0,2	0,4	1,2	1,1	0,7	0,4	6
78	21172	0,6	0,0	0,4	0,7	0,1	0,5	1,2	1,0	0,6	0,3	5
79	21901	1,0	0,5	0,3	0,4	0,4	0,8	2,2	1,8	1,3	0,7	9
80	22826	0,5	0,0	0,4	0,8	0,1	0,7	2,0	1,5	1,0	0,6	8
81	23763	1,3	0,5	0,4	0,5	0,5	1,0	3,0	2,2	1,6	0,7	11
82	24761	0,9	0,0	0,6	1,2	0,1	1,1	3,2	2,4	1,7	0,9	12